Spring 2006

Atmospheric-Pressure Plasma Sources for Polymer Surface Modification

Shujun Yang
Old Dominion University

ATMOSPHERIC-PRESSURE PLASMA SOURCES FOR POLYMER SURFACE MODIFICATION

by

Shujun Yang
B. S. Tsinghua University, Beijing, China
M.S. Institute of Electronics, Chinese Academy of Sciences, Beijing, China

A Dissertation Submitted to the Faculty of
Old Dominion University in Partial Fulfillment of the
Requirement for the Degree of

DOCTOR OF PHILOSOPHY

ELECTRICAL ENGINEERING

OLD DOMINION UNIVERSITY

May 2006

Approved by:

_____
Amin Dharamsi (Director)

_____
Ravindra Joshi (Member)

_____
Linda Vahala (Member)

_____
James Yuan (Member)

ABSTRACT

Atmospheric-pressure plasma sources for polymer surface modification

Shujun Yang
Old Dominion University, 2006
Director: Amin Dharamsi

Plasma processing is widely used in the microelectronics industry for deposition of thin films. It is also used in etching of semiconductors, metals and organic materials such as photoresists. In addition, plasmas are widely used to modify material surfaces. Plasma surface modification can improve the surface adhesion of polymeric materials, which can be used as insulating layers in multilayer semiconductor structures. In deposition and etching, relatively a large amount of material is added to or removed from the surface. In plasma surface modification, only the surface layer is changed in composition or structure, and no significant amount of material is added or removed. In this research, two atmospheric-pressure plasmas were generated and characterized, and were used to modify polyethyleneterephthalate (PET) surfaces.

An atmospheric-pressure helium plasma source was generated without any need of vacuum. The plasma was first characterized with a Langmuir Probe for electron density estimation. The emission spectrum was measured and the spectroscopic identification allowed main components of the plasma to be identified. In addition, absorption spectroscopy was used to measure the ozone density from the plasma. A PET surface was modified with this plasma. Contact angles were measured on the modified PET surface. Hydrophilic and Hydrophobic PET surfaces were obtained with different minority gas or chemicals added to the feeding helium gas. The changes of the contact angles of the modified surfaces were monitored as a function of time. The surface modification was determined to be mainly a chemical and photochemical process through analysis and experiments on ions, ultraviolet photons, oxygen atoms and ozone molecules.

An atmospheric-pressure air plasma source was developed without the need of vacuum and the need of expensive helium gas. The peak electron density was determined by measuring and analyzing current-voltage characteristics of the plasma. The emission spectrum was measured and the main peaks were identified. Absorption spectroscopy was used to estimate ozone density. This plasma was used to modify PET surfaces with very high throughput.

ACKNOWLEDGMENTS

I would like to sincerely thank Dr. Dharamsi for his advice and inspiration on my dissertation research. He gave my special helps when I was in a very special situation. He contributed his knowledge and patience to bring my research to a conclusion.

Great thanks to Dr. Gupta at Applied Research Center for his concern and financial support, which made it possible to finish the dissertation.

I also thank Dr. Joshi, Dr. Vahala and Dr. Yuan for their willingness to serve in my dissertation committee. They gave me a lot of comments and suggestions.

Special thank goes to my colleagues and friends at Applied Research Center: Dr. Johnston, Dr. Familant, Dr. Mohajer, Dr. Wong, Dr. Yang, Dr. Yan, Dr. Elbandrawy, Dr. Nayak, Dr. Zhu, Dr. Wang, Dr. Li, Brandt, and Richard.

Special thank also goes to my close friend Feng Chen, Huanqin Yuan, Changqing Song, Yuming Geng, Jincheng Gao, Shangping Guo, Feng Wu, Bing Xiao, and Chunqi Jiang.

Finally, I would like to express my gratitude to my parents in China.

TABLE OF CONTENTS

LIST OF FIGURES

LIST OF TABLES

VITA

Shujun Yang was born in Mingshui County, Heilongjiang Province, P. R. China. He received his B. S. degree in Physical Electronics in 1991 from Tsinghua University, Beijing, China. He got his M. S. in Physical and Optical Electronics in 1998 from Institute of Electronics, Chinese Academy of Sciences, Beijing, China. From 1991 to 1992, he was a production engineer at Sanmei Electronics, Beijing, China. From 1993 to 1995, he worked as an electronic design engineer at Chinese International Enterprises Co-operation Corp, Beijing, China. From 1998 to 2000, he was a research assistant at PERI Lab, ODU, Norfolk, Virginia. From 2000 to 2005, he was a research assistant at ARC-ODU in Thomas Jefferson Lab, Newport News, Virginia. He authored three journal papers. His research interests include plasma, semiconductor processing and characterization, electronic circuits, microprocessors, RF and microwave, and acoustics.

Chapter I

Introduction

1.1. Polymer surface modification

Polymers are being extensively used because of their low cost and high performances. But their low surface energy, and hence their poor adhesion, limits their applications. Their poor surface adhesion can be greatly improved by surface modification. Surface modification changes the composition and the structure of surface layers without affecting the polymer bulk. Several methods have been used to modify polymer surfaces to improve their surface adhesion. They include mechanical and wet-chemical treatments, exposure to flames, photons, ion beams, corona discharges, and low-pressure plasma [1-3]. Mechanical treatments just make the surface rough to increase the surface areas. These treatments are too rough and their effects are limited. The treatment with wet chemicals can be very effective due to the extensive chemical reactions at the surface. But modifications by wet-chemical treatments are not uniform and hard to control, and the results are not reproducible. Exposure to flames may cause degradation of polymers and even destroy the polymers. Exposure to ions whose kinetic energies are not more than several keV is another way to modify polymer surfaces [4-8], but the efficiency is low, and the cost is very high. Exposure to photons, such as UV light and laser, has also been used to modify polymer surfaces [9-12]. The use of UV light is a practical way for large area applications, but it lacks the resultant effects generated by ion bombardment. Corona treatment is being widely used [1, 13-17], and it is realized in air without any vacuum requirement. One problem with corona treatment is that the modification effects decay quickly, and the treated surfaces need to be treated again

before being used [14, 15, 18, 19]. Low-pressure plasma surface modification can overcome this problem, and the modification effects are good. But this method requires vacuum, and hence the cost is high.

1.2. Plasma surface modification of polymer

Plasma refers to a quasi-neutral gas of charged and neutral particles exhibiting collective behavior [20, 21]. From this definition, plasma is a partially charged gas. It is neutral as a large body. Most particles are neutrals inside plasma, and some of them are at excited states. The key plasma species are charged particles, such as electrons and ions. Plasma also has some photon emissions. Plasma is usually characterized by electron density, electron temperature, ion density, ion temperature, gas temperature and gas pressure.

To be surface modified, a polymer sample is usually submerged inside or exposed to plasma. All the plasma species may interact with the polymer surface. Surface cleaning, ablation, cross-linking, surface chemical reactions may happen during the modification process [1]. Unlike plasma etching and deposition, no significant mount of material is added or removed during surface modifications. Only the surface layer is changed in composition or structure, and the polymer bulk is not influenced. New polar or unpolar groups may be formed at the polymer surface, and the surface energy may increase or decrease. The modified polymer surface is usually characterized by contact angle measurement, XPS (X-ray photoelectron spectroscopy), and other analytical techniques [1-3].

There are three fundamental mechanisms for plasma surface modification of polymers [1]. They are ultraviolet photochemistry, ion bombardment, and direct reactions. These three theories are widely accepted, although people still have disputes over some special cases. According to ultraviolet photochemistry theory, UV photons from a plasma source have short wavelengths and high energy, and they can break chemical bonds at a polymer surface and in its surrounding gases. These broken bonds lead to a series of chemical reactions at the surface layers. Through these chemical reactions, elements from the surrounding gases can be incorporated into the surface layers. According to the ion bombardment theory, some ions inside the plasma have enough energy to break chemical bonds on polymer surfaces, and then initiate a series of chemical reactions. These reactions change the polymer surface composition and structure. In some cases, ion dose can be the main factor of polymer surface modification. The third theory is called direct reaction. According to this theory, chemically active species generated by the plasma may react directly with polymer surfaces, and the reactions modify the polymer surfaces.

1.3. Goals of this research

This research has three goals. The first research goal is to generate two atmospheric-pressure plasma sources to overcome the vacuum limitation of low-pressure plasma surface modification. These two plasmas are different from other plasmas that have been used in polymer surface modification. The second goal is to characterize the two plasma sources on electron density, emission spectrum, ozone density, and etc. The third goal of this research is to modify polymer surface with these two plasmas and to investigate the modification mechanism.

1.4. Structure of this dissertation

This dissertation has six chapters. Following this introduction is a chapter that describes the low-pressure plasma and high-pressure plasma, the characterization of high-pressure plasma, and plasma surface modifications. Although most materials come from other researches, we put them together with our contributions in a systematic way to give readers a clear picture of relevant phenomena and mechanisms. Chapter three and chapter four have similar structures. In each of these two chapters, we describe the experimental setup of each plasma source, the characterization of each plasma source on electron density, emission spectrum, and ozone density. In chapter five, we describe the plasma surface modification setup, the modification results, and the investigation of modification mechanisms. In chapter six, after a short summary of this research, we give several possible future developments in this area.

Chapter II

Plasma and Plasma Surface Modification of Polymers

2.1. Fundamental Plasma theory [20, 21]

2.1.1. Definitions of plasma

Plasma is the fourth state of matter. If the temperature is increased, a solid will become a liquid. The liquid can become a gas if the temperature is increased more. If the gas temperature is high enough, some gas molecules can be decomposed into atoms. If the temperature is further increased, some of the atoms and molecules can be decomposed into electrons and ions, and the matter becomes plasma. The temperatures required to form plasmas are different for different materials. Plasma is firstly characterized by the electron density. Since electrons and ions are moving, the plasma is secondly characterized by electron temperature and ion temperature. In some plasmas, electrons and ions are in thermal equilibrium. While in cold plasma, only electrons are extremely hot, and ions and neutrals are cold.

Plasma has another definition. The word plasma originally means to mold. Plasma refers to a quasi-neutral gas of charged and neutral particles exhibiting collective behavior. From this definition, plasma is a partially charged gas. It is neutral as a large body. But it is not neutral in a certain small volumes. Since plasma is a gas, it is also characterized by its pressure.

2.1.2. Maxwell-Boltzman Distribution

The electrons in plasma or a gas has a distribution on speed or energy. The most popular description is Maxwell-Boltzman Distribution. This distribution is based on the kinetic theory of the ideal gas. It has four assumptions. The first assumption is that the

gas only consists of a very large number of point particles with no size or internal structure. In practice, the distance between molecules is much larger than the size of the molecules. The second assumption is no other forces except elastic collisions. The potential energy changes from electrical, gravitational, and nuclear forces are much smaller compared with the particle's kinetic energy. The third assumption is that the kinetic energy and momentum are conserved in collisions. The fourth assumption is that the movements of particles are randomized.

Maxwell-Boltzmann Distribution is expressed as

$$f(v) = 4\pi v^2 \left(\frac{m}{2\pi kT}\right)^{3/2} \exp\left(-\frac{mv^2}{2kT}\right), \qquad (2\text{-}1)$$

where f is the distribution function, v is velocity, m is particle mass, k is Boltzmann constant, T is temperature. In terms of kinetic energy, the distribution has another expression described as

$$f(E) = \frac{2E^{1/2}}{\pi^{1/2}(kT)^{3/2}} \exp\left(-\frac{E}{kT}\right), \qquad (2\text{-}2)$$

where E is the kinetic energy.

The averaging over Maxwell-Boltzmann Distribution can be calculated as

$$\bar{g} = \int g(v) f(v) dv, \qquad (2\text{-}3)$$

where g is a physical quantity. In this way, the average speed can be calculated as

$\bar{v} = \sqrt{\dfrac{8kT}{\pi m}}$, and the average kinetic energy can be calculated as $\bar{E} = \dfrac{3}{2}kT$. Similarly,

electron or ion flux on wall can be calculated as $\Gamma = \dfrac{1}{4}n\bar{v}$.

The spatially distribution of electrons and ions can be influenced by the potential difference inside the plasma. This effect can be described by Boltzmann's relation, which can be expressed by

$$n_e = n_0 \exp\left(-\frac{e\Phi}{kT_e}\right),$$
(2-4)

where T_e is electron temperature, Φ is the potential difference, and n_e and n_0 are the electron densities at two locations with a potential difference Φ, e is electron charge quantity, and k is Boltzmann constant.

2.1.3. Collisions

In inside plasma, electrons play a key role. The external energy is first usually applied to electrons. Electrons can transfer their energy to other particles through collisions. The electrons flux is changes by collisions. This effect is described by

$$\Gamma(x) = \Gamma_0 \exp(-n\sigma x),$$
(2-5)

where Γ_0 is the initial electron flux, $\Gamma(x)$ is the electron flux after the electrons travel a distance x, n is the gas density, and σ is the collision cross section. The mean free path of electrons can be expressed by

$$l = \frac{1}{n\sigma}.$$
(2-6)

The averaging collision frequency per electron can be calculated by

$$\gamma = n\sigma v,$$
(2-7)

where v is electron velocity.

Plasma is a partially ionized gas, and there are countless collisions inside plasma. Collisions are usually divided into elastic collisions and inelastic collisions. In elastic

collisions, sum of the kinetic energies of colliding partners is conserved, and internal energies of the colliding partners do not change. The total momentum is also conserved. There is momentum transfer and kinetic energy transfer between colliding partners. In inelastic collisions, the total kinetic energy is not conserved. Most inelastic collisions lead to excitations and ionizations, and the total kinetic energy is reduced. One special case is superelastic collision, in which an exited atom can relax through a collision with an electron, and the total kinetic increases. Electrons can have elastic and inelastic collisions with ground state and excited neutrals, ions. Electrons can have superelastic collisions with excited neutrals. These elastic collisions determine electron transport properties, such as diffusion, electrical and thermal conductivity, and gas heating. Inelastic collisions determine excited state density, degree of dissociation. Both elastic and inelastic collisions determine the degree of ionization.

2.1.4. Plasma species

There are many species inside plasma, such as neutrals, electrons, ions, photons. Most neutrals are at ground state, and some are at excited states. Most ions are positive and at ground states. Some ions are negatively charged, and some are even at their excited states. Photons come from the relaxations of particles from higher states to low states. Photons can have different wavelengths to form an emission spectrum.

Figure 2.1 shows different kinds of plasma with different electron density and electron temperature. We would like to mention two kinds of discharges. Both of them are widely used in material processing. The most import kind is low-pressure glow discharge. Electron temperature is between 1 and 10 eV. Electron density is between 10^8 and 10^{11} cm^{-3}. Ion temperature is much lower than electron temperature. The gas pressure

is between 1 mTorr and 1 Torr. The second kind of important plasma is the high-pressure

arcs. Electron temperature is between 0.1 and 2 eV. Electron density is between 10^{14} and

10^{19} cm^{-3}. Ions and electrons are nearly in thermal equilibrium.
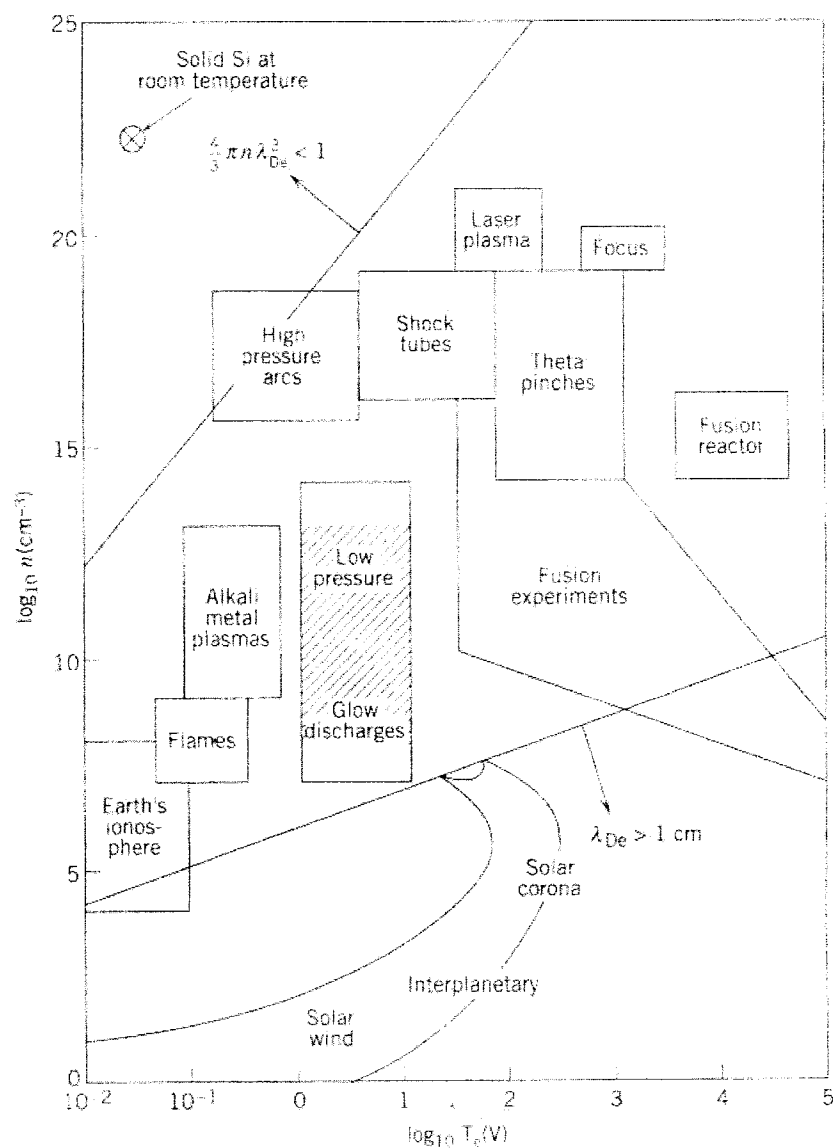
Figure 2.1. Plasmas with different electron densities and temperatures [20].

2.1.5. Diffusion

External energy is always needed to sustain the plasma because electron density can decay through different mechanisms. If gas pressure is higher than 10 Torr, the main decay mechanism is electron-ion recombination. If an electric negative gas is used, the main decay process is electron attachment to neutrals. For most low-pressure plasmas, electrons are lost mainly due to the electron diffusion to walls. Electrons should diffuse fast than ions, but the established new electric field tend to keep the overall space-charge neutrality. As a result, electrons have to diffuse at the same rate as ions. This effect is called Ambipolar Diffusion expressed by

$$\frac{\partial n}{\partial t} = \frac{D_e \mu_i + D_i \mu_e}{\mu_e + \mu_i} \nabla^2 n = D_a \nabla^2 n, \qquad (2\text{-}8)$$

where n is electron density, t is time, D_a is ambipolar diffusion coefficient, D_e is electron diffusion coefficient, D_i is ion diffusion coefficient, μ_e is electron mobility, and μ_i is ion mobility.

2.1.6. Plasma properties

Debye Length is the characteristic length of plasma. It is the shielding length of plasma. If a charge is placed inside plasma, its field will be shielded by the charges over several Debye Lengths. Debye Length is also the distance over which significant charge density differences can exist. Debye Length can be express by

$$\lambda_D = \sqrt{\frac{kT_e \varepsilon_0}{ne^2}}, \qquad (2\text{-}9)$$

where λ_D is Debye Length, k is Boltzmann's constant, T_e is electron temperature, n is electron density, ε_0 is the dielectric constant in vacuum, e is electron charge quantity.

Debye Length is also a distance over which significant derivations from quasi-neutrality are possible. From this point of view, the dimension of plasma must be much larger than Debye Length, or the discharge is not good plasma, and it will be dominated by wall effect. Quantitatively, for good plasma, there must be large number of electrons inside a Debye Sphere. This effect can be expressed by

$$\frac{4}{3}\pi\lambda_D^3 n >>> 1.$$ (2-10)

Plasma has a characteristic electron frequency and ion frequency. These frequencies are used to describe how fast electrons and ions oscillate caused by any charge perturbation. Plasma electron frequency can be expressed by

$$\omega_{pe} = \sqrt{\frac{ne^2}{m\varepsilon_0}},$$ (2-11)

where ω_{pe} is electron frequency, and m is electron mass. Similarly, plasma ion frequency can be expressed by

$$\omega_{pi} = \sqrt{\frac{ne^2}{M\varepsilon_0}},$$ (2-12)

where M is ion mass. Ion frequency is much lower than electron frequency. Plasma electron frequency is usually called plasma frequency. An electromagnetic wave with a frequency higher than plasma frequency can penetrate the plasma. If an electromagnetic wave has a frequency lower than plasma frequency, it will be absorbed by the plasma.

Plasma has its conductivity and effective dielectric constant. The conductivity can be express by

$$\sigma_p = \frac{\varepsilon_0 \omega_{pe}^2}{j\omega + v_m},$$ (2-13)

where σ_p is plasma conductivity, ω_{pe} is plasma frequency, ω is the frequency of applied external electric field, and ν_m is the electron-neutral collision frequency. The plasma effective dielectric constant can be expressed by

$$\varepsilon_p = \varepsilon_0\left[1 - \frac{\omega_{pe}^2}{\omega(\omega - j\nu_m)}\right],$$ (2-14)

where ε_p is the plasma dielectric constant. For $\omega \gg \nu_m$, the plasma dielectric constant reduce to

$$\varepsilon_p = \varepsilon_0\left(1 - \frac{\omega_{pe}^2}{\omega^2}\right).$$ (2-15)

For $\omega > \omega_{pe}$, plasma dielectric constant is positive, and the electromagnetic wave can propagate at this frequency. If $\omega < \omega_p$, plasma dielectric constant is negative, and the electromagnetic wave cannot propagate inside the plasma. If $\omega = \omega_p$, ε_p is infinitely small, and oscillation happen inside the plasma. In this case, voltage drop on the plasma in reduced greatly.

2.1.7. Plasma sheath

The plasma should contain equal numbers of electrons and ions. Electrons are hotter than ions. More electrons reach the wall first, and the plasma has a positive potential to the wall. As a result, ions are accelerated to the wall, and electrons are expelled away from the wall. Between the plasma and the wall, a special non-neutral region is formed. This region is called plasma sheath. Inside the sheath, there are more ions than electrons, and electron flux and ion flux are balanced at the wall. From this mechanism, the wall potential to the plasma can be expressed by

$$V_p - V_w = \frac{kT_e}{e} \ln\left(\frac{MT_e}{mT_i}\right)^{1/2} , \qquad (2\text{-}16)$$

where $V_p - V_w$ is the wall potential, T_e is electron temperature, T_i is ion temperature, M is ion mass, m is electron mass.

Between the plasma body and the plasma there is neutral region called plasma presheath. It can be shown that ions at the starting point of sheath must have enough speed to reach the wall. This minimum speed can be expressed by

$$u_B = \left(\frac{kT_e}{M}\right)^{1/2} , \qquad (2\text{-}17)$$

where u_B is called Bohm Speed. This effect is called Bohm Sheath Criterion. Bohm Sheath Criterion is the evidence of the existence of plasma presheath. Through the presheath, there is a voltage drop, and ions are accelerated to get Bohm Speed. The voltage drop across the presheath is

$$\Phi_P = \frac{kT_e}{2e} . \qquad (2\text{-}18)$$

The ion density at the sheath edge (between the sheath and the presheath) can be calculated as

$$n_s \approx 0.61 n , \qquad (2\text{-}19)$$

where n_s is ion/electron density at the sheath edge, and n is electron/ion density inside the plasma.

If sheath voltage is larger compared to electron temperature, the case is different as above. The simplest high-voltage sheath model is the Matrix Sheath. In a Matrix Sheath, ion density and electron density are constant, and the sheath thickness can be expressed by

$$s = \lambda_D \left(\frac{2V_0}{T_e} \right)^{1/2},$$

(2-30)

where s is sheath thickness, λ_D is Debye Length, V_0 is sheath voltage, and T_e is electron temperature. Matrix Sheath is not a good model, since it does not consider the decrease in ion density as ions accelerate across the sheath. A better model is called Child Law Sheath. In this model, the constant ion current can be expressed by

$$J_0 = \frac{4}{9} \varepsilon_0 \left(\frac{2e}{M} \right)^{1/2} \frac{V_0^{3/2}}{s^2},$$

(2-31)

where V_0 is the sheath voltage, and s is the sheath thickness. The sheath thickness can be calculated as

$$s = \frac{\sqrt{2}}{3} \lambda_D \left(\frac{2V_0}{T_e} \right)^{3/4}.$$

(2-32)

2.1.8. Langmuir Probe

Langmuir Probe refers to a metal probe inserted into plasma and biased positively and negatively to collect a current. It is a very general and usefully tool to characterized plasma. The probe is surrounded by a plasma sheath. The size of probe is usually very small compared with dimension of the plasma, and the perturbation to plasma can be small if certain conditions are met. Langmuir Probe is usually used to measure electron density and electron temperature.

A typical current versus bias voltage curve is shown in Figure 2.2. When a large

negative bias voltage is applied, the probe collects mainly ions, and the current is ion

current. When a large positive bias voltage is applied, the probe current is electron

current. At a certain positive bias voltage Φ_f, the probe current is balanced by ion

current and electron current. This bias voltage is called floating potential. When the bias

voltage equals plasma potential Φ_p, the probe only collects electrons. Above plasma

potential, probe current tends to saturate.
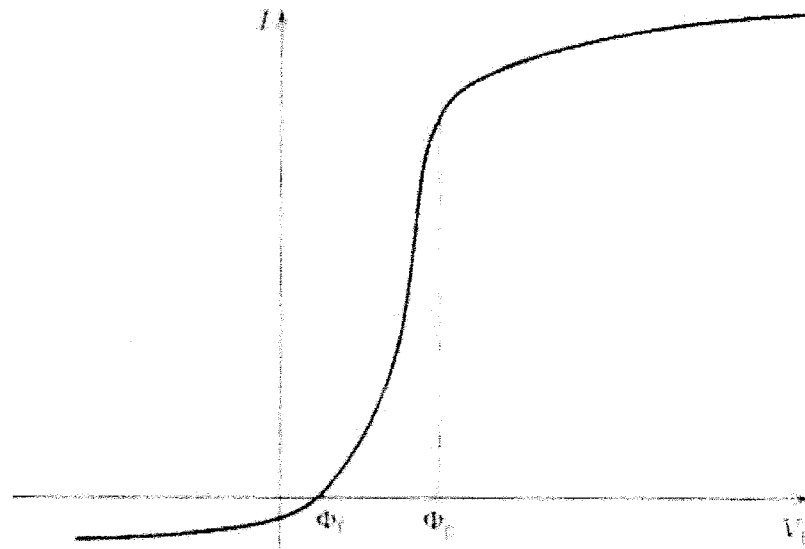
Figure 2.2. Typical I-V curve for Langmuir Probe [20].

When a planar probe is biased with a large negative voltage, the probe current is

ion current. It can be expressed by

$$I = -en_s u_B A,$$
(2-33)

where $u_B = \sqrt{\dfrac{kT_e}{M}}$ is the Bohn velocity, and $n_s = 0.6n$ is the plasma density at the sheath

boundary. For most low-pressure plasmas, electron temperature is at a few eV, and

plasma density can be estimated by above formulae. Electron temperature can also be measured by applying a positive bias a little bit lower than plasma potential. Applying Boltzmann's relation, we can get

$$\ln\left(\frac{I_e}{I_{esaturation}}\right) = \frac{V_B - \Phi_p}{T_e}.$$

(2-34)

By fitting the line, and we can get electron temperature T_e.

When the sheath thickness s is large, the condition probe area $A \gg s^2$ cannot be met, planar probes cannot be used. Under these conditions, a thin cylindrical wire probe can be used. The radius of the wire is much smaller than the sheath thickness s. The probe length d is much larger than the sheath thickness. With certain approximations, the probe current can be expressed by

$$I = 2en_s ad\left(\frac{2e|\Phi_p - V_B|}{m}\right)^{1/2}.$$

(2-35)

The calculation of plasma density from this formula is only semi-quantitative, since three conditions need to be met. The first condition is the collisionless sheath. It is right for low- pressure plasmas. The second condition is isotropic distribution function. Ions do not met this condition due to the Bohn velocity. The third condition is that low ion drift velocity compared to ion thermal velocity. This condition cannot be met at low pressure.

If there is no well-defined ground electrode in the plasma, double probes are usually used. A bias voltage is usually applied between two probes. The distance between the two probes must be much larger than the plasma sheath thickness. The current between the two same sized probes can be expressed by

$$I = I_i \tanh\left(\frac{V}{2T_e}\right), \qquad (2\text{-}36)$$

where I_i is the ion saturation current, and V is the voltage between the two probes.

Electron temperature T_e can be calculated through

$$\frac{dI}{dV}\bigg|_{V=0} = \frac{I_i}{T_e}. \qquad (2\text{-}37)$$

With electron temperature available, it is easy to calculate plasma density from the ion

saturation current.

2.2. High-pressure plasmas and their characterizations

2.2.1. Low –pressure plasmas

Low-pressure plasmas refer to the plasmas generated in vacuum where the pressure ranges from 1 millitorr to 1 torr. The density of low-pressure plasma is from $10^8 cm^{-3}$ to $10^{13} cm^{-3}$. The electron temperature is usually from 1eV to 10eV. Electrons are much smaller than ions, and the mean free path length of electrons is much larger than that of ions. The ion temperature is much lower than the electron temperature. Low-pressure plasmas are usually operated in normal glow discharge region where the applied voltage is constant or slightly decrease with increasing current.

Low-pressure plasmas have several advantages. First, it is easy to generate low-pressure plasmas due to the relatively low breakdown voltages (less than 1kV). Second, the plasmas are stable in a large operation region. Third, the plasmas are cold, and neutral temperature can be lower than $150^{\circ}C$. Fourth, plasma densities are high enough for material processing. Fifth, a large volume of uniform low-pressure plasma can be generated. Due to these advantages, low-pressure plasmas have wide applications in material processing and semiconductor industry, such as deposition and etching.

Low-pressure plasmas have several drawbacks. First, vacuum systems are needed to generate the plasma. Vacuum systems are expensive and maintenance is needed. Second, load systems are needed to place the materials into the vacuum chamber. Third, the dimension of the materials is limited by the size of the vacuum chamber. In order to overcome these shortcomings, air-pressure plasmas are highly desired.

2.2.2. High-pressure plasmas

Generally, it is very hard to generate high-pressure plasmas due to the high breakdown voltages. Different kinds of high-pressure plasmas have been generated in different ways. Transferred arcs were used to cut and melt solids [22-26], but they are hot plasmas, and the neutral temperature can reach 10^4k. Plasma torches are similar as transferred arcs, and they are used to spray materials onto the substrate [22, 27-29]. The breakdown voltages of transferred arcs and plasma torches are above 10kV. The generation and applications of a cold plasma torch have been reported [30-37], but the size of the torch was too small. Corona is a nonuniform discharge generated around a point tip, such as between a sharp electrode and a plate electrode. The ions density inside a corona ranges from 10^9cm^{-3} to 10^{13}cm^{-3}[38, 39], but the size of a corona is small (such as 1mm), and its applications are limited. The breakdown voltage of a corona is above 10kV. Dielectric barrier discharge can be operated in air pressure. It has been used in surface cleaning [40] and plasma-assisted CVD [41]. Since it is not uniform (randomly distributed micro arcs), its applications of deposition and etching are limited to cases where the surfaces do not need to be smooth. An array of micro-hollow cathode discharge was used as cathodes of a discharge [42]. This discharge was operated at DC mode in high gas pressure, but the neutral temperature was high (above 2000°C). Capillary-plasma-electrode discharge can also be operated with high gas pressure [43], but apparently this discharge is not uniform. In brief, to generate a large volume of uniform plasma at high-pressure is extremely challenging.

One main problem of high-pressure plasma is its stability, or how to prevent the glow discharge from transferring to arc. An arc refers to equilibrium plasma, whose

neutral temperature equals its electron temperature. Plasma instabilities can be divided into electronic and thermal instabilities. In electronic instabilities, a change in the electron energy distribution and subsequent change in the number of excited states, leads to an increment in the ionization rate and positive feedback on the electron temperature distribution. Thermal instabilities are associated with the heating of neutrals. When the neutrals are heated, the number of neutrals in the ground state decreases, and electron distribution shifts to higher energy. This effect increases the ionization rate and current density, and also generates a positive feedback on the heating of neutrals.

The glow-to-arc transition limits the intensity of high-pressure plasmas and the operations with high input power. Several ways have been proposed to overcome this problem. One basic way is to operate the plasma in pulsed mode. The second way is to separate the cathode into sections each connected to the power supply through a large resistor [44]. The third way is use a plasma cathode [45-47]. The mechanism behind the second and the third methods is to dampen the perturbations in cathode boundary region. The combination of these three methods can be used to generate large volume plasmas at high gas pressure.

2.2.3. Characterization mechanisms for high-pressure plasmas

2.2.3.1. Absorption Spectroscopy

When a light beam passes a plasma body, some of the photons may be absorbed by the species inside the plasma, and the intensity of the light beam decreases (Figure 2.3). The decrement of the light intensity can be described by

$$I = I_0 \exp(-n\sigma z),\qquad\qquad (2\text{-}38)$$

where I_0 is the original light intensity (without plasma), and I is the light intensity after the light beam passes the plasma, and n is the density of the effective species, and σ is the absorption cross section of the effective species, and z is the light beam's path length inside the plasma. Generally, I_0 and I can be measured, and σ can be found in references, and z can be easily determined, and the density of the effective species can be calculated.

Absorption Spectroscopy is theoretically good, but it is not widely used because of its limitations. In the experiment, the wavelength of the light source must be properly selected for different species inside the plasma. A tunable laser is a good choice of the light source, and special lamps can also be used. The main disadvantage of absorption spectroscopy is its low sensitivity. In order to improve the sensitivity, high-density light source is needed, and experiment result is only good for species with large absorption cross sections at the chosen wavelength.
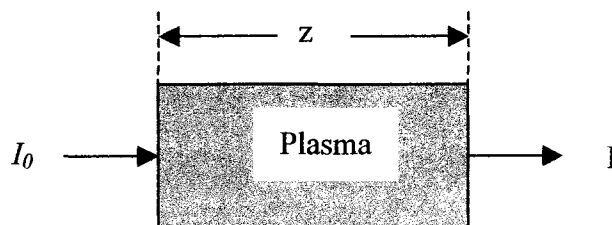
Figure 2.3. Schematic show of Absorption Spectroscopy.

2.2.3.2. Cavity Ring-down Spectroscopy (CRDS) [48]

The main problem of Laser Absorption Spectroscopy is its low sensitivity. It is not effective to measure weak absorptions due to the possible fluctuations of the laser intensity. In order to improve the low sensitivity of Laser Absorption Spectroscopy, Cavity Ring-down Spectroscopy was proposed. This method, which is insensitive to the laser intensity fluctuation, has become an ultra-sensitive, quantitative absorption measurement.

Cavity Ring-down Spectroscopy is a modified Laser Absorption Spectroscopy. The main idea of CRDS is to increase the path length of the laser beam inside the plasma. The schematic experimental setup is shown in the flowing Figure 2.4. The fundamental components are a tunable laser source, two highly reflective (reflectivity above 99.9%) concave mirrors, a photo- sensitive detector and the data processing equipment.

When a laser pulse enters the cavity, it will reflected back and forth, and its intensity will decrease due to the absorption inside the cavity and the transmission by the two mirrors. The laser pulse intensity is reduced by a certain proportion on each round trip, and the detector monitors the exponential decay of the laser pulse. An ideal detector can see a series of pulses with the decay envelope, and a practical detector and data processing equipment will see the envelope due the lose of the high frequency components. The change of the laser pulse intensity with time can be described by

$$I(t) = I_0 \exp\left(-\frac{t}{\tau_0} - n\sigma c t \right),$$
(2-39)

where τ_0 is the laser pulse decay time constant without the plasma, and n is the density of the absorption species, and σ is the absorption cross section, and c is the light speed,

and t is time. The measurements need to be conducted with and without the plasma, and the decay constants with and without the presence of the plasma can be used to calculate the density of the absorption species inside the plasma.

CRDS has several drawbacks. First, as general Absorption Spectroscopy, it is not absolutely species-selective, and all absorption species are counted. Second, the reflectivity must keep constant for a long time, and the spectrum range for the two mirrors is typically limited within 50nm. Third, it cannot measure the spatial distribution.

CRDS can also be operated in continuous mode, and the technique was patented. Pulsed CRDS was widely used in research. Commercial products in continuous mode are available from a few pioneer companies.
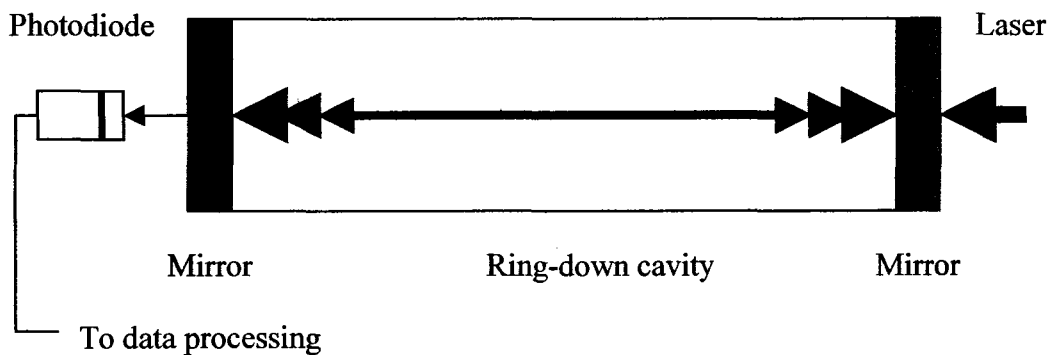
Figure 2.4. Schematic show of Ring-down Spectroscopy.

2.2.3.3. Motional Stark Effect [49]

Motional Stark Effect is used to measure the magnetic field in hot plasmas. In high-temperature plasmas, any probe will be destroyed by the high temperature, and non-intrusive measurement is needed. Motional Stark effect is based on Stark Effect and basic electrodynamics. Stark effect refers to the splitting and shifting of atom energy levels due to the existence of an external electric field. In the experiment, an atom beam with tens keV energy enter the plasma. According to electrodynamics, the magnetic field inside the plasma is transformed into a magnetic field and an electric field in the moving atom reference frame. The presence of the electric field in the moving reference frame leads to Stark Effect. As the atoms moving inside the plasma, collisions with ions and electrons excite some ground state electrons in the moving atoms, and the excitations result in the emission of radiations. Stark Effect polarizes the emitted electromagnetic field along the direction of the electric field, or the direction perpendicular to the direction of the magnetic field. By measuring the polarization of the radiation, information on the direction of the magnetic field can be determined.

2.2.3.4. Laser Induced Fluorescence (LIF)

Laser-induced fluorescence (LIF) refers to the optical emission from species that have been excited to higher energy levels by absorption of laser energy. The excited species relaxes from higher energy level to lower levels, which are higher than the ground state. The fluorescence wavelengths, which are longer than the laser wavelength, are the fingerprint of the effective species. Compared with Absorption Spectroscopy, LIF can achieve much higher sensitivity due to the very weak background at the fluorescence wavelength.

In the experimental set up, a laser shines at the plasma, and the resultant fluorescence is picked up by a detector. The generation of LIF is limited by the fluorescence quantum yield, and the detection of LIF is restrained by the quantum efficiency of the photomultiplier tube. Laser wavelength is generally restricted to UV and visible range, and at longer excitation wavelength, the fluorescence yield is low. LIF can give quantitative and qualitative results. In quantitative analysis, calibration is needed. If a tunable laser is used, and the line width of the exciting laser is substantially narrower than the thermal Doppler shift of the plasma ions, scanning the dye laser wavelength maps out the ion velocity distribution $f(x,v,t)$ for the effective species.

2.2.3.5. Infrared and microwave interferometer

Microwave and infrared light beam can be used to diagnostic plasmas, especially for hot plasmas. While traveling through the plasma, an electromagnetic wave interacts with the plasma, and the properties of the plasma may be found by detecting the transmitted wave. The presence of the electromagnetic wave should not perturb the plasma, and the weak interaction of the wave and the plasma can be used to detect the plasma.

Infrared and microwave interferometer is an important tool to measure the electron density inside the plasma. The plasma electron frequency must be lower then the microwave or the infrared laser frequency to guarantee that the electromagnetic wave can propagate inside the plasma. The fundamental mechanism is that the phase shift of the electromagnetic wave is proportional to the average electron density on the propagation path of the EM wave inside the plasma. In the instrument, one EM beam is separated into two beams. One beam travels through high vacuum or the air, and another beams travels

through the plasma. By comparing the phase shifts of the two beams, the electron density can be determined. The interference of the two waves has two modes: homodyne and heterodyne. In homodyne mode, the two waves interfere directly. In heterodyne mode, one wave is phase modulated. Homodyne mode has at least two drawbacks. First, it is sensitive to the amplitude instability of the two waves. Second, it is impossible to decide the sign of the phase shift difference between the two waves. In heterodyne mode, the phase shift difference can be calculated conveniently. The phase modulation can be realized through a moving mirror or a rotating grating. In these two ways, phase modulation is realized through Doppler effect. Two finely tuned lasers can also be used in heterodyne mode. The main disadvantage of the interferometer is its high cost.

2.2.3.6. Thomson Scattering

Thomson Scattering refers to the scattering of an electromagnetic wave by the plasma. It is a non-destructive method to measure the plasma. It has the potential to give detailed information on electrons and even ions. These two advantages offset the drawback that the measurements are very hard to perform.

Thomson Scattering can be described in a classical way. When an incident electromagnet wave reaches a charged particle, the charged particle is accelerated, and emits electromagnetic waves. The emitted electromagnetic wave is the scattered wave. Since ions are much heavier than electrons, the acceleration and the scattering of ions are much weaker than those of electrons. But this does not mean that ion scattering is always negligible compared with electron scattering. If the product of the wave vector and the Debye length is less than one, the scattering from an electron and the scatterings from its shielding electrons are canceled, and ion scattering is the main contribution for Thomson

scattering. This kind of scattering is called coherent scattering. In incoherent Thomson Scattering, the product of the wave vector and the Debye length is much larger than one, and electrons scattering is the main contribution.

In the experiment, only a very small fraction of scattered photons are generated. In order to improve the signal intensity, an intense pulsed laser is usually used. Some baffles are needed to reduce the intensity of stray light. The frequency of the scattered light is different from the frequency of the incident light due to the Doppler effect, and this is good for the signal detection. In incoherent Thomson Scattering, the signal intensity reflects the electron density, and the line shape of the scattered light reflects the electron temperature. In coherent Thomson Scattering, the information of ions can be obtained.

2.3. Plasma surface modification of polymers

2.3.1. Adhesion mechanism [50, 51]

The purpose of polymer surface modification is to improve the surface adhesion. Adhesion can be defined in two ways. In physical chemistry, it refers to the attraction between a solid and a liquid [52]. In this way adhesion is measured as the contact angle of a liquid drop on a solid surface. In technology, adhesion refers to the resistance to the separation of two joined material surfaces [53], such as the breaking force and the breaking stress. In the first definition, the quality of the adhesion is not emphasized. While by the second definition, the joint surfaces will be destroyed if one wants to measure the adhesion property.

Several theories have proposed to explain the mechanisms of adhesion [1, 50, 51]. They are the adsorption theory, the mechanical hooking theory, the electrostatic theory, the rheological theory, and the diffusion theory. Every theory has its owner advantages and shortcomings. They are summarized in the following:

The first theory is called adsorption theory. It emphasizes the roles of physisorption and chemisorption. In this theory, the strength of the adhesion is mainly determined by the interface force, and good adhesion comes from covalence bonds or some polar groups, and also, weak interface forces lead to poor adhesion. One shortcoming of this theory is that it cannot explain how mechanical parameters, such as stress and deformation, influence the adhesion strength.

The second theory of adhesion is the mechanical interlocking or hooking theory. It emphasized the function of micro-geometry. By this theory, rough surfaces produce more contact area and possible strong interlocking between two surfaces, and therefore

good adhesion. This theory works well for some cases, but it is too rough, and it cannot explain the strength adhesion between two smooth surfaces.

An electrostatic theory of Deryagin [54] can also be used to describe the adhesion phenomenon. This theory is based on the contact charging effect, in which the adhesion junction acts as a charged capacitor when two different materials are joined. By this theory, the strength of adhesion is determined by the electrical charge distribution. This theory has also been criticized. First, the electrical phenomenon was observed during the breaking process of a joint, and a breaking joint is different from an adhesion joint. So this theory should be use to explain the breaking process, not an adhesion phenomenon. Second, this theory cannot explain that two conductive materials can adhere each other well.

The fourth adhesion theory is called diffusion theory. Voyutskii and co-workers [55] measured the breaking strengths of adhesive joints, and their results were similar to what should be expected by diffusion theory. According to this theory, the adhesion strength is determined by the diffusion and mixture of different materials at the joint. This theory cannot explain the good adhesion between a hard material, such as a metal, and a relatively soft polymer.

The fifth adhesion theory is the rheological theory by Bikerman [56]. By this theory, the adhesion strength is determined by the mechanical properties of the materials at the joints, and the local stress inside the joint. Also by this theory, interfacial forces, which appear in breaking process, cannot account for the adhesion performance. This theory does not consider the function of interface forces across the joints.

The last adhesion theory is called interphase (not interface) theory. An interphase is the region between two contacting solids, and its composition, structure and properties are different from the two contacting solid phases. L. H. Sharpe summarized some early evidences supporting the existence of the interphase [50]. A good schematic diagram with an interphase was given by M. R. Wertherimer [2]. E. M. Liston also gave a similar schematic show [1]. The interphase between a polymer layer and another solid layer determines the adhesion strength of the two solid layers, and the stability of the adhesion. In such cases, the interphase includes a crosslinking layer and a covalent bonding layer. The covalent bonding layer catches the solid layer for the polymer layer. The underlying crosslinking layer improves the polymer surface strength, prevents agents inside the bulk polymer from diffusing into the interface, therefore, keep the bonding stable. The interphase theory has been widely accepted.

2.3.2. Contact angle

When a water drop is placed on a flat polymer surface, contact angle is used to describe the shape of the water bead (Figure 2.5). Contact angle is the angle between the tangential line of the water surface and the polymer surface. Surface energy refers to the interfacial tension between a solid and vapor (or air). Surface energy and contact angle are related by Young's Equation, which is expressed by

$$\gamma_{SV} - \gamma_{SL} = \gamma_{LV} \cos\theta, \qquad (2\text{-}40)$$

where γ_{SV} is the interfacial tension between the solid (polymer) and vapor (air), γ_{SL} is the interfacial tension between the solid (polymer) and the liquid (water), γ_{LV} is the interfacial tension between the liquid (water) and the vapor (air) (γ_S is the balance force due to the deformation of the solid (polymer)), and θ is the contact angle.

Contact angle can be measured by a goniometer. The surface tension of a liquid (water) can be determined easily, or can be found in books. The surface tension of a solid (polymer) and the interfacial tension between the solid (polymer) and the liquid (water) are unknown. To solve this problem, five models have been used to calculate the surface tension of the polymer and the interfacial tension between the polymer and water. The details of the five models are beyond the scope of this dissertation. It is well know that larger polymer surface energy insults in smaller contact angle. Therefore, contact angle is widely used to describe polymer surface energy.
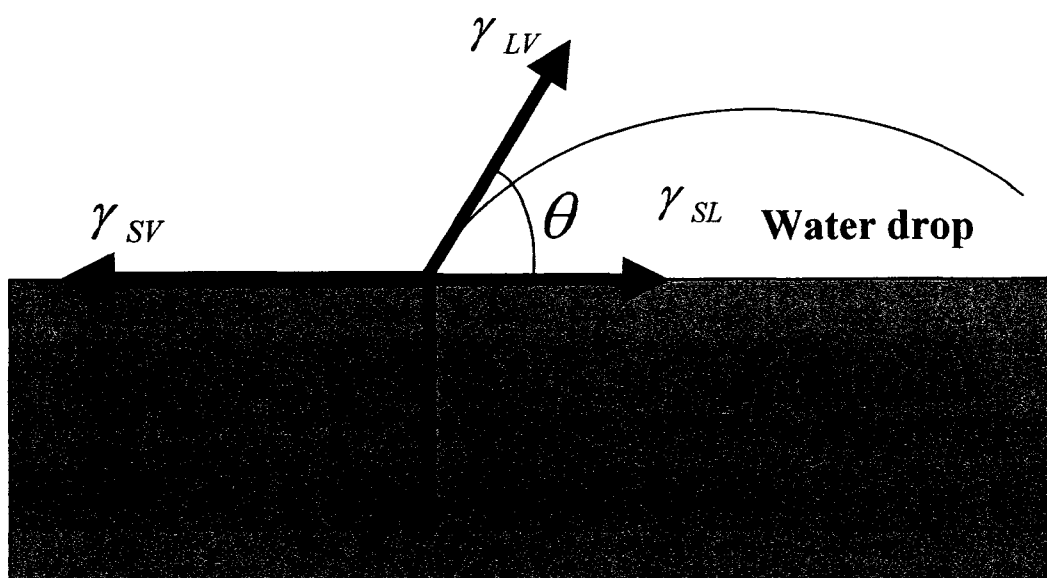
Figure 2.5. A water contact angle on a polymer surface.

2.3.3. Plasma and polymer surface interactions [1,2]

Besides neutrals, plasma has many species, such as electrons, ions, radicals, and photons. Ions are much heavier compared with electrons, and most of them are positively charged. Since the total electrical charges from electrons and ions are always balanced, the density of electrons and positive ions are roughly equal. Most of each species are at their ground states. But some of them are excited, and when they relax photons are generated. The optical emission powers differ from plasma to plasma. The density of radicals can be very high, several orders higher (such as 10^5) than electron density. Some of the radicals may be active.

When a sample is placed inside plasma, the case can be quite different from the situation in which only neutral gases and the sample exit. There are many kinds of reactions at a solid surface submerged in plasma. The first kind is surface neutralization, such as a positive ion at a surface is neutralized by an electron. The second kind is adsorption, including physical (bonding energy less than 1 eV) and chemical surface adsorption. The third kind is fragmentation due to the impact of high-energy ions and neutrals. The forth kind is sputtering, which is due to the floating potential or an applied bias. The fifth is pure chemical reactions, in which active radicals may play import roles. The sixth kind is the reaction of two adsorbed species. The seventh kind is reaction of adsorbed with an impinging gas molecule.

Plasma surface reactions are the competitions of formations and destructions. Formations mean new materials are generated at the surface, and usually refer to depositions and surface modifications. Destructions refer to the etching effect, or the

formation of gas product from the surface. If a solid sample is place inside plasma for a certain long duration, either deposition or etching effect may be distinguished.

Inside the plasma, energetic particles and photons are generated. During the plasma treatment of a polymer surface, these particles and photons interact intensively with the polymer surface. In the case without thin film deposition, these interactions usually lead to four major effects, and they are: surface cleaning, ablation or etching, cross-linking or branching, modification of surface chemical structures. These four major effects are discussed below.

Surface cleaning refers to the removal of contaminations from polymer surfaces. This effect is mainly due to the ion bombardment onto the surfaces. Generally, any cleaning process leaves a layer of organic contaminations, and any clean surface will also acquire a layer of contamination when it is exposed to air. These contaminations may lead to poor adhesive properties of the polymer surface. Most polymers have some additive or contaminations added intentionally into the polymer to improve its properties. These additives always like to diffuse onto the polymer surface from polymer bulk. These additives often have similar chemical compositions as the bulk polymer, and it is hard to detect them by most analysis measurements. To clean these additives and contaminations is a major task of plasma surface modification.

The second effect on plasma surface modification of polymer surfaces is the ablation. Ablation refers to the etching of polymer surfaces. Ablation removes a large amount of materials from the surface compared with surface cleaning. It can clean a heavily contaminated surface, remove weakly bonded lays on a polymer surface, and improve the adhesion strength of the surface. Amorphous polymer structures are much

easier to be ablated than crystal structures and inorganic filler materials. An uneven surface morphology is generated by ablation, since more amorphous materials have been removed from some regions. This surface structure may improve mechanical hooking, and increase the surface area for chemical interactions at the polymer surface, and hence, improve the surface adhesion

The third effect of plasma and polymer surface interaction is cross-linking. It happens when polymers are exposed to inert gas plasmas. After the treatment, new free radicals are generated at the surface layers, but no new chemical components come from the gas phase. Ion bombardment and ultraviolet photons can break C-C and C-H bonds, and free radicals are generated. These free radicals can react with other radicals at the surface, or with other chains. These reactions tend to make polymer surface more stable. If polymer chains are flexible, these surface reactions may lead to recombination, unsaturation, branching, or cross-linking. Cross-linking can increase the surface bond strength and surface stability, and improve surface adhesion.

The most important effect by plasma modification is the surface chemical structure changes. Some functionalities can be added into the surface layer, and they can interact with adhesives and materials deposited onto the polymer surface. These chemical changes happen only at the surface layer, and the bulk polymer remains unchanged.

2.3.4. Ultraviolet photochemistry

The most popular theory on plasma surface modification mechanism is the ultraviolet photochemistry. According to this theory, the UV radiation from a plasma source can break chemical bonds at a polymer surface and in its surrounding gases, and then these broken bonds lead to a series of chemical reactions at the surface layers.

During these chemical reactions, other elements from the surrounding gas can incorporate into the surface layers. The reason why UV photons are needed is that they have enough energy to break certain chemical bonds.

Many experiments support the ultraviolet photochemistry theory. Hiroyuki Niino and coworkers used an ArF excimer laser (193nm) to modify a PTFE surface in the air [57]. They found that the water contact angle reduced 100 degrees and that Nitrogen in the air was incorporated into the surface layers. Polymer surface modification by UV laser is a powerful proof for the photochemistry theory. Heitz used UV excimer lamps to modify PTFE samples in an ammonia atmosphere [58]. He also found reduced contact angles. The photochemical reactions let nitrogen, oxygen, and hydrogen enter the surface layer. Beil used excimer lasers and excimer lamps to modify polybutyleneterephthalate (PBT) in the air [59]. After the modification, metal films were selectively deposited on the PBT surfaces with improved bonding. Callen used a mercury vapor lamp to modify polystyrene [60], and the modification effect is very stable. Hollander used the UV light from a plasma source to modify polyethylene surrounded by oxygen [61]. He found that the restriction factor in the experiment is the UV radiation intensity, not the oxygen concentration.

There are several restrictions for the UV photochemical reactions to happen on polymer surfaces. Not all UV light is capable of breaking chemical bonds at polymer surfaces. Generally, UV light with wavelength less than 180nm has photons with enough energy to generate rapid photochemical reactions. Second, the polymer material must have a large absorption coefficient or a small absorption depth. In other wards, the polymer must be black to the UV light.

The next problem for plasma surface modification of polymers is the big difference between pure plasma and real plasma. The pure plasma refers to the plasma source without any polymer samples. The UV spectra are usually measured from this kind of pure plasma. The real plasma refers to the plasma source with polymers sample inside. The modification process always contaminates the plasma source, and changes its emission spectrum and even the modification effects. This contamination to the plasma source must be considered.

2.3.5. Ion bombardment

Inside the plasma, there are a large number of particles, including electrons, ions, and neutrals. Some of these particles have enough energy to break chemical bonds on polymer surfaces, and then initiate a series of chemical reactions. This is the other mechanism for plasma surface modification of polymer surfaces. Ion beams with energy of a few hundred eV to a few thousand eV have been used to modify polymer surfaces [4-8]. All the results were promising. Therefore, ions with proper energy have the potential for surface modification. But most ions inside the plasma usually do not have such high energy. But ion energy has its distribution inside the plasma, and a small percentage of ions have relative high energy to generate the modification effects. Ions inside plasma also have the ability of surface cleaning, which is a major aspect of surface modification.

In some cases, ion dose can be the main factor in polymer surface modification. Groning's experiment is a good example [62, 63]. In the experiment, for the same sample and the same plasma, different ions dose generated different modification effect. For the

same sample and the same ion dose, even with different plasmas, the modification effects

are the same.

Chapter III

An atmospheric-pressure helium plasma source

3.1. Plasma source generation

3.1.1. Electronic structure of the plasma source

The structure of the atmospheric plasma jet is very simple, and no vacuum is needed. The plasma is generated through a capacitive RF discharge. A 13.56 MHz RF voltage is applied to a couple of electrodes, and helium gas flows between the two electrodes. The RF power supply is Advanced Energy's RFII 1250 Generator. Its maximum output power is 1250 W, and the highest reflected power is 250 W. The gas between the two electrodes is at air pressure. The two electrodes are separated by two pieces of dielectric materials. The RF power ignites and sustains the discharge. The currents through the discharge body lead to ohmic heating, while the sheath voltage leads to sheath heating through electron reflection.

The RF signals from the RF power supply cannot be added directly to the two electrodes of the plasma jet. A tuner is needed to match the capacitance of the plasma jet to the output impedance of the RF power supply, which is 50 ohms [64, 65]. The tuner is Advanced Energy's AZX10. The schematic structure of the tuner is shown in Figure 3.1. In this Figure, R is the output impedance (50 ohms) of the RF power supply, C1 is the shunt capacitor, C2 is the series capacitor, L is an inductor, and the load is our plasma. By adjusting the two capacitors inside the tuner, the equivalent impedance at the tuner input end can match the RF power supply's output impedance. This mechanism can be expressed by

$$\frac{\left(\dfrac{1}{j\omega C_1}\right)\left(j\omega L + \dfrac{1}{j\omega C_2} + Z\right)}{\left(\dfrac{1}{j\omega C_1}\right) + \left(j\omega L + \dfrac{1}{j\omega C_2} + Z\right)} = R.$$
<div style="text-align:right">(3-1)</div>

The tuner cannot match any load to the RF power supply. The tuning region of the tuner is shown in Figure 3.2. The capacitance of the plasma jet was calculated as 44 PF, which is equivalent to an impedance of −j270 ohms. This impedance is not within the tunable region. When the plasma is ignited, it cannot be considered as a pure capacitor, and it is equivalent to a capacitor and a resistor. As a result, the imaginary part of the total equivalent impedance will be smaller than −j270 (such as −j400). In order to move the impedance at the tuner's output into the middle of the tunable region, a 470 PF parallel capacitor was added.
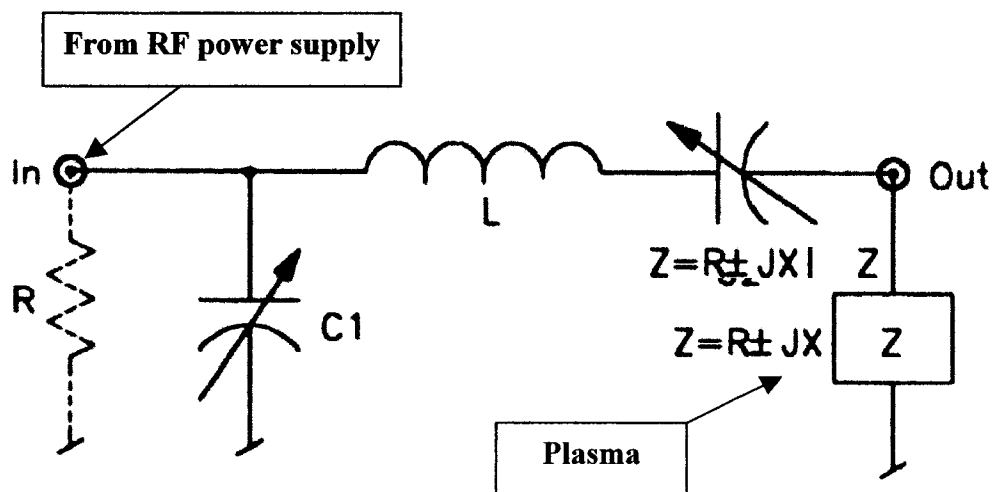
Figure 3.1. Schematic structure of a tuner [65].
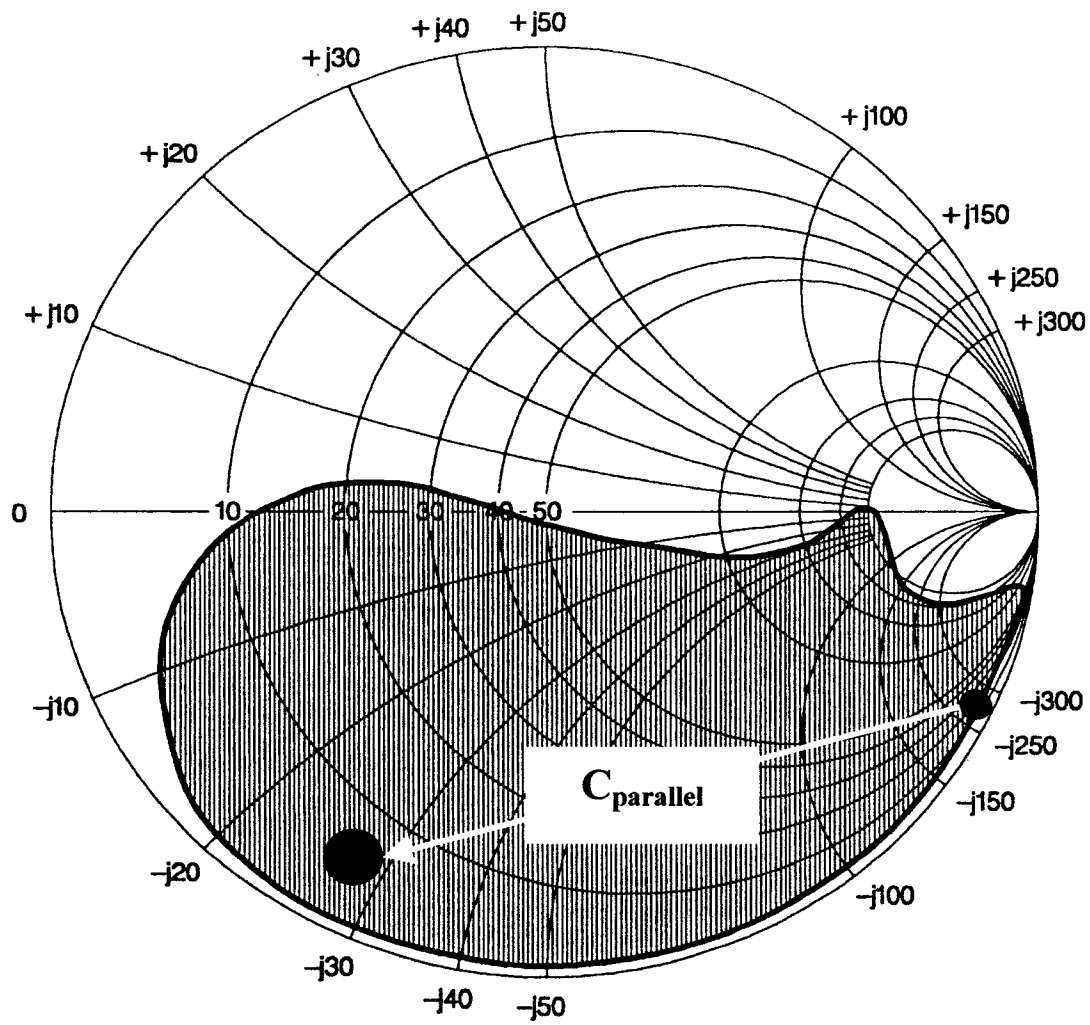
Figure 3.2. Smith Chart for the tunable range for a standard AZX 10 tuner [65]. The two black ovals represent the characteristic impedance with and without the parallel capacitor.

3.1.2. Physical structure of the plasma source

The plasma consists two electrodes, two quartz slices, one ceramic manifold, gas pipes, cooling water pipes, and the holder. The structure of the plasma jet is shown in Figure 3.3 to Figure 3.5. The two electrodes are made of aluminum, and each has an area of 10 cm by 10 cm. The ground electrode is about one inch thick, and is cooled by circulating water. Another electrode is 3.0 mm thick, and it is not cooled. The two electrodes are separated by two quartz slides. The dimension of each quartz slice is 10cm by 1.0 cm by 1.50 mm. The two electrodes and the two slices are hold together by four clamps. The two electrodes with the two slides are installed onto a ceramic manifold. On the top of the manifold, there are seven small holes with a diameter of 0.15 mm. Gases enter the manifold through a pipe and flow out of the manifold through the small holes, and then enter the space between the two electrodes, and finally flow out of the plasma jet into air. The plasma is full of the space surrounded by the two aluminum electrodes and the two quartz slides. The setup of the plasma source is similar to the one described by Park et. al. [66-69].
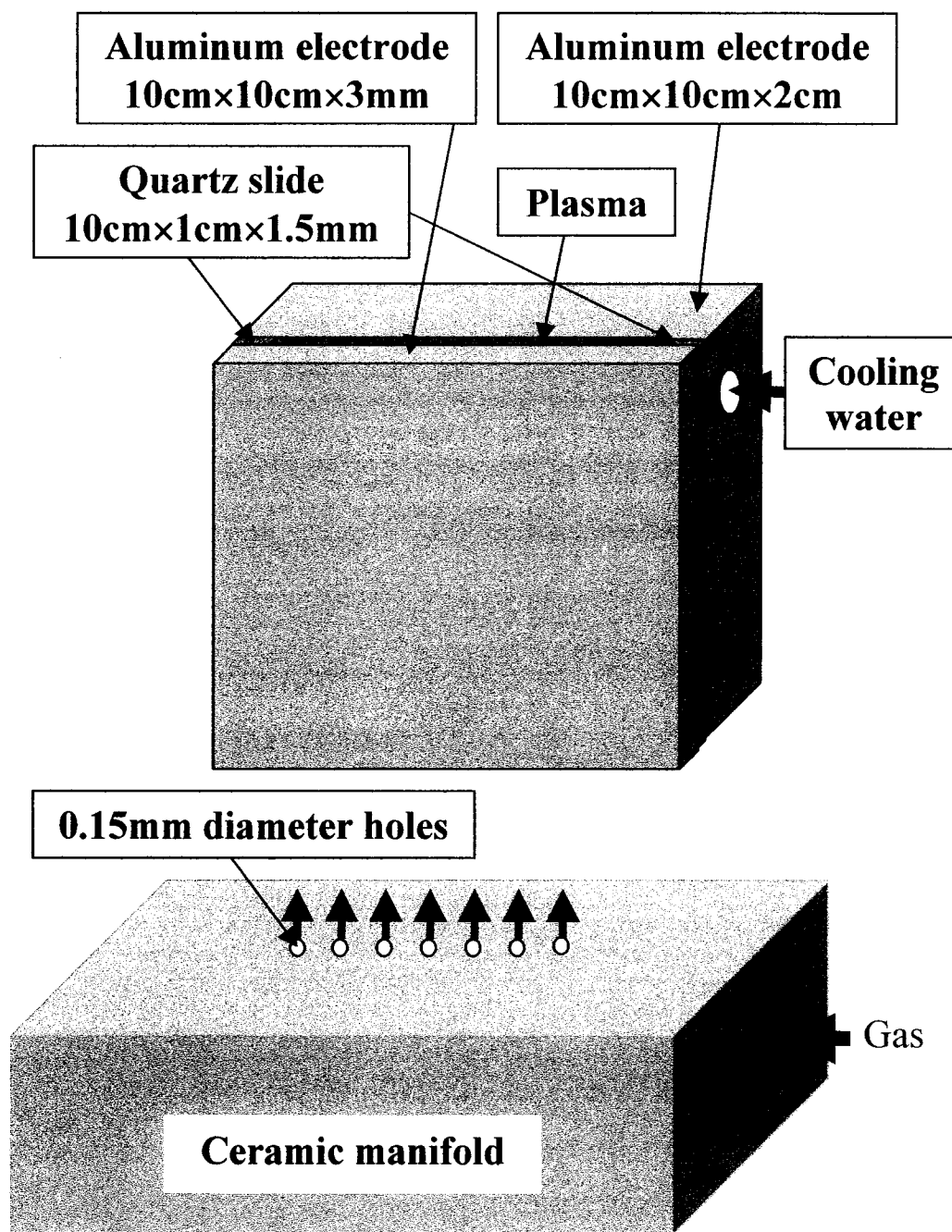
Figure 3.3. Schematic show of the structure of the plasma jet. The ceramic manifold is separated from the rest parts in the figure.
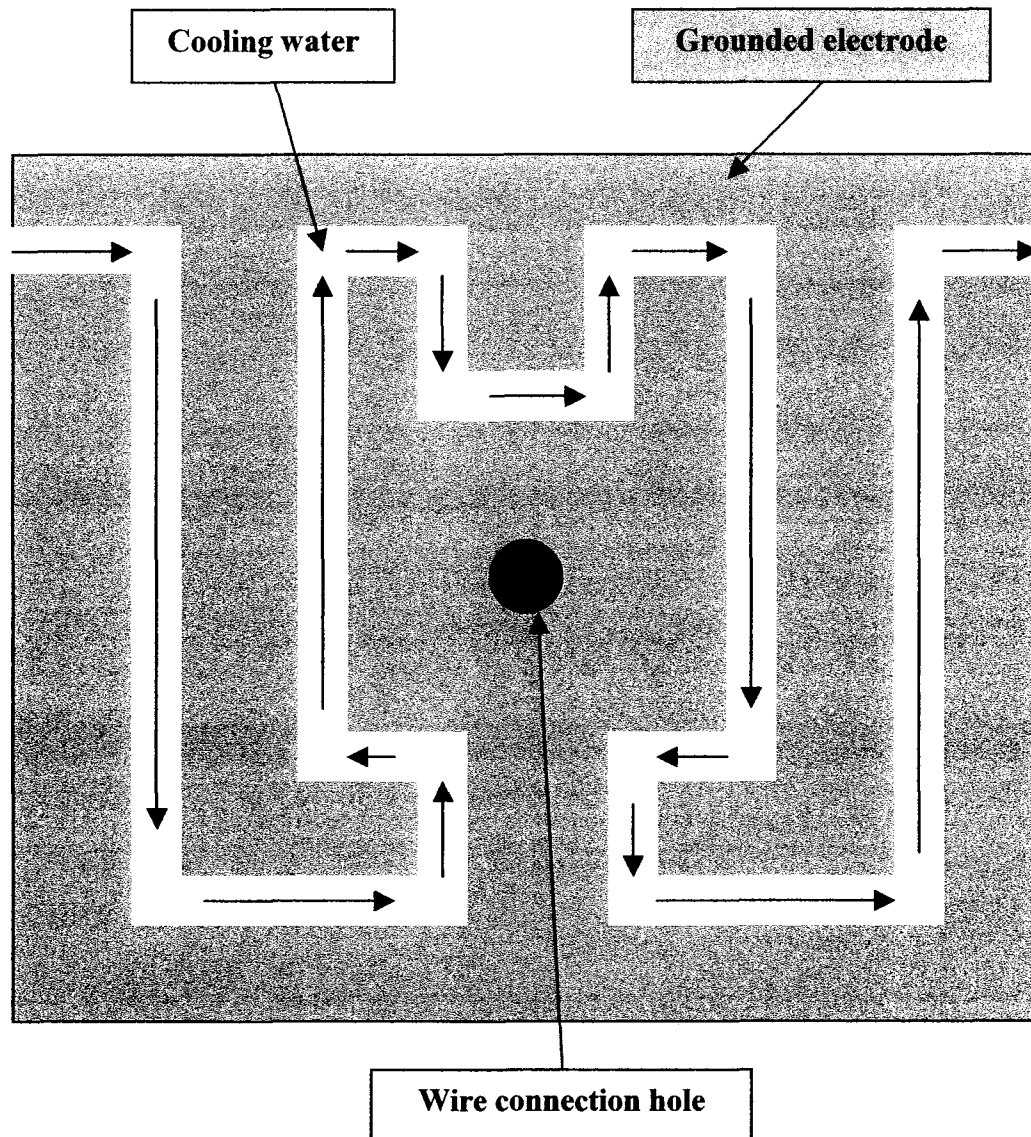
Figure 3.4. Schematic show of the cooling water flow.
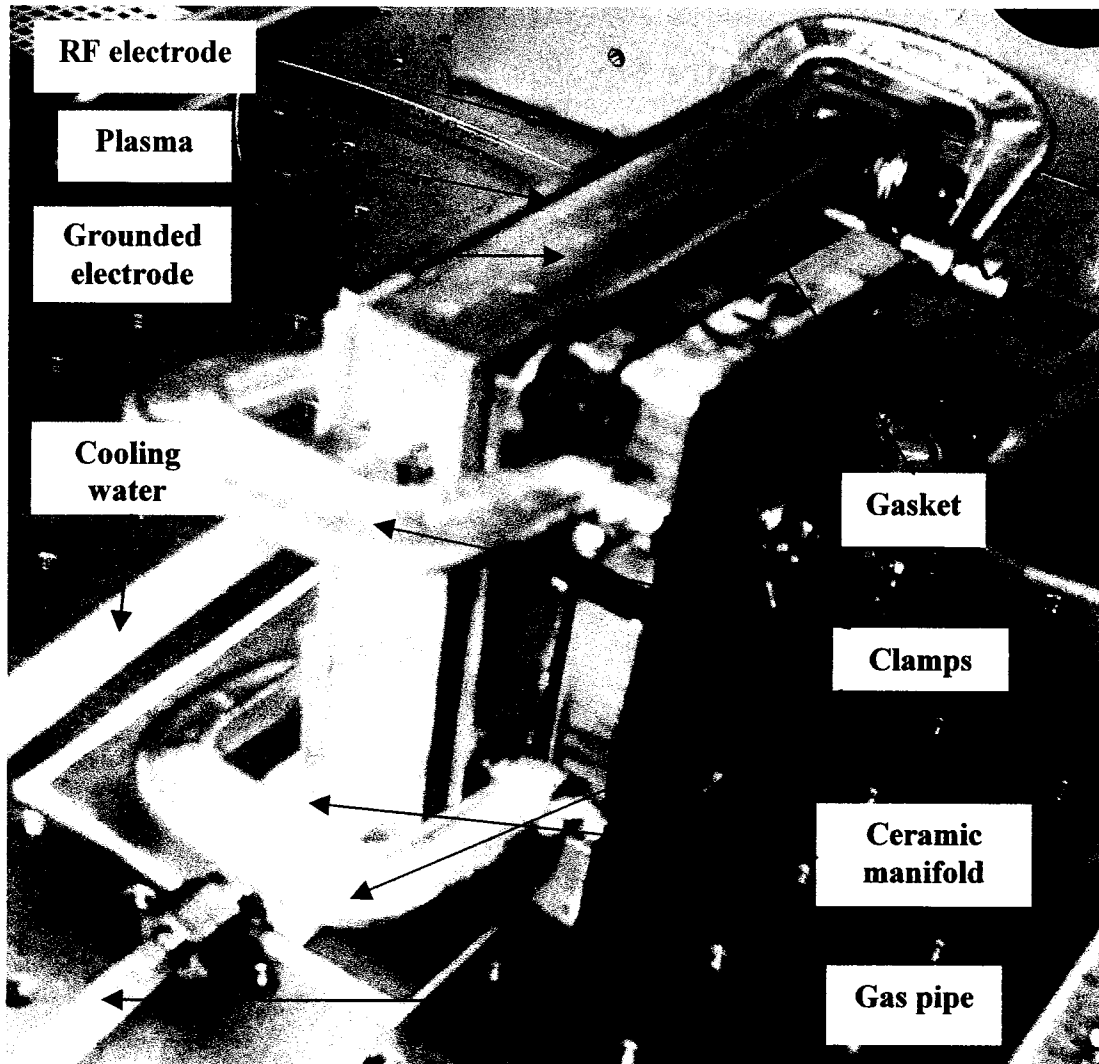
Figure 3.5. The picture of the plasma jet.

The structure of the gas pipelines is shown in Figure 3.6. In the Figure, helium and oxygen are used. They flow along the two separate pipelines, then mix, and finally enter the plasma jet. The three purge valves are used to purge the pipelines before the experiment. The two flow meters are used to measure the flow rates of the two gases. The two metering valves are used to control the flow rates of the two gases.
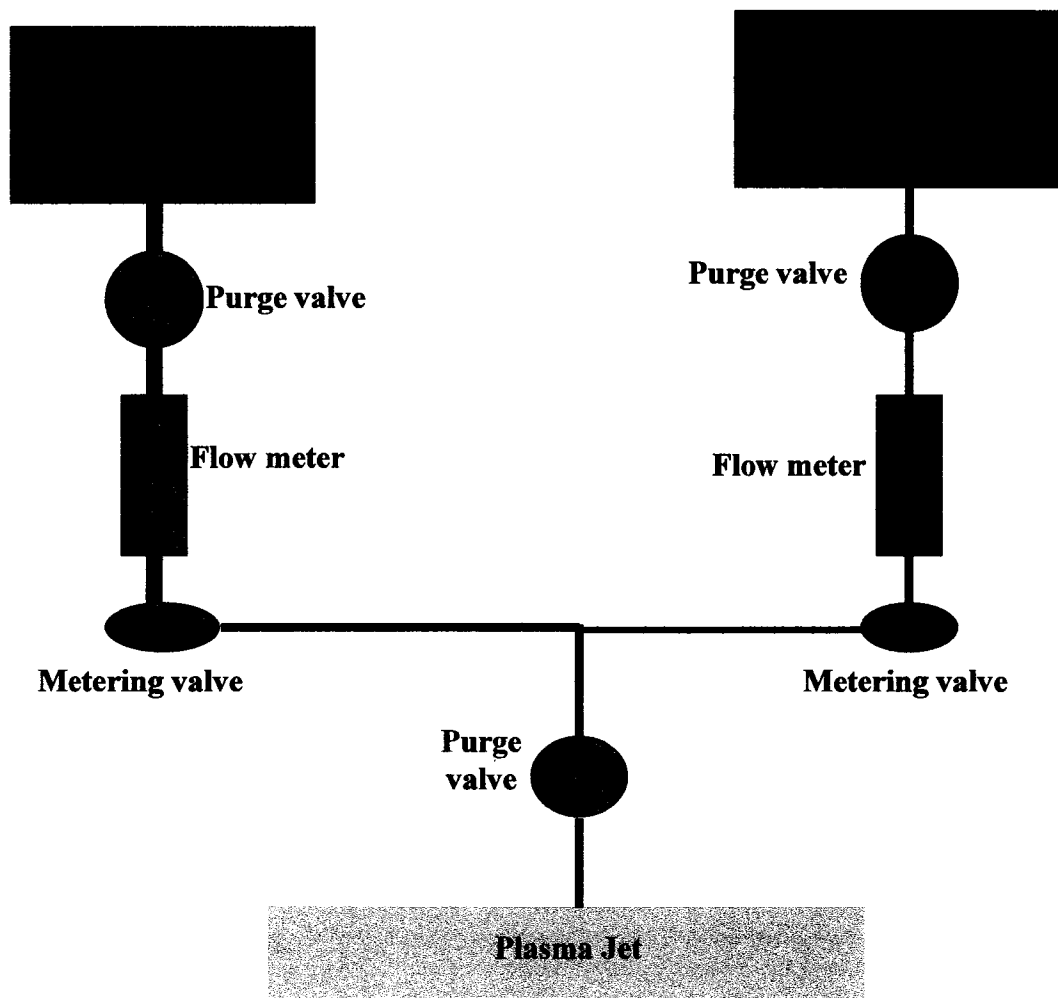
Figure 3.6. Schematic show of the gas pipelines.

3.1.3. Setup with liquid chemicals

In the previous experiments, we have used helium or the mixture of helium and another minority gas, such as oxygen or nitrogen. When a mixture is used, helium is the dilute gas to keep the plasma, while the minority gas provides the active components to modify the polymer surface. Even when pure helium is used, it is still the mixture of real pure helium and some impurities. We could only use the mixture of helium and other gases.

When a mixture is used in the plasma, the minority gas provides the necessary elements and active species to modify the polymer surface. Liquid chemicals can take the functions of minority gases. They have many species with different compositions needed to modify polymer surfaces. If liquid chemicals are properly chosen and mixed with the majority helium, different active species will be generated in the plasma and the polymer surface may be modified in different ways.

The mixture of helium and a liquid chemical can be realized through bubbling. Bubbler is a standard instrument in chemistry. The schematic setup is shown in Figure 3.7. There are two helium flows in the setup. The large flow goes to the plasma directly while the small helium flow goes through the bubbler. When helium passes the bubbler filled with liquid chemical, it is saturated with the chemical. The small helium flow takes the chemical vapor, and joins the main helium flow. In this way, the mixture of the majority helium and very small amount of chemical is formed. The small helium flow can be adjusted by the regulator, and the chemical concentration in the mixture is controlled through this regulator. In the experiment, perfluorohexane (PFH) liquid was

used, and the plasma source and the bubbler were placed in the hood for safety considerations. The setup is shown in Figure 3.8.
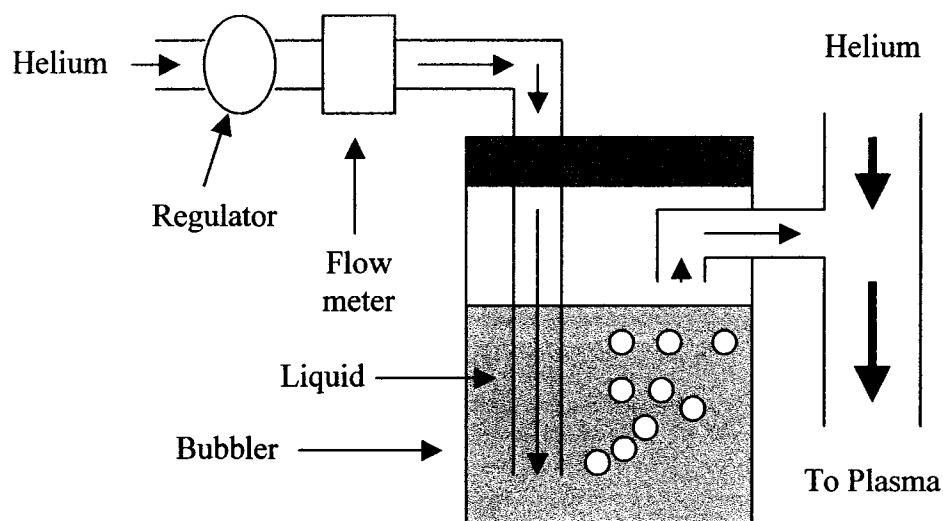
Figure 3.7. Schematic show of the bubbler.
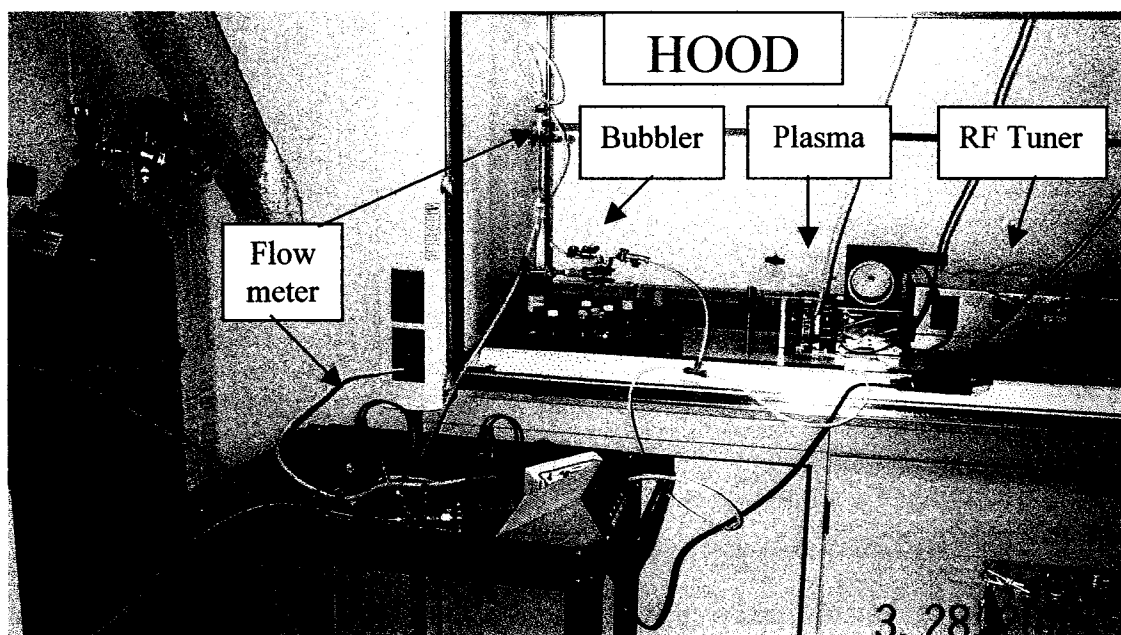
Figure 3.8. Setup with liquid chemicals.

3.1.4. Plasma source

The plasma was full of the space surrounded by the two aluminum electrodes and the two quartz slides. The dimension of the plasma was 8 cm by 10 cm by 1.5 mm. The picture of the plasma is shown in Figure 3.9. The plasma was very stable for several hours during our experiment. The plasma is shallow blue if helium is used, and it is shallower if the mixture of helium and oxygen is used, and it becomes pink if helium and nitrogen are used.

Certain RF power is required to sustain the plasma. When pure helium is used, for moderate helium flow rates (from 10 sccm to 20 sccm), the lowest RF power to sustain the plasma was from 15 W to 30 W. This value may change with the thickness of different quartz slides. If this value is too high, such as 50 W or 60 W, the structure of the plasma jet needs to be adjusted.

The plasma was cold, but the gas temperature was higher than room temperature after certain duration of operation. Some of the light from the plasma was absorbed by the electrodes, and electrodes were heated, and electrodes heat the gas. To lower the gas temperature, the ground electrode was cooled by circulating water. The gas temperature was measured by a thermal meter, and it was below 60°C. The gas temperature increased with RF power, and decreased with gas flow rate.

The most important parameters of the plasma are the RF power and gas flow rates. The RF power can be from 30W to several hundred Watts. Operation with higher RF power is hard because arc will be generated and the plasma will be distinguished. On the other hand, higher RF power may increase the gas temperature to the range in which the plasma jet will be destroyed. Helium flow rate can be from a few slm (standard liter

per minute) to much higher. Low flow rate may let air enter the plasma jet, and high flow

rate is a waste. Usually, helium flow rate is from 10slm to 20slm.
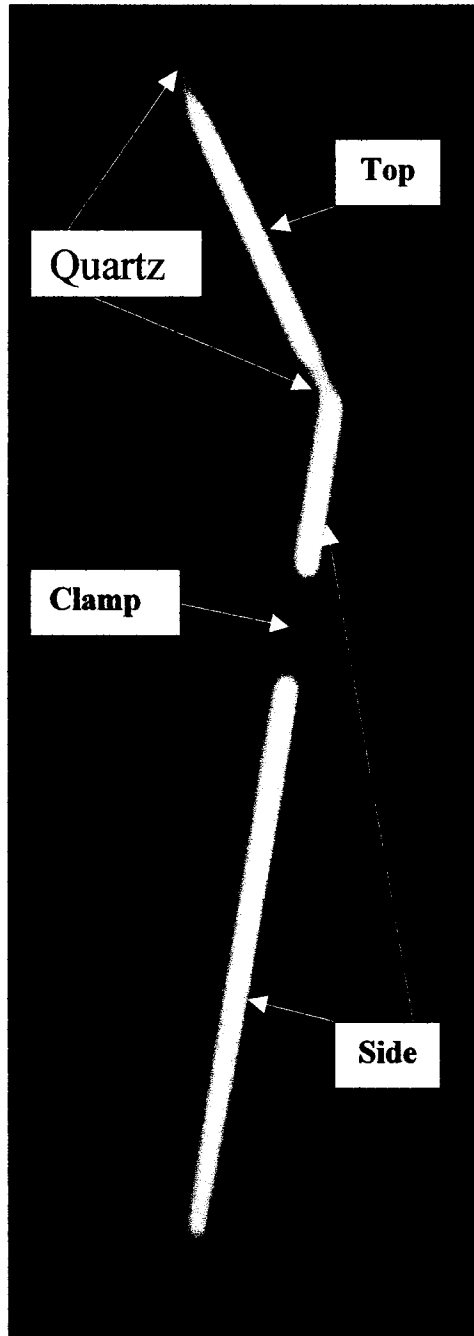
Figure 3.9. Picture of the He plasma.

When the mixture of helium and oxygen is used, the oxygen flow rate has to be

much smaller (usually less than 1%) than the helium flow rate. The reason is that oxygen

is much harder to be ionized compared with helium. Detailed explanations are given in

the discussion section. With a certain helium flow rate (12 slm), the maximum oxygen

flow rate increases with increasing RF power. The result is shown in Figure 3.10. For

another helium flow rate (15 slm), the ratio of maximum oxygen flow rate to helium flow

rate is the same, or the maximum oxygen percentage is the same.
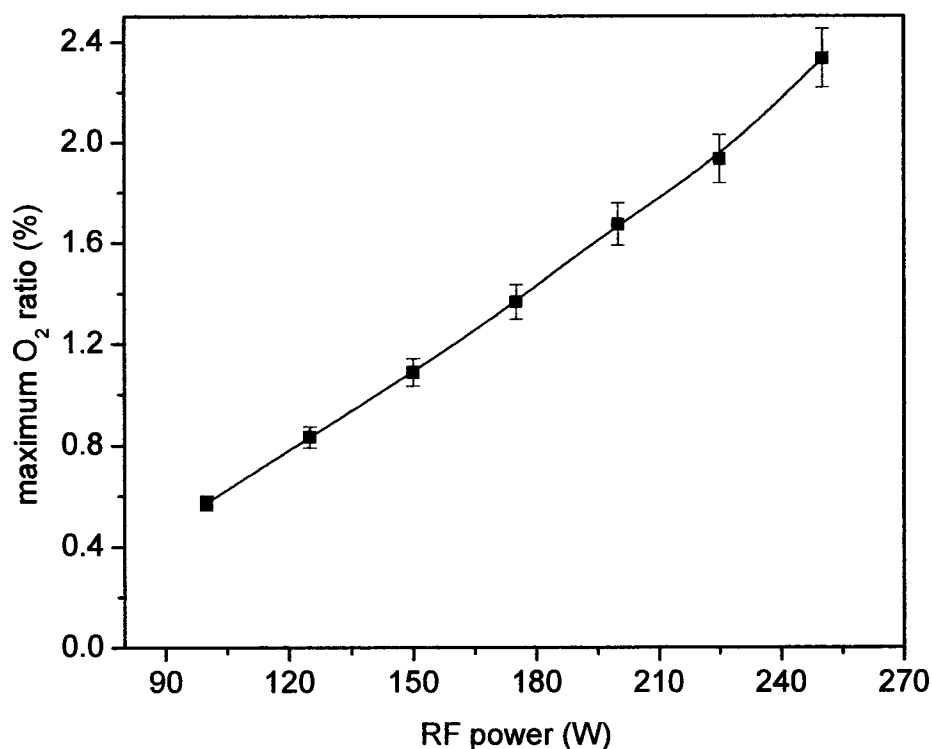
Figure 3.10. Maximum oxygen ratio versus RF power.

3.1.5. Operation of the plasma source

A. Turn on procedure

1. Turn on the cooling water for the RF power supply and for the plasma jet.

2. Turn on the tuner controller first, and then turn on the RF power supply.

3. Turn on the flow meter power supply. Wait for at least thirty minutes.

4. Turn on gas regulators, and purge the pipelines.

5. Adjust the regulators and the metering valves to get proper gas flow rates.

6. Set the shunt and series capacitors of the RF tuner.

7. Add RF power.

8. Adjust the shunt and the series capacitors to minimize the reflected power.

9. Decrease the RF power, turn off the lights in the lab, and then check quality of the plasma. If the plasma is not good, turn off the plasma, and repair the plasma jet.

10. Increase the RF power to desired value, and adjust the shunt and the series capacitors to minimize the reflected power.

B. Turn off procedure

1. Stop the RF power added.

2. Turn off the gases.

3. Turn off the RF power supply first, and then the tuner and the gas flow meters. Do not turn off the tuner when the RF power supply is on.

4. Turn off the cooling water.

C. Stabilization of the plasma

1. The RF power supply should work in Local control mode, Forward and Load output power regulation mode. In Local control mode, all parameters are set manually. In Forward mode, the output power is kept at the set value. In Load mode, the forward power minus the reflected power is maintained at the set value.

2. RF tuner has two operation modes: auto versus manual. In auto mode, the two capacitors are adjusted automatically to minimize the reflected power. In manual mode, the two capacitors are set and adjusted manually. For our experiment, the tuner should be set in manual mode, or it will be too hard to start the plasma.

3. Before RF power is added, set the shunt and series capacitors at proper values. After the RF power is added, watch the reflected power and the RF peak voltage. If the reflected power or the RF peak voltage is too high, stop the RF power, adjust the plasma jet, or adjust the tuner.

4. After the plasma is started, change the gas flow rate to desired value. Then wait for at least several minutes to stabilize the gas flow.

5. During the operation process of the plasma, notice gas flow rates, reflected RF power, and RF peak voltage. If necessary, change gas flow rates, or adjust the RF tuner, or even stop the RF power to turn off the plasma.

6. If the RF power is changed, change gas flow rates and adjust the tuner accordingly.

7. Always notice the color of the plasma. It should be shallow blue when room light is on, or white if the room light is off. If the plasma is pink, there must be serious leakage at the plasma jet.

8. To turn off the plasma, stop RF power first, and then turn off gases.

3.2. Plasma characterizations

3.2.1. Langmuir Probe

3.2.1.1. Setup of the probe

Langmuir Probe is one of the most useful tools for plasma diagnostics. The main idea is to insert a negatively or positively biased metal probe inside the plasma to draw ion current. By changing the bias, current versus bias voltage data are collected. From these data, some important parameters of the plasma can be obtained, such as electron density, electron temperature, electron energy distribution, and etc. Commercial products on Langmuir Probe are available.

There is a restriction on the usage of commercial Langmuir Probes. That is the collisionless sheath requirement. All the widely used formulae in this method are based on collisionless sheath. For this air-pressure plasma, the mean free paths of different ions and neutrals are on the order of microns [70]. The sheath thickness can be on the order of 0.1mm [66]. Hence, even inside the sheath ions have countless collisions. Commercial Langmuir Probe cannot be used to diagnostic the air pressure plasma. A new Langmuir Probe has been developed to diagnostic this plasma jet. The electronic structure of this probe is shown Figure 3.11. When electrons and ions arrive at the collector, a current is generated. The current passes a resistor, and the voltage across the resistor is the indication of the current. With different bias voltages, different currents are obtained. The practical structure of the Langmuir Probe is shown in Figure 3.12 and Figure 3.13.
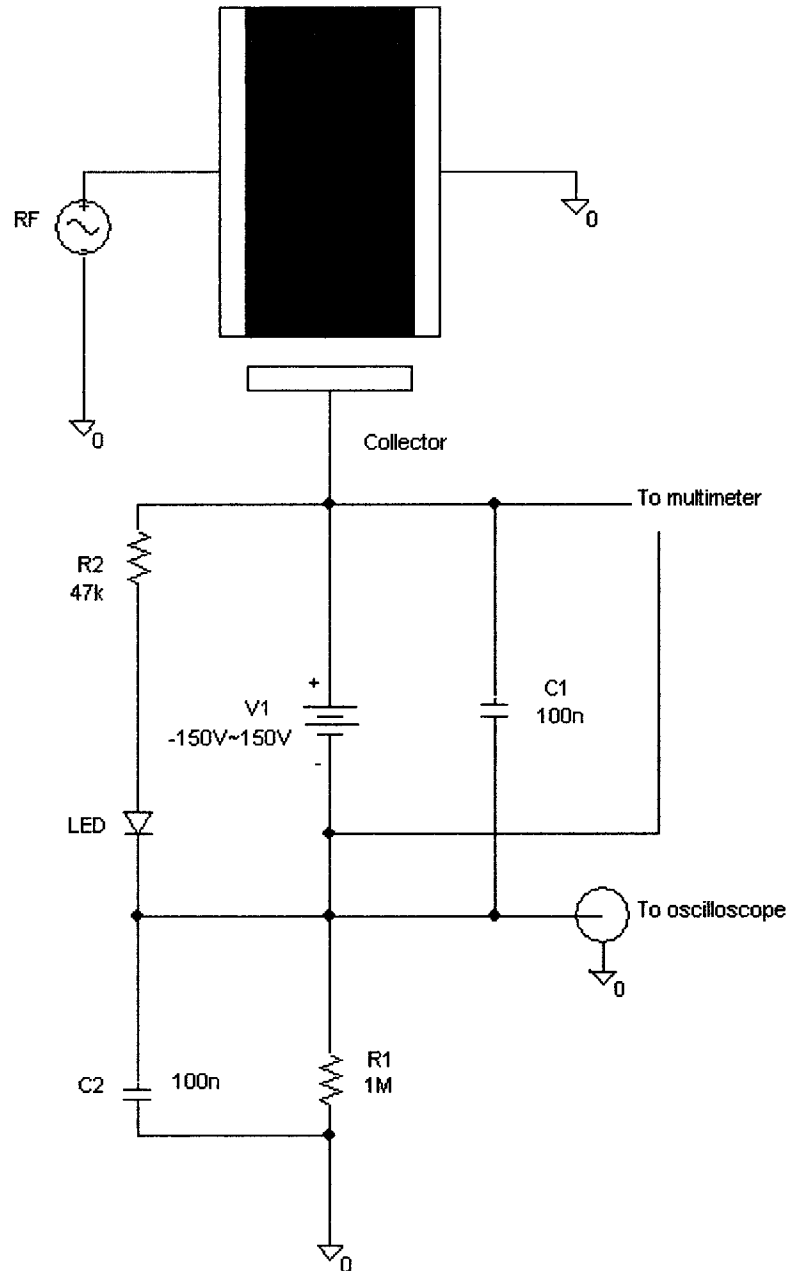
Figure 3.11. Electronic structure of the Langmuir Probe.
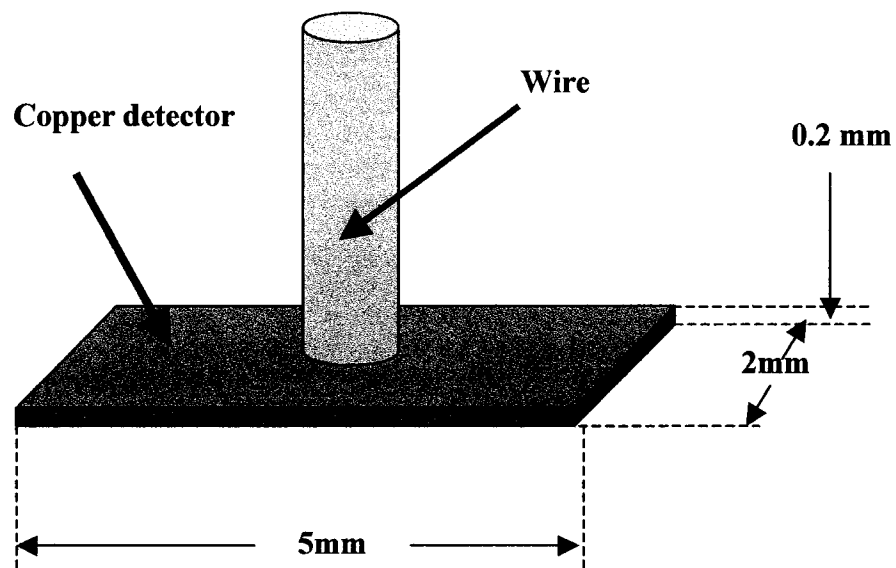
Figure 3.12. Schematic structure of the collector of the Langmuir Probe. The copper plate and the wire are soldered together.
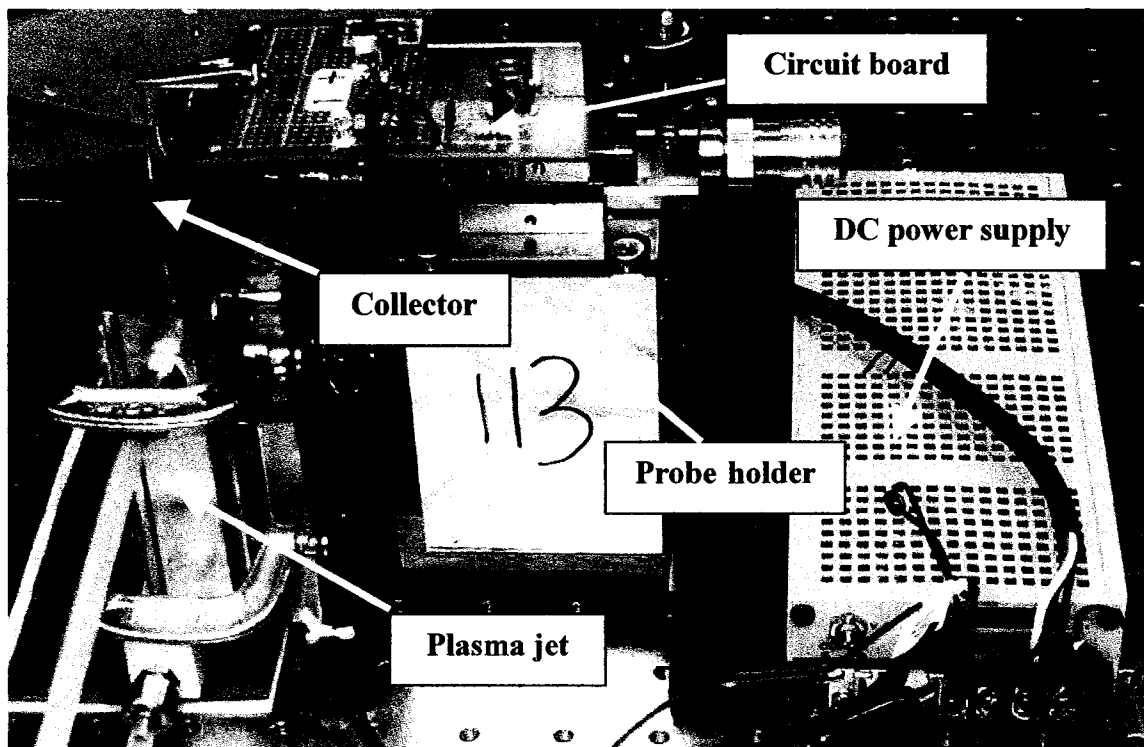
Figure 3.13. The picture of the Langmuir Probe.

3.2.1.2. Results from the Probe

Figure 3.14 shows how the ion flux changed with bias voltage. The ion current increased lineally with negative bias, and decreased quickly with positive bias. With a negative bias, the probe mainly collected positive ions. With relatively large positive bias, the probe mainly collected electrons. Since ions are much heavier than electrons, the slope with the negative bias was lower than that with large positive biases. With zero bias, the probe has a low potential to the plasma body due to the formation of the plasma sheath. Only when the positive bias was large enough, the probe could expel positive ions and collect electrons. This effect is shown by the transition region where both ions and electrons were collected for certain positive biases. The gas flow speed at the plasma exit is on the order of 100 cm/s, and the ion flux is on the order of 10^{13} cm^{-2}s^{-1}. It is estimated that the ion density inside the plasma jet is on the order of 10^{11} cm. The exact value of the ion density has not been determined. The ion flux does not change much with helium flow rate as shown in Figure 3.15. The ion flux decreases with the distance between the probe and the plasma exit as shown in Figure 3.16. Ion flux distribution at about one millimeter away from the plasma exit has been measured. Ion flux increased with RF power (Figure 3.17). In the middle of the plasma exit, the ion flux is roughly uniform (Figure 3.18). If the mixture of helium and oxygen is used for the plasma, the ion flux decreases with the flow rate of oxygen (Figure 3.19).
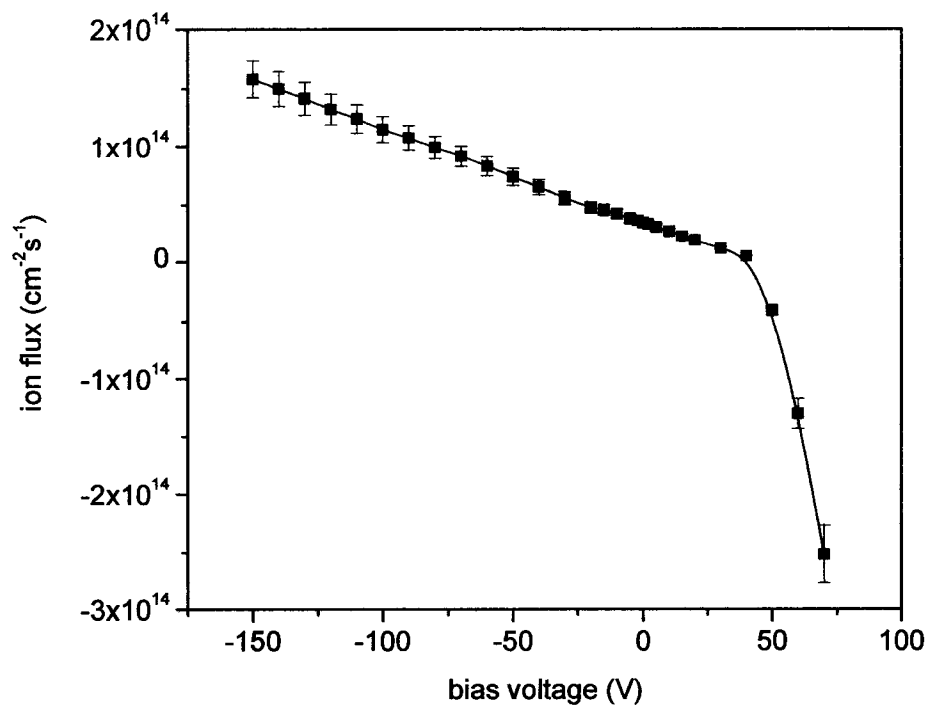
Figure 3.14. Ion flux versus bias voltage at 1 mm away from the plasma exit. RF power was 150 W, and helium flow rate was 12 slm.
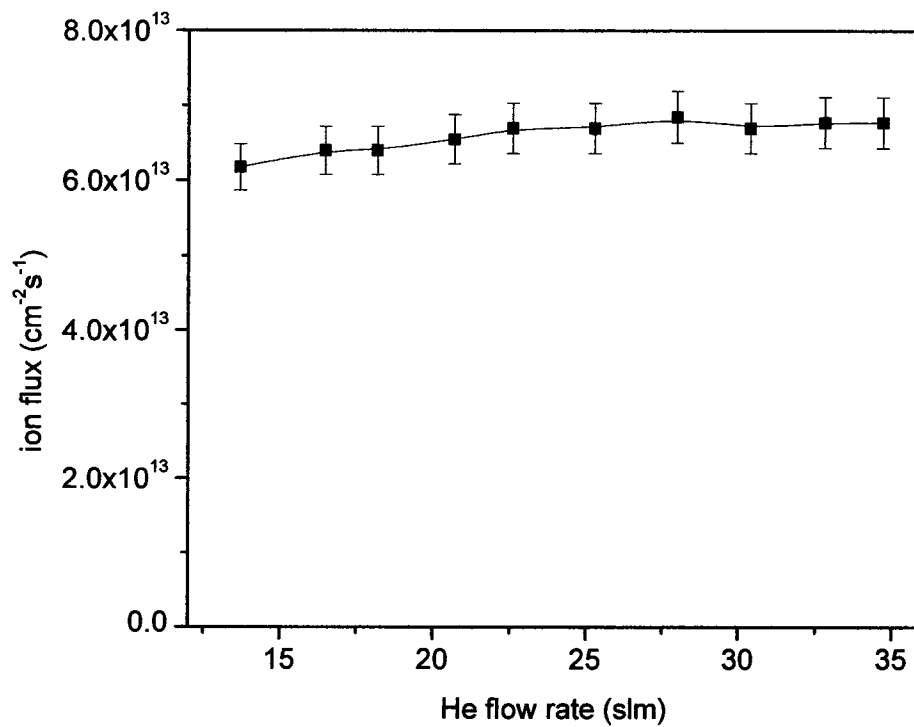
Figure 3.15. Ion flux versus helium flow rate at 1mm away from the plasma exit. RF

power was 150 W.
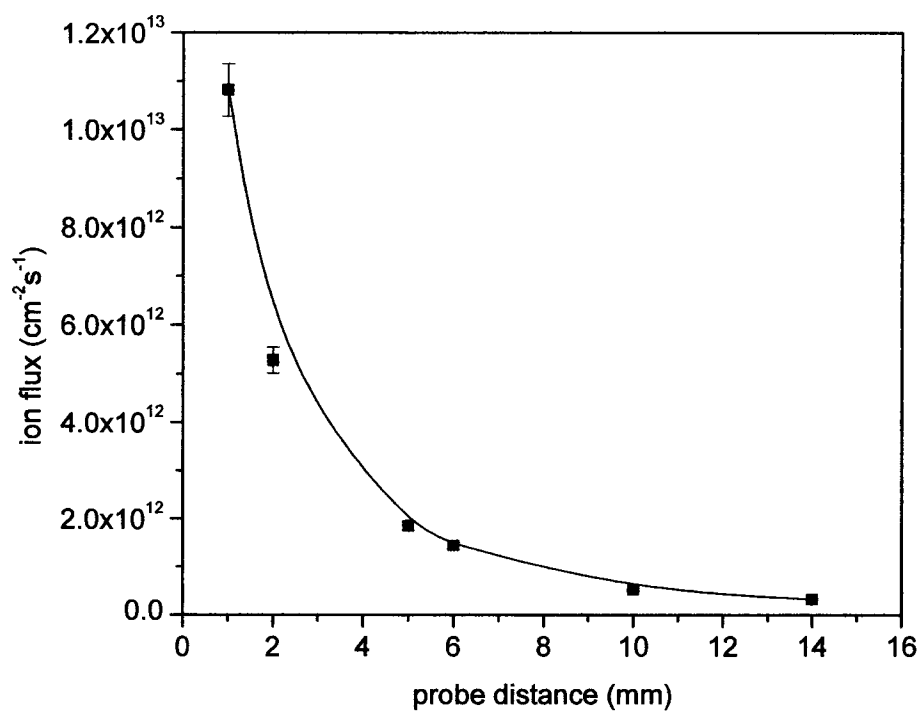
Figure 3.16. Ion flux decreases with probe distance. RF power is 150 W, and helium flow rate is 12 slm, and bias voltage is –0.3 V.
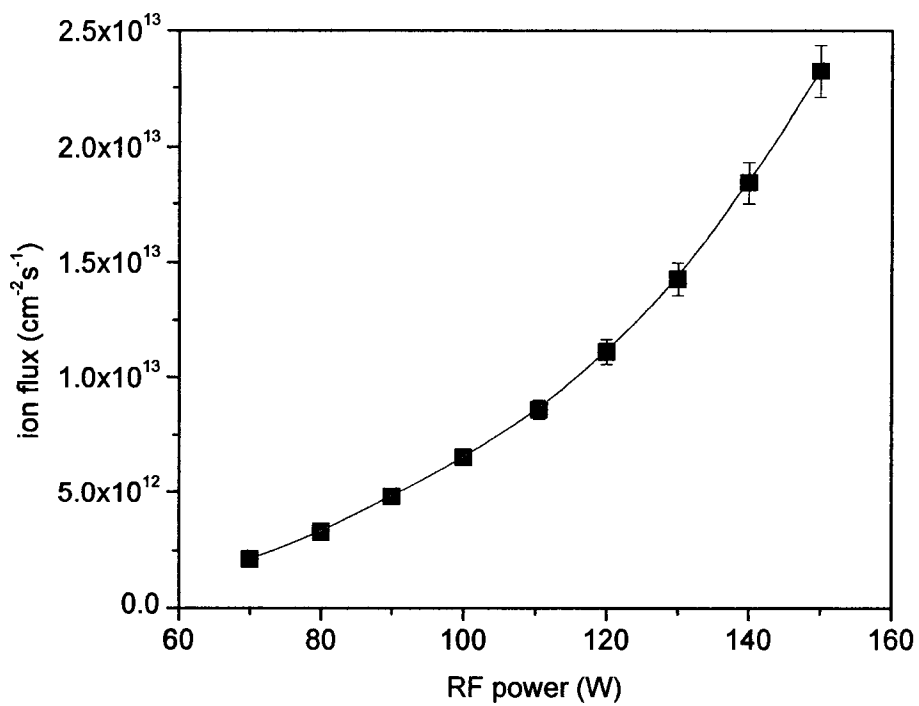
Figure 3.17. Ion flux versus RF power. Helium flow rate was 12 slm. Probe distance was 2 mm. Bias voltage was zero.
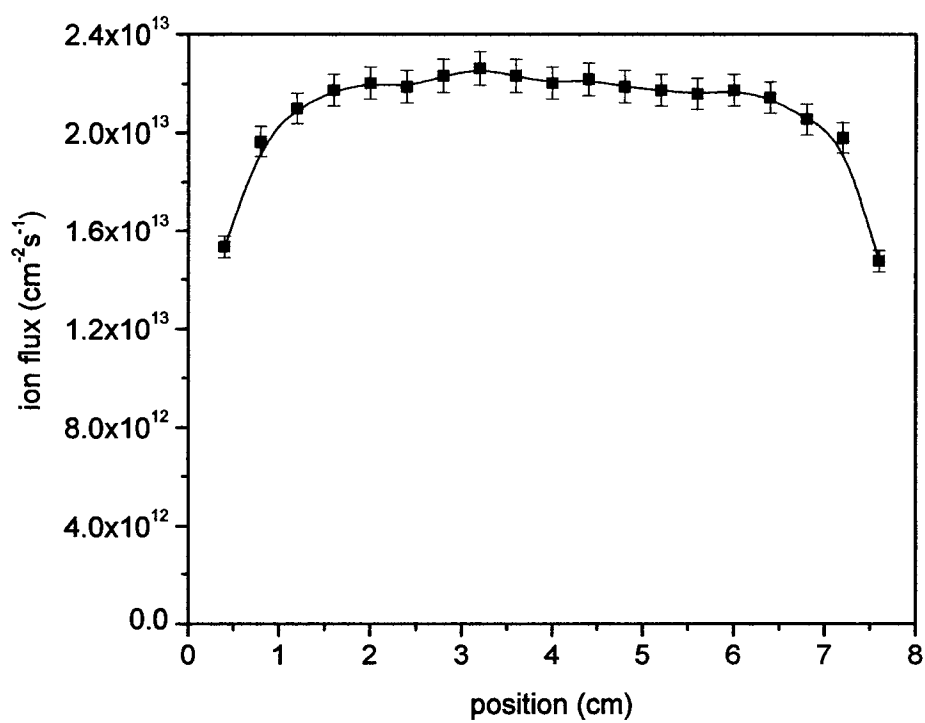
Figure 3.18. Ion flux distribution at the exit of the plasma jet. RF power is 100 W.

Helium flow rate is 14 slm. Probe distance is 1mm. Bias voltage is 0V.
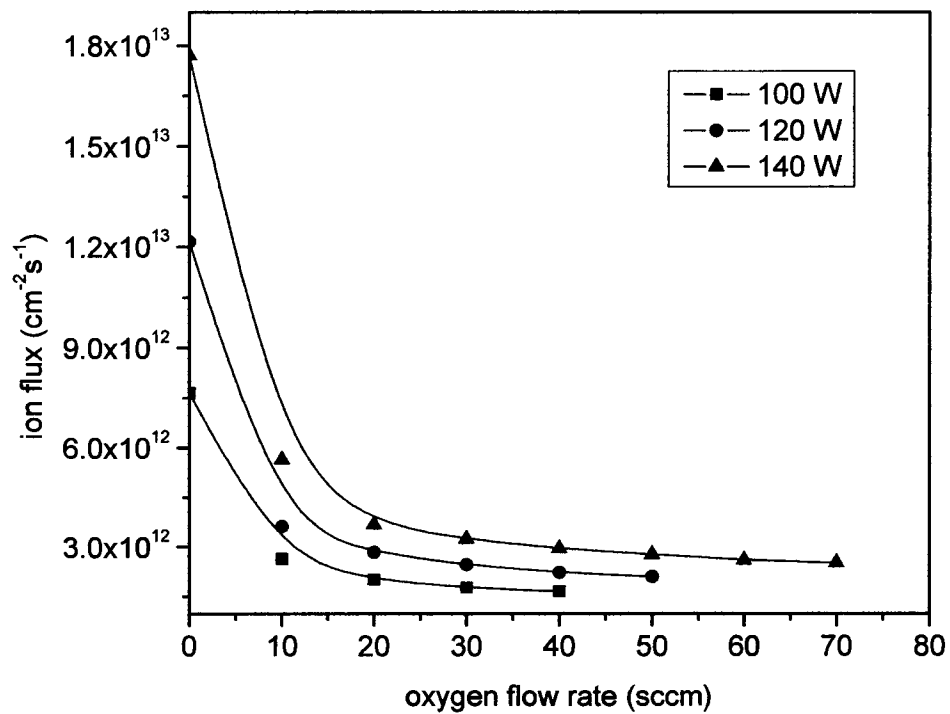
Figure 3.19. Ion flux versus oxygen flow rate for the helium-oxygen plasma. Helium flow

rate is 12 slm, and the bias voltage in Langmuir Probe is 0 V.

3.2.1.3. Calculation of electron density and electron temperature

The estimation of electron density

In order to estimate the electron density, we first assume that our plasma is uniform and the electron density is uniform everywhere inside the plasma. We also assume that the electric field is uniform in the plasma. The RF current density can be expressed by

$$J_{RF} = \frac{P_{RF}}{V_{RF} A}, \tag{3-2}$$

where J_{RF} is the RF current density, and P_{RF} is the RF power, and V_{RF} is the RF voltage, and A is the electrode area. The RF current can also be expressed by

$$J_{RF} = ne\mu E = \frac{ne\mu V_{RF}}{d}, \tag{3-3}$$

where n is the electron density, μ is the electron mobility, E is the RF field intensity, d is the distance between the two electrodes. By equating the above two equations, we have the electron density expressed by

$$n = \frac{P_{RF} d}{e V_{RF}^2 A \mu}. \tag{3-4}$$

Let us choose $P_{RF} = 100W$, $V_{RF} = 70V$ (It is an indication on the RF power supply, and it is not accurate), $A = 100 cm^2$, $d = 1.5mm$. The electron mobility can be found in a reference [69] as $\mu = 2.1 \times 10^3 cm^2 / V / s$. Substituting these values into the expression of electron density, we have

$$n = 1 \times 10^{11} cm^{-3}. \tag{3-5}$$

This result is only a rough estimation, and it agrees with the estimation by Langmuir Probe measurement.

The estimation of electron temperature

In order to estimate electron temperature, we assume that our plasma is uniform, and the electron density and electron temperature are also uniform. We also assume the electric field is uniform inside the plasma. The electric field energy density can be expressed by

$$\frac{\varepsilon_0 E^2}{2} = \frac{\varepsilon_0 V_{RF}^2}{2d^2}.$$
(3-6)

Next, we assume the electric field energy is only in form of electron kinetic energy, and the movement of electrons is only in one direction. Then, the electric field energy density can also be expressed by

$$\frac{nkT_e}{2},$$
(3-7)

where k is Boltzmann's constant, and T_e is the electron temperature. By equating the above two equations, we have

$$T_e = \frac{\varepsilon_0 V_{RF}^2}{nkd^2} \approx 1 \times 10^4 k \approx 1eV.$$
(3-8)

3.2.2. Absorption Spectroscopy

When the mixture of helium and oxygen is used for the plasma jet, ozone and oxygen atoms are generated. Oxygen molecules compete with helium and other molecules, and oxygen molecules are excited, and even dissociate into oxygen atoms. An excited oxygen atom may combine with an oxygen molecule to form an ozone molecule. An ozone molecule may dissociate into an oxygen molecule and an oxygen atom. Ozone density in the down plasma region can be measured by Absorption spectroscopy.
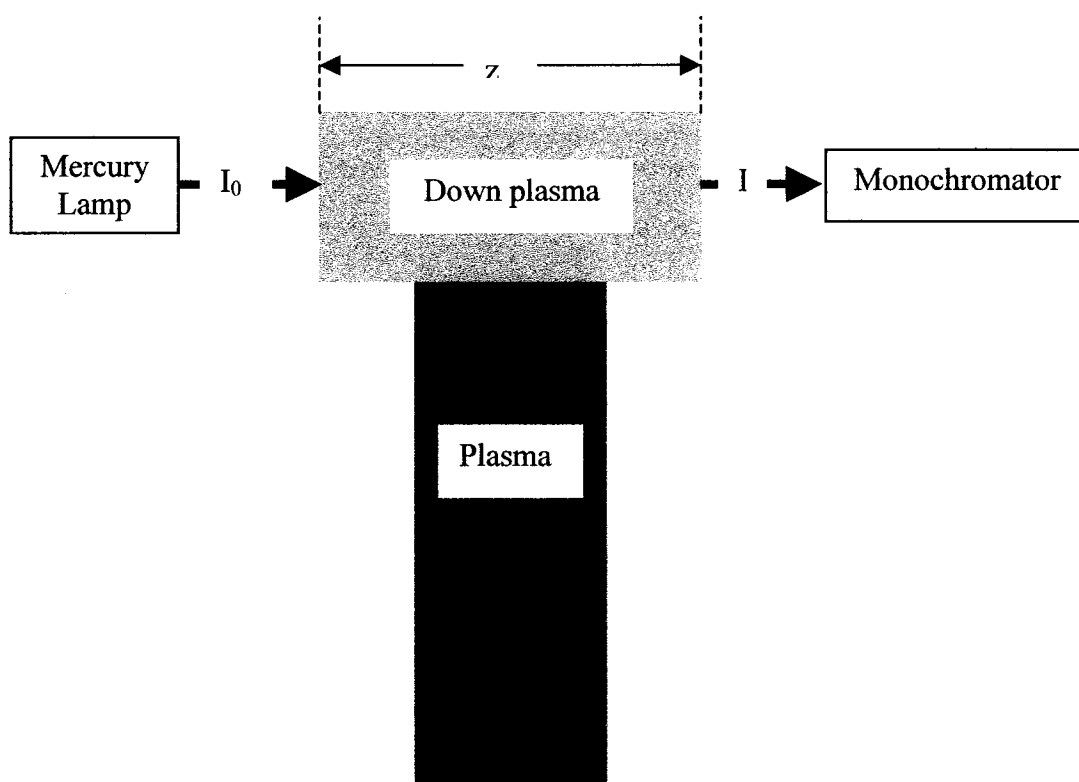
Figure 3.20. Schematic show of the experimental setup.

In the experiment (Figure 3.20), the mercury lamp was Acton Research Corp.'s MS416. The monochromator was made by McPHERSON Inc., its model number was 234/302. The monochromator picked up the fluorescence from the mercury lamp at wavelength 253.7 nm. The measurement point was about 5 mm above the exit of the

plasma jet. The mixture of helium and oxygen were used. Helium flow rate was 20 slm, and oxygen flow rate was 196 sccm. Oxygen occupies about one percent of the mixture. RF power was 200W, and the ground electrode was cooled. The indications of the monochromator with and without the plasma were taken to calculate the ozone density. From $I = I_0 \exp(-n\sigma z)$, we get

$$n = \frac{\ln I_0 - \ln I}{\sigma z},$$
(3-9)

where I_0 (32.8) is the original light intensity, and I (32.2) is the light intensity after absorption by the ozone layer, and z is the thickness of the ozone layer. From reference [71], we found that $\sigma = 1.1 \times 10^{-17} cm^2$. The exact value of ozone layer thickness z is not known. If z is taken as half centimeter, then we have

$$n = 4 \times 10^{15} cm^{-3}.$$
(3-10)

The ozone density in the downstream of the plasma is not uniform both horizontally and vertically, and effective fluorescence cross section is large (about 3 mm^2), so our result is just a reasonable estimation of the ozone density in the down plasma region and the oxygen atom density inside the plasma jet. This result is similar to that reported by others [66, 68].

3.2.3. Emission spectra

The emission spectra of the plasma were measured at the exit of the RF plasmas. The spectrometer was Ocean Optics' USB 2000 with a resolution of 1.5 nm. Its wavelength range is from 200 to 800 nm. The detector of the spectrometer was put one centimeter down the plasma. Helium, helium and oxygen, and helium and PFH were used respectively. The UV emission spectrum for the RF helium plasma was measured with a monochromator (Mcpherson's model 302) with a resolution of 0.2 nm.

Figure 3.21(a) shows the emission spectrum from 200 to 800 nm. The RF power was 120 W, and the helium flow rate was 12 slm. One strong oxygen atom peak was observed at 777 nm, and another weak oxygen atom peak was observed at 616 nm. Only one weak helium peak was observed at 707 nm. One strong N_2^+ peak was observed at 428 nm. Figure 3.21(b) shows the UV emission spectrum obtained with helium plasma. The emission peaks were mainly from the presence of NO and N_2 [72]. The NO peaks were observed at 205, 215, 226, 236, 247, 259, and 271 nm. The N_2 peaks were observed at 313, 316, 337, 354, 385 nm. An N_2^+ peak was observed at 391 nm. OH peaks were observed at 308 and 309 nm. N_2 and O_2 may present as an impurities inside the feeding helium gas. O should be formed from the dissociation of O_2. NO was formed from the reaction of N_2 and O_2. N_2^+ should be formed from N_2. OH might be formed from water impurity.

Figure 3.22 shows the emission spectra from 300 nm to 800 nm for different oxygen concentrations. The RF power was 120W. Helium flow rate was 12 slm. When mixtures of helium and oxygen were used, the intensities of the UV peaks decreased with higher oxygen concentration due to the decrease in plasma density as shown by the

Langmuir Probe measurements. An oxygen atom peak was observed at 777 nm. The intensity of this atomic oxygen peak increased with higher oxygen concentration at first. Above a certain oxygen concentration, its intensity decreased with higher oxygen concentration due to the quenching effect from the oxygen gas and the decrease in plasma density.

Figure 3.23 shows the emission spectrum from He-PFH plasma. The RF power was 120W. The main helium flow rate was 12 slm, and the small He-PFH flow rate was 10 standard cubic centimeters per minute (sccm). In this spectrum, the highest peak at 707 nm was from He. Other He peaks were also observed at 502, 588, 668, and 728 nm. One weak N_2 peak was observed at 357 nm. Only one weak N_2^+ peak was observed at 391 nm. A Ne peak was also observed at 640 nm. Two H peaks at 486 and 656 nm were also observed. One F peak was observed at 740 nm. A series of strong CF_2 peaks were observed around 300 nm. F and CF_2 should be formed from PFH. No O and O_2 peaks were observed. This effect may be caused by the fact that O and O_2 are depleted to form COF_2. While in the helium plasma, most He peaks were quenched by the O peak at 777nm.
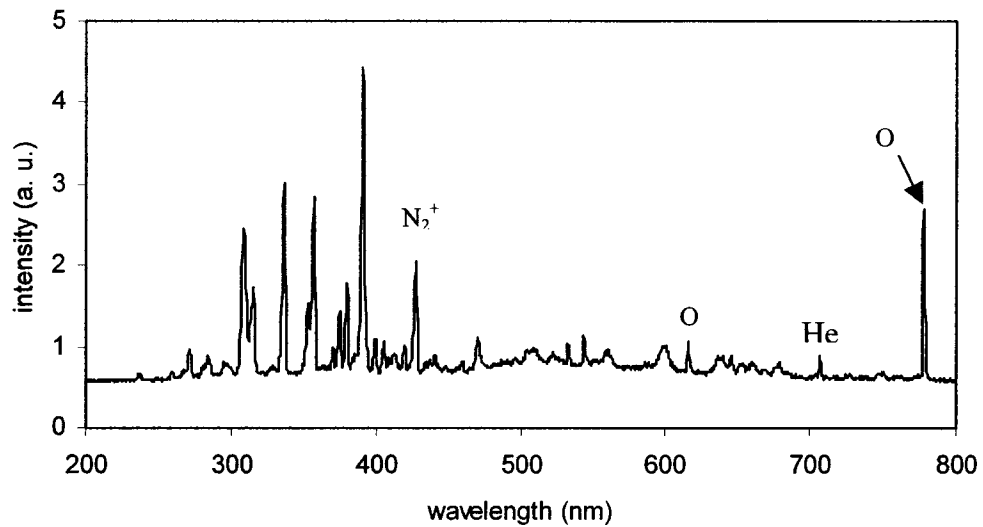
Figure 3.21(a). The emission spectrum from the RF He plasma.
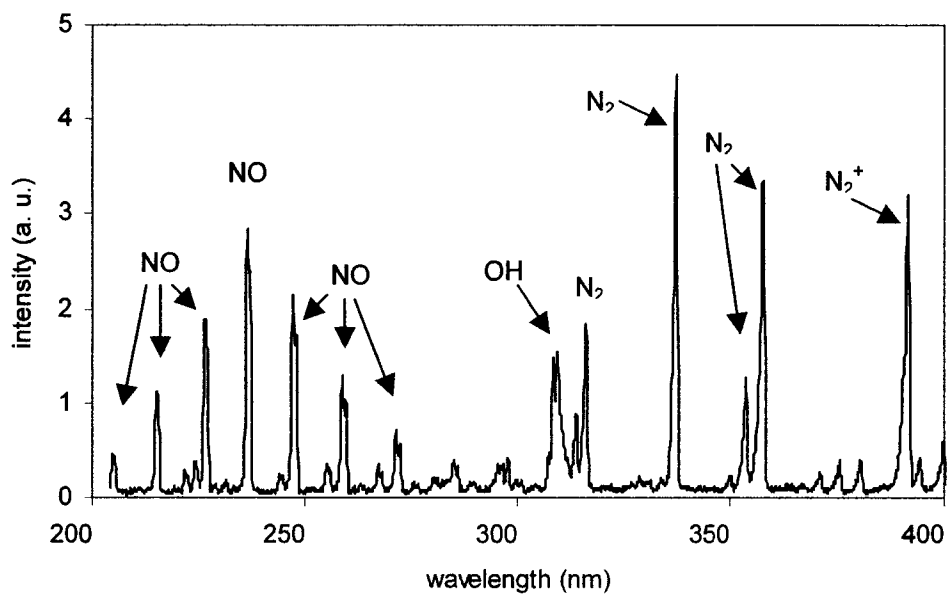
Figure 3.21(b). The UV emission spectrum from the RF He plasma.
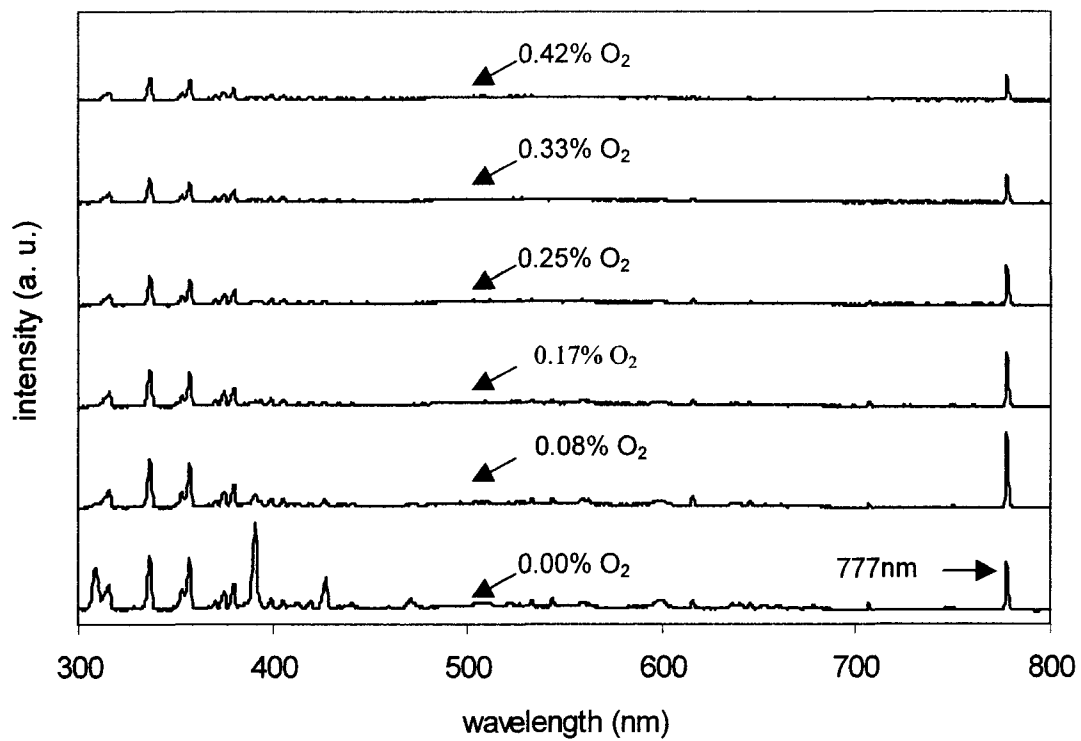
Figure 3.22. The emission spectra from the He plasma at selected oxygen ratio.
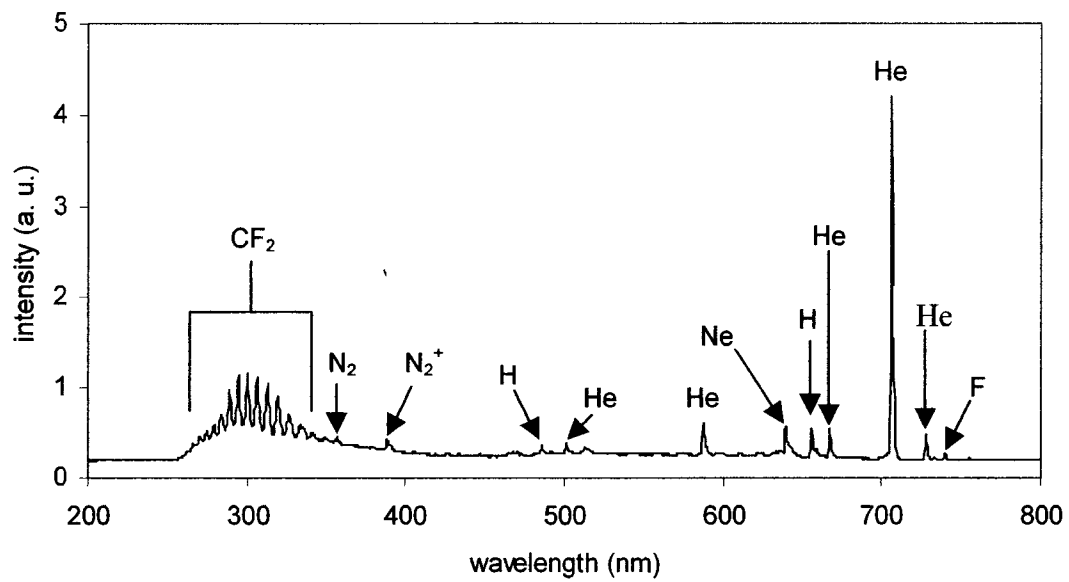
Figure 3.23. Emission spectrum from He-PFH plasma.

3.3. Discussions

3.3.1. On the plasma source

3.3.1.1. Why only helium works

This atmospheric-pressure plasma only works with helium gas, or a mixture of majority helium and another minority gas. We did not find it working with any other gas. One strange aspect is that helium has the highest ionization energy (about 24 eV) among single atom elements. Based on this aspect, helium should be very hard to be ionized, especially at atmospheric pressure. On the other hand, helium has the smallest electron collision cross sections among most gas species [21]. Based on this aspect, free electrons should have the longest mean free path, and hence the highest energy. With enough energy, electrons can have inelastic collisions with helium and helium may get ionized. This is the reason why pure helium works well. The ionization processes with pure helium are listed as

$$e \xrightarrow{\text{RF}} e$$

$$e + He \longrightarrow He^* + e, \ 20 \ eV$$

$$e + He \longrightarrow He^* + e, \ 25 \ eV$$

$$He^* + He^* \longrightarrow He^+ + He, \ -15 \ eV$$
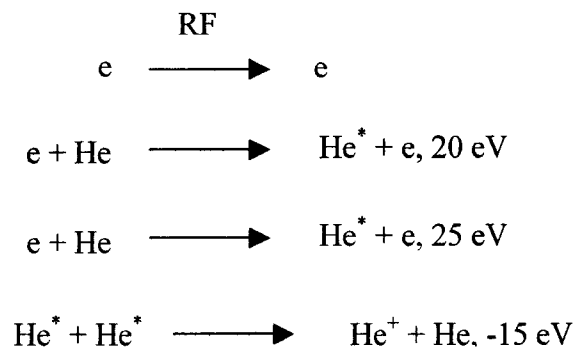
Let us look at the case when a mixture of majority helium and another minority gas. Helium can be exited to a meta-stable state at 20 eV. Helium at meta-stable state may collide with and transfer energy to minority gas molecules. As a result, minority molecules may get excited and even ionized. This is the reason why a mixture of helium and another minority gas also works with this high-pressure plasma. The ionization processes for N_2 and O_2 minority or impurity gas are listed as

$$e + N_2 \longrightarrow N_2^* + e$$

$$e + N_2 \longrightarrow N_2^+ + 2e$$

$$e + N_2 \longrightarrow N + N + e$$

$$He^* + N_2 \longrightarrow N_2^+ + He + e$$

$$He^* + N_2 \longrightarrow N_2^* + He$$

$$e + O_2 \longrightarrow O_2^* + e$$

$$e + O_2 \longrightarrow O_2^+ + 2e$$

$$e + O_2 \longrightarrow O + O + e$$

$$He^* + O_2 \longrightarrow O_2^+ + He + e$$

$$He^* + O_2 \longrightarrow O_2^* + He$$

$$O + O_2 + M \longrightarrow O_3 + M$$

$$N + O \longrightarrow NO$$
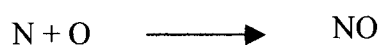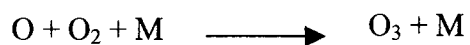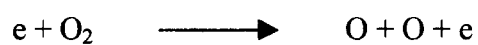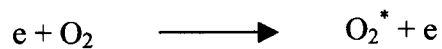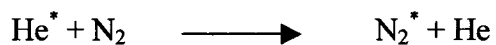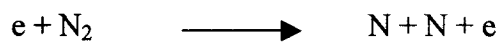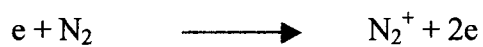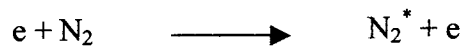
High energy electrons can excite, ionize and dissociate N_2 and O_2. Helium at meta-stable state can also excite and ionize N_2 and O_2. Majority or impurity gases take electrons and meta-stable Helium. Ozone can be generated through three-body process. Minority N_2 and O_2 decrease electron mean free path and the electron energies. At a result, higher percentage of minority gas leads to low plasma density. For a certain power density, above a certain percentage of minority gas, the helium plasma is distinguished.

3.3.1.2. Two types of discharges

RF capacitive discharge can be stable in two different operation modes: alpha (α) type and gamma (γ) type [73]. Alpha type discharge is sustained by volume ionization, while gamma type discharge is sustained by wall ionizations. Compared with alpha type discharge, gamma type discharge is characterized by thin sheath and high current density. If the RF power applied on discharge is raised to a critical value, an alpha discharge can transfer to a gamma discharge. Even in an alpha RF discharge, wall ionization process exists. Some energetic electrons are generated through ion and meta-stable species bombardments, photon radiation on the instantaneous negative electrode. Then, these secondary electrons are accelerated across the sheath. When the RF power for an alpha type discharge is high enough, the wall ionization becomes the dominant ionization mechanism, and the transition to gamma type happens.

The plasma is essentially an Alpha mode capacitive discharge. First, the voltage and current waveforms showed that the plasma is a capacitive discharge, not arc-type discharge. Second, the I-V curves and their dependence on the gas pressure and RF frequency are very similar to those of alpha mode discharge used for gas lasers. Third,

the I-V characteristics vary little with different electrode materials, indicating the passive role of the electrode material in the alpha mode discharge.

The spatial profile of emission intensity between the two electrodes were measured by Jaeyoung Park et. al. The emission intensity is both low near the two electrodes and in the middle of the discharge [69]. This emission profile keeps unchanged with different input power, RF frequency, and gas mixture. This emission profile can be explained by electron density distribution and electric field distribution. The emission profile is the effect of electron excitation. The electron density is low near the electrode (sheath region), and hence, emission intensity is low. In the middle of the plasma body, the electron density is not low, but the electric field is low, and hence the electron energy is low, and the emission intensity is also low. Theoretical calculations show that the RF voltage mainly drops in the sheath, and the voltage drop in the plasma body is relatively small.

3.3.1.3. An equivalent circuit

Suppose that the plasma is generated through RF discharges between two electrodes on which an RF voltage is applied (one electrode is grounded, and the other is really driven by the RF signal). In the two regions close to the two electrodes are the two plasma sheaths, and between the two sheaths is the plasma body. We also suppose the plasma body is uniform. In the sheath region, there are only ions (no electrons), ions are accelerated to the electrode, and electrons are expelled away from the sheath into the plasma body (this is called stochastic heating). The plasma body is neutral, and it has a positive potential to the ground.

A typical equivalent circuit of the RF plasma is shown in Figure 3.24 [20]. C_a and C_b, R_a and R_b, D, and I_i are used to describe the plasma sheath. L_p, R_p and C_0 are used to describe the plasma body. The current I_i represents the ion current to the electrode. The power dissipated by R_a and R_b represent the stochastic heating. The two capacitors C_a and C_b represent the charging effect of the two sheaths. The RF voltage is a quickly changing AC signal. When the sheath voltage changes from positive to zero, electrons are transferred to the RF electrode. This process is described by the diode D, whose preferred current direction is from the RF electrode to the plasma body. The energy dissipation through R_p is used to describe the ohmic heating effect in the plasma body. The combination of L_p and C_0 can be used to decide the plasma body is inductively or capacitive discharged.
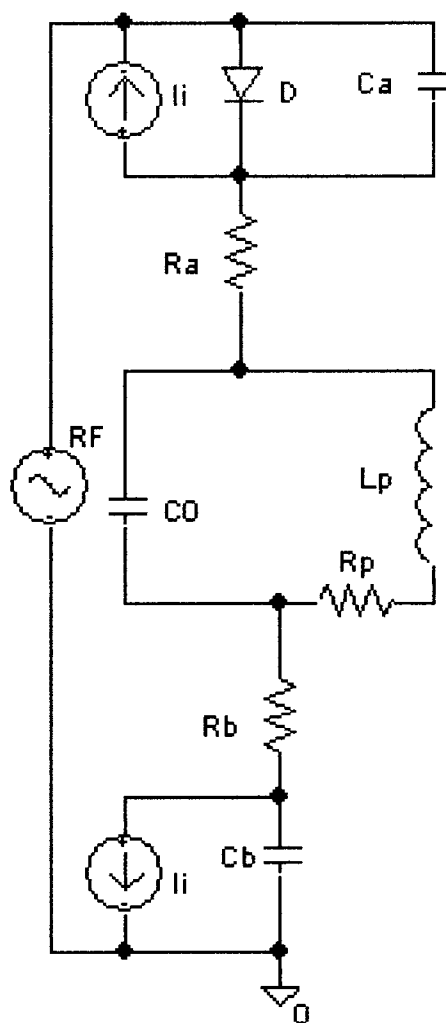
Figure 3.24. An equivalent circuit for the RF plasma.

3.3.2. On characterizations

3.3.2.1 On Langmuir probe

Langmuir Probe is a general tool to characterize low-pressure plasma. Its main idea is to use a biased metal probe to collect current from plasma. By changing the bias voltage applied to probe, people get a current versus voltage curve to calculate some parameters, such as electron density, electron temperature and so on. For our atmospheric-pressure plasma, we can only use Langmuir Probe to measure the total ion flux due to the non-collision sheath limitation for this technique.

Our Langmuir Probe is specially designed for our plasma. The probe collector is placed at the exit of the plasma, instead of the body of the plasma. To keep this condition in mind, we need to place the collector far enough from the plasma body. If it is too close, a discharge is generated between the probe and the plasma body. If it is too far, then the signal is too weak. Since we assume the plasma and the down plasma are uniform, the resultant total flux is an indication of the average plasma density in the down plasma region. We found that the total ion flux decreased with larger distance between the collector and the plasma. We also found that the total ion flux increased with higher RF power, and decreased with oxygen flow rate. The ion density in the down plasma is lower than the ion density inside the plasma. The final resultant ion density from the Langmuir Probe is only a very rough indication of the plasma density inside the plasma. Our conclusion is that the plasma density is on the order of 10^{11}cm^{-3}. We can use our Langmuir Probe to diagnostic the plasma roughly, or to see how the ion total ion flux changes with some operational parameters.

3.3.2.2 Main ion species

The main impurities inside helium are N_2 and O_2 as shown in the emission spectra. Some helium atoms are excited to the meta-stable states. They can transfer their energy to impurities to ionize impurities, or continue to get excited to higher ionization states. Both helium and impurities can be ionized. Minorities are much less than helium atoms. Helium atoms at meta-stable states collide mainly with other helium atoms. Minorities should have less chance to collide with excited helium atoms. But still, we cannot decide the main ion species. The majority ions should not come from oxygen, since it is an electron negative gas and hard to be ionized. When a mixture of helium and nitrogen was used, the N_2^+ peak in the emission spectrum decreased (Figure 3.25). At same time, the total ion density decreased (Figure 3.26). From this point of view, the main ion species may be N_2^+. When a mixture of helium and nitrogen was used, Langmuir Probe measurement showed that the total ion density decreased greatly. At the same time, the intensity of the N_2^+ peak in the emission spectrum increased. From this point of view, the main ion should not be N_2^+. In summary, the main ion species should be He^+, since other minority gases are harder to be ionized compared with helium.
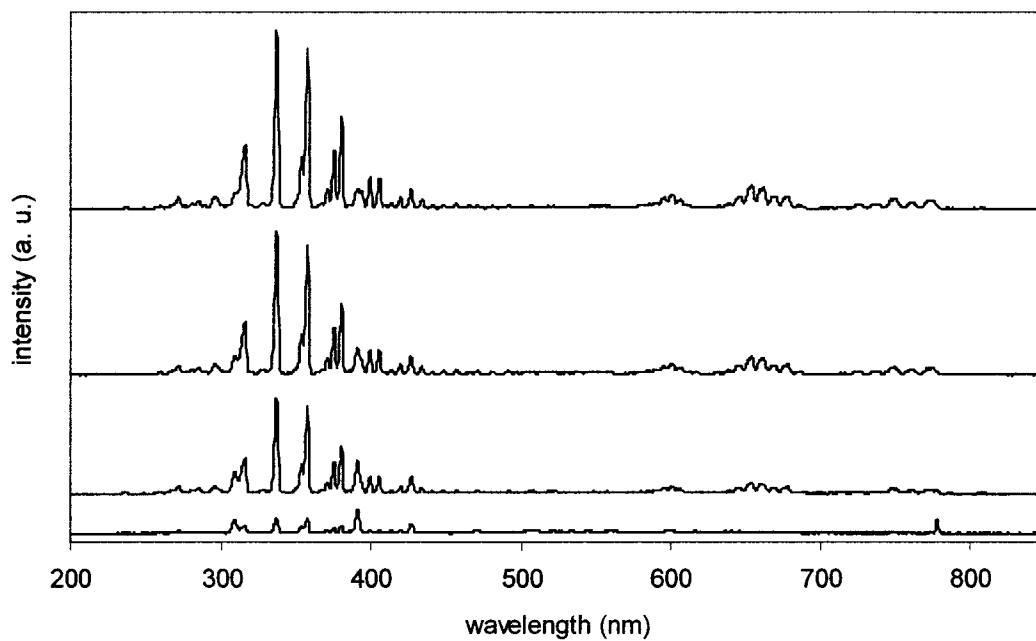
Figure 3.25. The emission spectra of He-N₂ plasma. Helium flow rate was 12slm, and nitrogen flow rate was 0, 10, 20, and 30sccm from bottom to top respectively. RF power was 120 W.
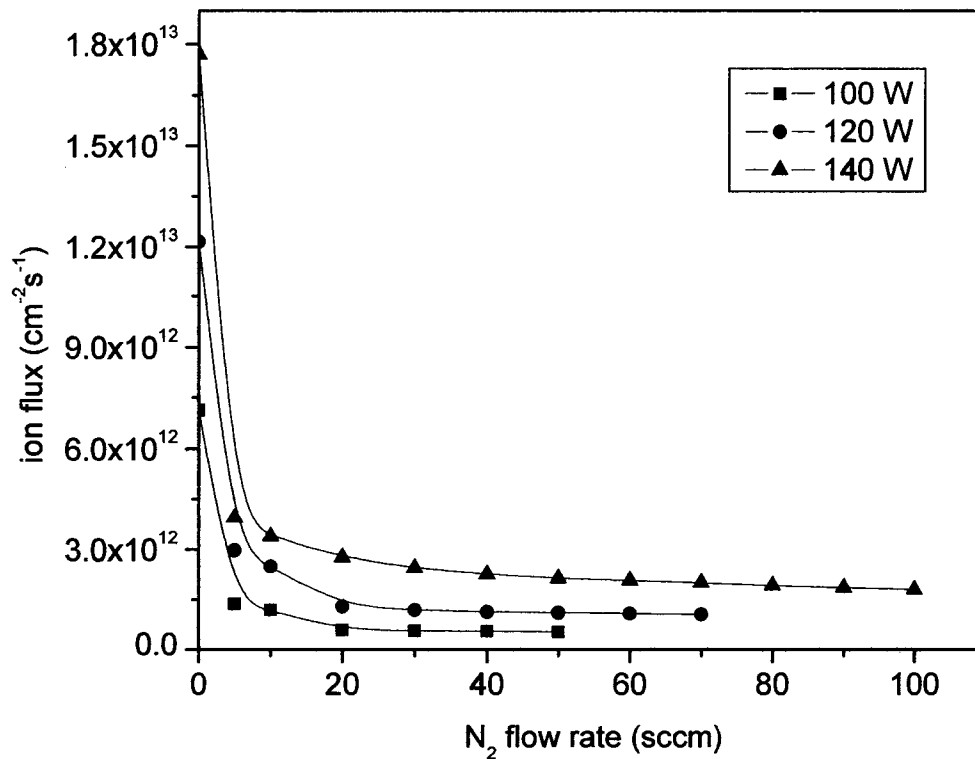
Figure 3.26. Ion flux versus nitrogen flow rate for the helium-nitrogen plasma. Helium flow rate was 12slm, and the bias voltage was 0V.

3.3.2.3. Absorption Spectroscopy

Absorption Spectroscopy is usually used to measure relative high densities species inside the plasma. In our experimental setup, the absorption region was in the down plasma. We also assume that the down plasma region is uniform. The absorption length in the calculation was an estimated value. Therefore, the result is an estimation of the ozone density in the down plasma region. We believe that the ozone density at the exit of the plasma source was on the order of $10^{15} cm^{-3}$.

The result from the Absorption Spectroscopy is also the estimation of oxygen atom density inside the plasma. Inside the plasma, oxygen molecules are dissociated into oxygen atoms. At the same time, an oxygen atom and an oxygen molecule can react to form an ozone molecule, and an oxygen molecule can be dissociated into an oxygen atom and an oxygen molecule. These ozone creation and consumption processes are balanced. Since densities of excited species and electrons are lower in the down plasma region, the ozone consumption process is weaker, in a certain range, the zone density is higher than inside the plasma. On the other hand, the oxygen atom density is lower than inside the plasma. Considering these ozone related reactions inside the plasma and in the down plasma region, we believe that the oxygen atom density inside the plasma and the ozone density at the exit of the plasma are on the some order. Hence, the oxygen atom density inside the plasma body is also on the order of $10^{15} cm^{-3}$.

3.3.2.4. Emission spectra

The emission spectrum can be used to diagnostic the plasma. We measured the emission spectrum from 200 nm to 800nm. The helium peak was very weak compared to other peaks. The UV peaks were mainly from the impurities of NO, N_2, H_2O. In the

visible spectrum region, there are weak peaks. The oxygen atom peak at 777 nm was very strong. Some low peaks between 600 nm and 700 nm are related to N_2. The pink color is from these low peaks. If the plasma is pink, the there must be a leakage because a certain amount of N_2 is inside the plasma. A big air leakage can be noticed by observing the plasma color.

If the plasma is white and shallow blue, we need to check the emission spectrum to see if there are small leakages. In this case, we need to check the relative intensities of the some high peaks. For good plasma, the oxygen atom peak at 777 nm should be lower than some UV peaks, and the UV peaks from 300nm to 400nm should be stronger and stronger in the order. We can seal the leakage at the connections of the two aluminum electrodes and the ceramic manifold. To measure the emission spectrum is the most convenient and reliable way to characterize the quality of the plasma source.

3.3.2.5. On electron density and electron energy calculations

During the calculation process, we assume that the plasma is uniform and the electron density is uniform everywhere inside the plasma. Of course these assumptions are not right. Based on these assumptions, we also assume that all the electrons have the same mobility. We also assume the electric field is uniformly distributed in the plasma. Based on so many assumptions, we calculated that the electron density is $1 \times 10^{11} \text{cm}^{-3}$ when the RF power was 100 W. This value is calculated average electron density with those assumptions. This average value agrees with our Langmuir measurement result. Based on our calculations and measurement, we conclude that the electron density was on the order of 10^{11}cm^{-3}.

To calculate the electron temperature we made additional assumptions. We assumed that the electron temperature is uniform. This assumption is acceptable if we need to calculate the average electron temperature. The second additional assumption is that the electric field energy is only in form of electron kinetic energy. This assumption is absolutely false, and more investigations are needed to understand to what extent it affects the calculation result. The third assumption is that the electron movement is one directional. This is also not true. Our result one electron volt is a very rough estimation of average electron temperature.

Chapter IV

An atmospheric-pressure air plasma source

4.1. Introduction of DBD

4.1.1. A brief description

In a typical DBD, a high AC voltage is applied between two parallel electrodes, and at least one electrode is covered by a dielectric material. A discharge can be generated in the gas gap. DBD usually operate at high pressure, such as 0.1-1 atm. The gas gap is usually from 0.1 mm to about 1 mm, an even to several centimeters. DBD only works with high AC voltage. When a DC HV is applied between the two electrodes, all the voltage will drop on the dielectric material, and no gas breakdown happens. The amplitude of the AC HV is usually between 1 kV and 100 kV. The frequency of the AC HV usually varies from 1 kHz to 10 MHz [74-88]. The dielectric material can be made of glass, quartz, ceramic or polymers.

DBD has different kinds of structures [74]. The first kind is planar structures. In this kind of DBD, the two electrodes are metal plates, and one or both electrodes are covered by dielectric material. One special case is that only one piece of dielectric material is placed in the between of the two electrode, and discharge happens in the two gas gaps between the dielectric material and the two electrodes. The second kind of DBD structure has a cylindrical arrangement. The out electrode is grounded, and inner electrode is connected to HV. The cylindrical dielectric material is attached to the inner or the outer electrode. Discharge happens in the gas gap. The third kind of DBD structure is surface discharge. In this setup, a piece of dielectric material is inserted between the two electrodes, and they are bonded together without typical gas gap. One electrode is

much smaller than the other. Discharge can happen around the smaller electrode. The forth kind of DBD structure is called coplanar discharge. In this setup, a series of electrodes are inserted into the dielectric material beneath its surface. All the electrodes are parallel, and ground electrodes and HV electrodes are arranged in an alternate order. Discharge happens above the surface of the dielectric material.

DBD is non-thermal plasma. Gas temperature is usually very low, such as room temperature. Ion temperature is much lower than electron temperature. Generally, ions and neutrals can be in thermal balance. DBD can generate a lot of active species, such as atoms, radicals, excited neutrals, and ions. DBD can also generate strong UV radiations.

4.1.2. Microscopic behavior of dielectric barrier discharge

Filamentary DBD

The electrical breakdown in DBD happens in the forms of many tiny filaments, or micro discharges. The development of these discharges can be divided into three steps [74]. The first step is called pre-breakdown. A negative charge (electrons and negative ions) space is formed in front of the anode. The step lasts more than half microsecond. As a result, a high electric field is formed in front of the anode. If the field strength reaches a critical value, breakdown can start from the anode surface. The second step in filamentary DBD is called propagation phase. It refers to the spreading of the high electric field to the cathode direction. During the process, many pairs of electrons and ions are generated. This step takes only one to two nanoseconds. The third step is called decay phase. In this step, charges are accumulated at the dielectric surface, and an electric field is formed to compensate the external field. As a result, the discharge becomes weaker.

In filamentary DBD, many tiny filaments are generated. Each tiny filament is within nanometers, and lasts only a few nanoseconds [74, 75]. The function of the dielectric is to prevent arching. Once a tiny filament is large and strong enough, surface charges at the dielectric will cut off the filament. In this way, no filament can develop into arch. Or we can look at this mechanism in another way. Once a filament is strong enough, its equivalent resistor is low enough. More external voltage applied will drop on the dielectric, and less voltage will be left on the filament. As a result, the filament will distinguish itself.

Glow DBD

DBD usually happens in the form of filamentary discharge, but not always. In some cases, DBD does happen in the form of glow discharge [74]. The generation of glow DBD at atmospheric pressure requires special operational conditions. The most important condition is the feeding gas. The main requirement feeding gas is its ability to generate pre-ionization, Penning Ionization through metastables and primary ionization at low electric field. The second main condition of glow DBD is the applied voltage frequency. The residual species from the former half period can generate glow discharge in the later half period. Some dielectric can trap a large mount of charges on its surface. When the applied electric field changes its direction, the surface charges are expelled away to initiate a glow discharge. Glow DBD has been generated with helium, neon, and nitrogen.

4.2. Plasma source development

4.2.1. Plasma source setup

The experimental setup is basically a standard DBD structure driven by an AC high voltage signal. The schematic structure of the AC power supply is shown in Figure 4.1. The output from the functional generator is a low voltage and low power AC signal. Through the power amplifier, the AC signal gains power, but the voltage is still low. The transformer pumps up the signal amplitude. The output signal after the HV transformer gains both power (500 W) and amplitude (10 kV). The setup is shown in Figure 4.2. The functional generator was purchased from Instek (model GFG 8215A). The power amplifier was from Industrial Test Equipment (model 500A). The HV transformer was also purchased from Industrial Test Equipment (# 113671 for 25 k to 50 kHz and #113533 for 1k to 7 kHz).

The DBD structure is similar to that of the RF helium plasma source (Figure 4.3). The same ceramic manifold was used. The two aluminum electrodes were shorter (25 mm high). The ground electrode was cooled by circulating water. The other electrode was covered by 1 mm thick aluminum oxide slide. The gas gap was kept at 1.00 mm by two glass spacers at the two sides.

The high voltage applied to the DBD structure was measured by a digital oscilloscope (Tektronix's TDS380) through a high voltage probe. The total AC current through the DBD structure was determined by measuring the voltage drop across a 10 Ω series resistor. The emission spectrum was also measured by a spectrometer (Ocean Optics' USB2000). The ozone density at the exit of the plasma was also estimated by Absorption Spectroscopy.

One special consideration is needed for the loading problem [89]. The DBD

structure has a capacitor of 16 PF. The ratio of the transformer is 300 to 1. The equivalent

capacitor at the primary side is 1.4 μF, and its impedance is about $-2j\Omega$ at 50 kHz. Then

its imaginary power is about 200 W. Of course, the DBD capacitor does not take any real

power theoretically. But it does occupy the power, and the power factor will be low. In

order to solve this loading problem, we installed an inductor at the primary side of the

transformer (Figure 4.4). The inductance was chosen in such a way that it resonated with

the equivalent capacitor. During one half of the AC cycle, the inductor will take the

current from the capacitor. During the other half of the AC cycle, the capacitor will take

the current from the inductor. In this way, during any AC cycle, no current is taken from

the power amplifier.

Functional Generator	→	Power Amplifier	→	Transformer	→	Plasma
~1V 10Hz-2MHz ~ 1 mW		12 V 10Hz-40kHz 500 W		10 kV 1 k-7 kHz / 25 k-50 kHz 500W		DBD
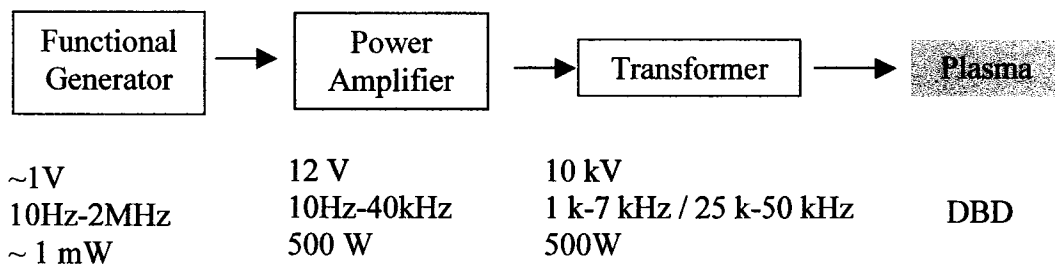
Figure 4.1. Schematic shown of the HV generation.
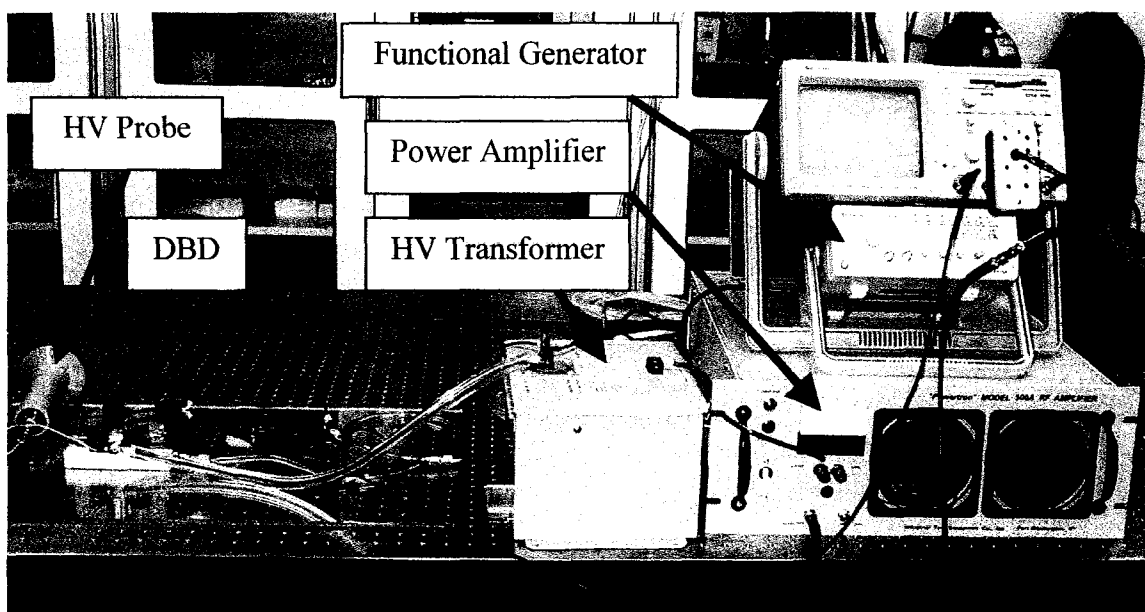
Figure 4.2. Picture of the DBD setup.
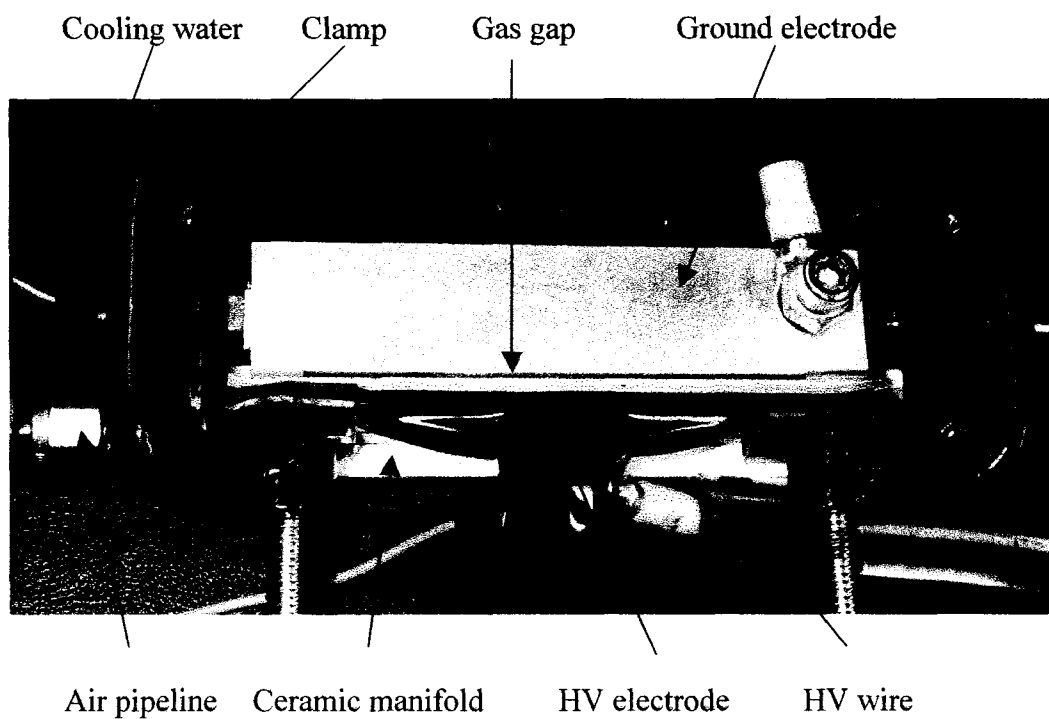
Figure 4.3. Picture of the DBD structure.
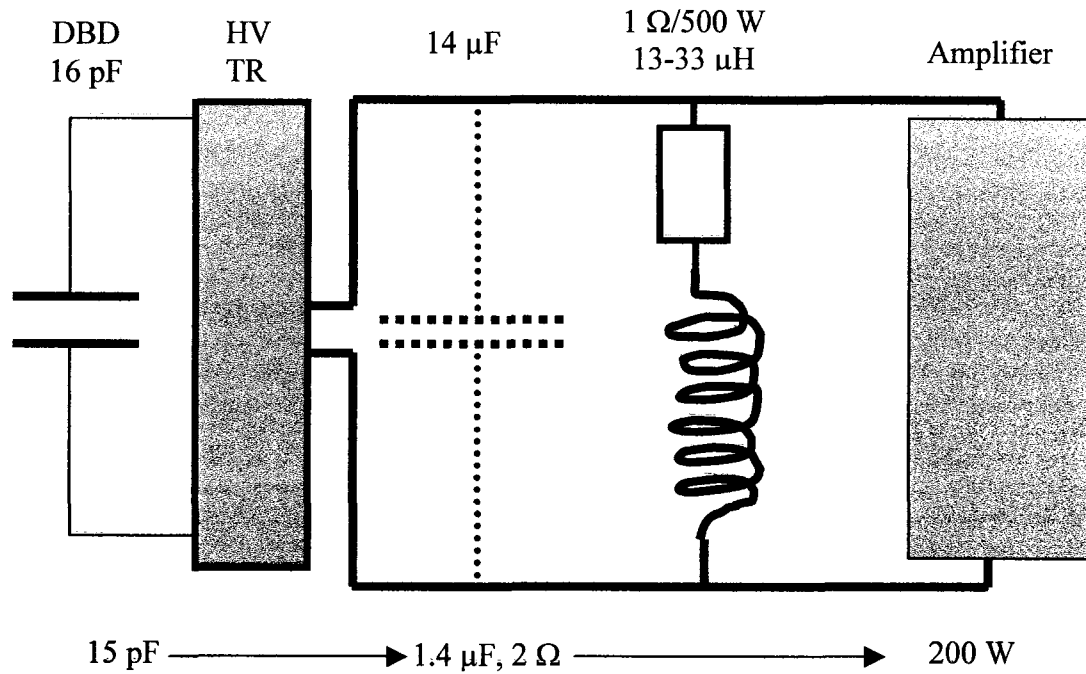
Figure 4.4. Schematic structure of the load.

4.2.2. Plasma source and its operation

Plasma source

The atmospheric-pressure air plasma source was very stable. Figure 4.5 shows the pictures of the plasma source. No apparent arcing was observed for the applied operational parameters. The gas temperature was measured by a thermometer, and it was below 60°C for the plasma sources. It increased with the power applied to the two plasma sources.

Figure 4.5. Picture of the air DBD.

Assembly of the plasma jet

The plasma jet has two aluminum electrodes, one dielectric sheet, one ceramic manifold, two glass spacers, two clamps, and two rubber spacers. Two glass spacers are situated between the ground electrode and the dielectric sheet, and dielectric sheet covers the AC electrode. The two clamps hold the structure tight. The two small rubbers are installed under the AC electrode to lift it up. The AC electrode is covered by two layers of electric tapes at the side and the top, and by one layer of the tape at the bottom. The two rubber spacers keep the bottom of the AC electrodes about two millimeters higher than the bottom of the ground electrode and the bottom of the dielectric sheet.

To assembly the plasma jet, we need to follow the certain procedures. First, prepare all the components well. Second, put the ground electrode on the manifold. Second, install the two glass spacers and the dielectric sheet. Third, install the two rubber spacers against the bottom of the dielectric sheets. Adjust the positions of the two rubber spacers to keep the structure stable and tight. Forth, install the AC electrode on the two rubber spacers. Fifth, use the two C-clamps to tight the plasma jet.

High voltage safety considerations

To generate the air plasma, we need at least 6 kV high AC voltage. Safety is our big concern. We must follow all the general lab safety rules. Additional considerations are needed to operate the plasma. First, we need at least two persons to operate the plasma. Once something happened, the second person can help. Second, when the plasma is working, never touch or come too close to any nearby components. Third, after operating the plasma, always discharge all the nearby components by the grounding

cable. Forth, never touch the plasma jet before discharging all the components, even when the plasma is not in use.

Operation procedure

Turn on the plasma

A. Check the DBD structure and the all the wire connections.

B. Turn on the cooling water.

C. Turn on the air flow, adjust the air flow rate.

D. Connect the wire between the power amplifier and the HV transformer.

E. Turn on the power amplifier.

F. Monitor the plasma, turn off the plasma if find anything abnormal.

G. Start other experiment.

Turn off the plasma

A. Turn off the power amplifier.

B. Take off the wire between the power amplifier and the HV transformer.

C. Discharge all the necessary components with the grounding cable.

D. Turn off the cooling water and air flow.

Arc prevention

To prevent arcing is also a big concern for the air DBD. Arcing not only influence the experimental results, but also can destroy the plasma jet. Before the experiment, we need to check the plasma jet to find any possible arcing path. Any possible arcing path must be blocked. Secondly, the power should be increased slowly. If the power is too high, then arc may happen. After increase the power a little bit, wait for a while and check the plasma. Thirdly, monitor the AC voltage and the current through an

oscilloscope. Any jitter is the sign of arcing. Decrease the power or turn off the plasma at

once. Check the plasma jet. If necessary, assemble the plasma jet again.

4.3. Plasma characterization

4.3.1. Electron density

An equivalent circuit (Figure 4.6) is used to describe the DBD plasma source [77]. The capacitance C_b and C_{gas} are used to describe the dielectric glass layer and air gas gap. The resistance R_{dis} is used to represent the plasma body. The voltage u is the total voltage across the plasma jet, while u_b and u_{gas} are the voltage across the dielectric layer and the gas gap. The current is the total current flowing through the plasma jet. The current I_{cgas} is the displacement current across the gas gap. The current i_{dis} is the conduction current flowing through the plasma body.
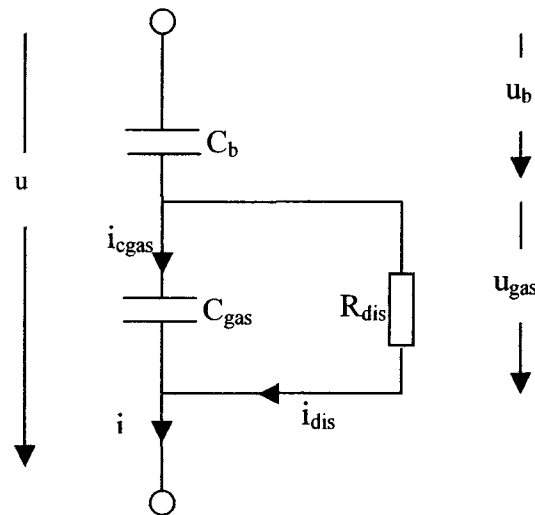
Figure 4.6. An equivalent circuit.

Apparently, we have

$$u_{gas} = u - u_b \tag{4-1}$$

$$u_b = \frac{1}{C_b} \int i\, dt \tag{4-2}$$

Substituting (4-2) into (4-1), we get

$$u_{gas} = u - \frac{1}{C_b} \int i\, dt \qquad\qquad (4\text{-}3)$$

The displacement current across the gas gap can be expressed as

$$i_{cgas} = C_{gas} \frac{du_{gas}}{dt} \qquad\qquad (4\text{-}4)$$

Substituting (4-3) into (4-4), we can get

$$i_{cgas} = C_{gas} \frac{du}{dt} - \frac{C_{gas}}{C_b} i \qquad\qquad (4\text{-}5)$$

Then discharge current can be expressed by

$$i_{dis} = i - i_{cgas} \qquad\qquad (4\text{-}6)$$

From (4-5) and (4-6), we finally get the discharge current

$$i_{dis} = i\left(1 + \frac{C_{gas}}{C_b}\right) - C_{gas} \frac{du}{dt} \qquad\qquad (4\text{-}7)$$

The total voltage was measured through a high voltage probe and an oscilloscope. A small resistor was put in series with the plasma jet, and the voltage drop across the resistor was used as the indicator of the total current. The total voltage and the total current are shown in the Figure 4.7. The dielectric capacitor and the gas gap capacitor were about 80 PF and 16 PF respectively. From equation (7), we computed the discharge current (Figure 4.8).

The total power consumed by the plasma jet can be calculated as

$$P = \frac{1}{T} \int_0^{0+T} u i\, dt , \qquad\qquad (4\text{-}8)$$

where T=40 μs is the period of the total voltage and the current. Then we found that the total power was about 88 W.

The highest discharge current was about 70 mA. The corresponding electric field was about 1 kV/mm, or 1×10^6 V/m. The gas density was calculated as $n=2.4 \times 10^{25}$ m^{-3}. Then the reduced electric field was $E/n=0.42 \times 10^{-19}$ $Vm^2=42$ Td (1 $Td=10^{-21}Vm^2$). From reference [76] we found the electron drift velocity was $v=5 \times 10^4$ m/s. From the electron drift velocity and the discharge current, we found the spatially averaged peak electron density

$$n = \frac{i_{dis}}{eSv} = 5 \times 10^9 cm^{-3}. \qquad (4\text{-}9)$$
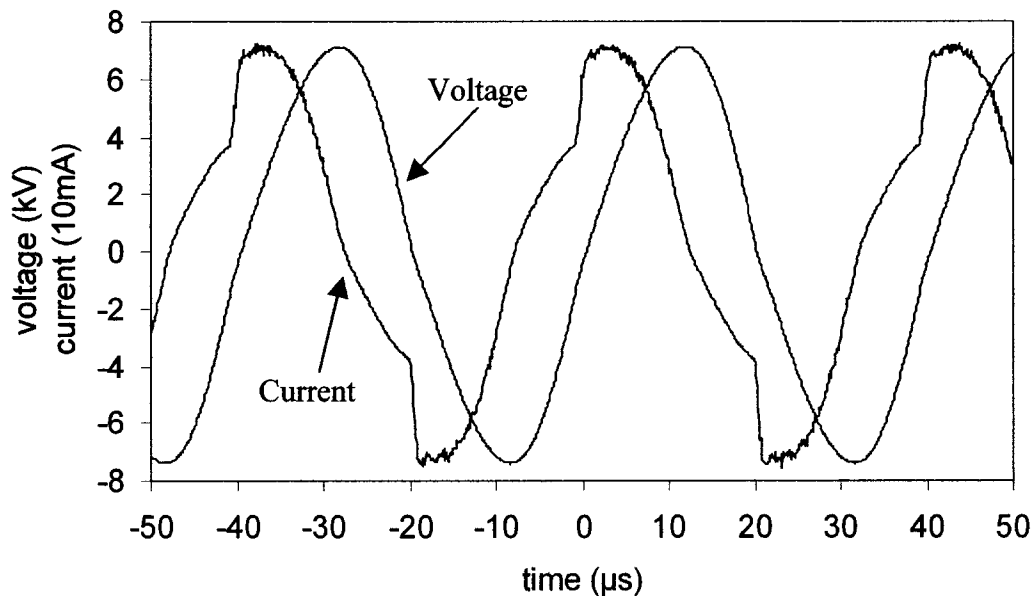
Figure 4.7. Waveforms of voltage and total current at 25 kHz.
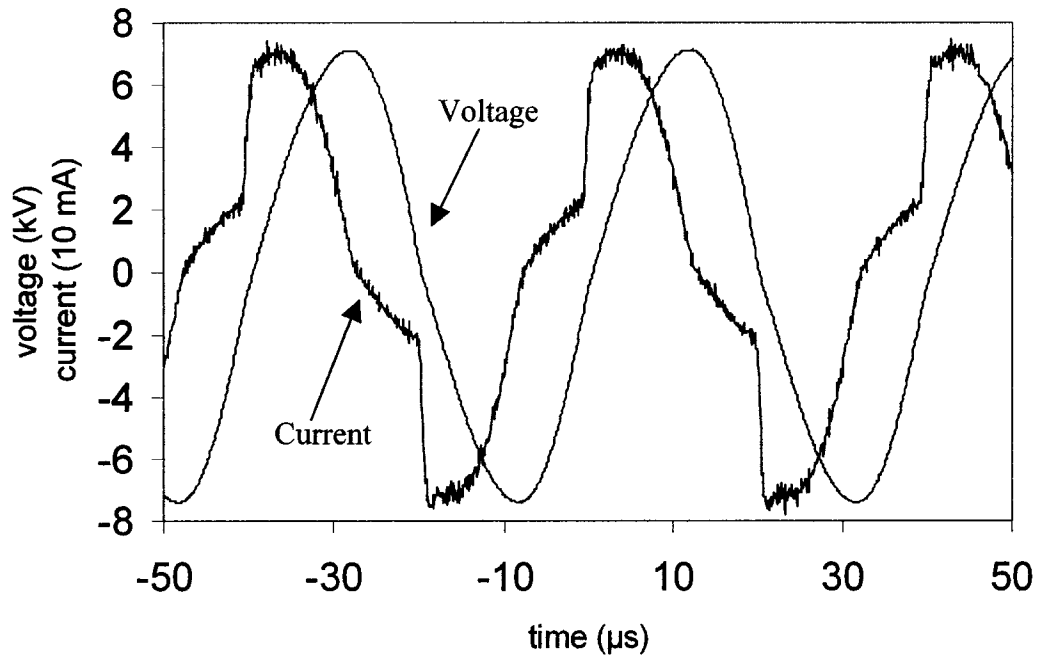
Figure 4.8. Waveforms of voltage and discharge current.

4.3.2. Emission Spectra

The emission spectrum was also taken by a spectrometer (Ocean Optics USB 2000). Figure 4.9 shows the emission spectrum of the air plasma. All the main peaks are from N_2, and no any O_2 peak was observed. This effect agrees well with others [72]. These N_2 peaks are at 316, 337, 354, 357, 372, 375, 380, 394, 400, 406, 420, 427, and 434 nm.
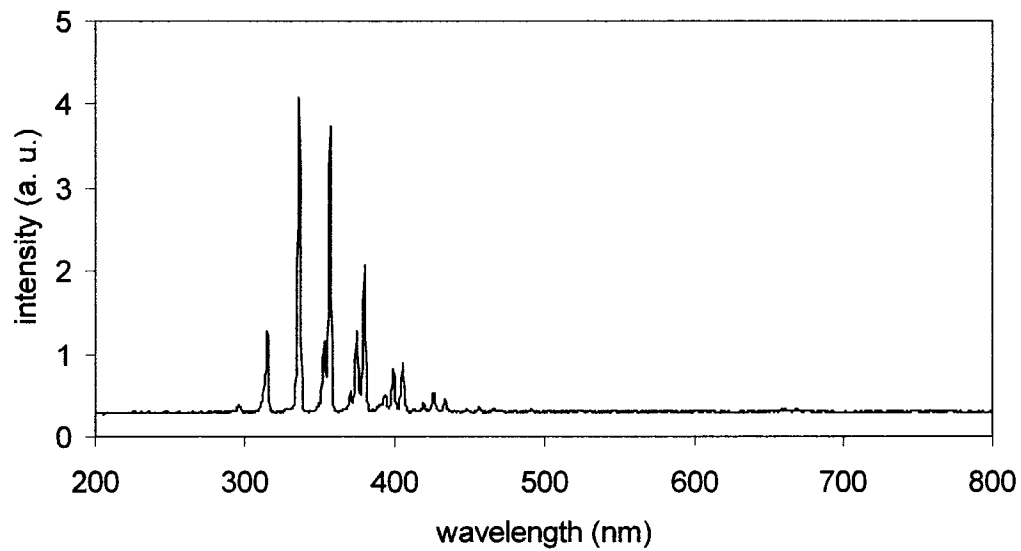
Figure 4.9. BDB emission spectrum.

4.3.3. Absorption Spectroscopy

The plasma source produced a large amount of ozone. We measured the ozone density at the exit of the plasma sources by Absorption Spectroscopy (Figure 4.10). A 253.6 nm wavelength absorption line was selected from a mercury lamp. The absorption cross section is 1.1×10^{-17} m^2. For the air plasma, the ozone density at the exit was found to be on the order of 10^{16} cm^{-3}. Since an ozone molecule is the reaction product of an oxygen atom and an oxygen molecule, it is reasonable to estimate that the density of oxygen atoms at the exit of the plasma source was on the same order.

Monochromator

UV Lamp   DBD
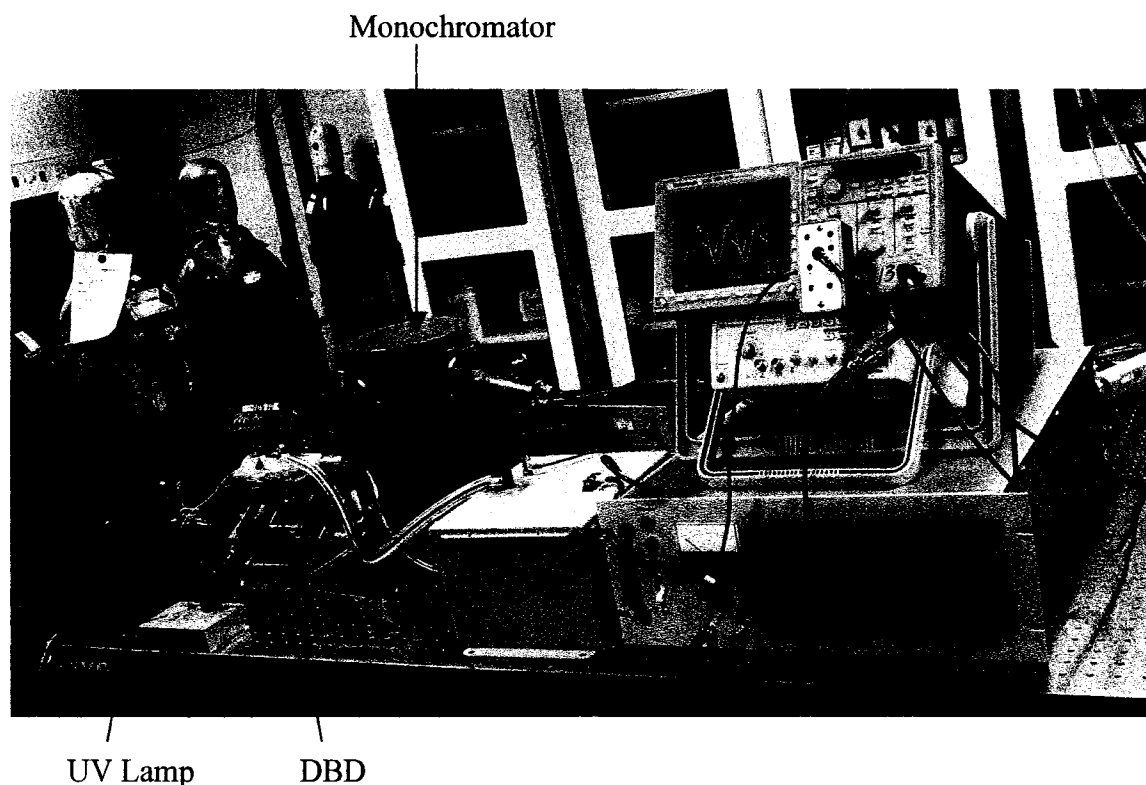
Figure 4.10. Setup of absorption spectroscopy.

4.4. Discussions

4.4.1.The voltage and the current waveforms

The total voltage and the total current waveforms are not sinusoidal. The voltage waveform is almost sinusoidal, and its deformation is small. The waveform of the total current is not sinusoidal at all. But, the phase of the total current is in front of the phase of the total voltage since the DBD has a capacitive structure. The reason for the deformation of the voltage and the current waveform is that the plasma always keeps changing. In the equivalent circuit of our DBD, the equivalent resistor representing the plasma keeps changing, since the plasma density keeps changing due to nature of the external AC voltage. As a result, the voltage and the current waveforms deform from their sinusoidal form.

4.4.2. Total current waveform

The current waveform is a direct measurement result. The waveform has two important characteristics. One aspect is the presence of many sharp peaks. These peaks correspond to the micro arcs in the DBD. The second property of the total current waveform is that the amplitude of the positive current is a little larger than that of the negative current (with glass dielectric sheet). The phenomenon can be explained by the surface charging effect on the dielectric material. Our DBD structure is not symmetric, and only one electrode is covered by dielectric slide. The other electrode is grounded, and the covered electrode is either positive or negative to the ground. When the covered electrode is negative (half of the AC period), positive ions can be trapped at the dielectric surface. When the covered electrode becomes positive in the next half period, these trapped positive ions are expelled away from the glass, and they lead to more ionizations

and increase the plasma density. The uncovered electrode is of aluminum, and it cannot trap any ion. Due to the contributions of these trapped ions, the plasma density is higher during the half period when the AC voltage is positive. Therefore, the positive amplitude of the total current can be a little higher.

4.4.3. Air plasma emission spectrum

In the air plasma, both nitrogen and oxygen molecules can be excited, dissociated, and ionized through inelastic collisions with hot electrons and meta-stable helium. But in the emission spectrum, only nitrogen peaks show up, and there is no any oxygen peak. To understand this effect, we need to check the plasma emission mechanism. The emissions come from the relaxation of the excited species. In the plasma, there are excited nitrogen molecules and excited oxygen molecules. The nitrogen peaks come from the relaxation of these excited nitrogen molecules. The difference between the excited oxygen and nitrogen molecules is that the oxygen molecules are at metastable states, which have much longer lifetime. These excited oxygen molecules prefer to stay at their metastable states than to relax. At the same time, they may transfer their extra energy to nitrogen molecules through collisions. As a result, the emissions from oxygen molecules are much weaker than those from nitrogen molecules.

4.4.4. Electron density calculation

To calculate the electron density, we use an equivalent circuit to present our DBD structure. In the circuit, we use a resistor to present the plasma. This means we assume that the plasma is spatially uniform without any sheath. Due to the existence of the plasma sheath, the plasma body has the trend to have a high potential to the electrode. As a result, the actual drift velocity of electrons approaching the electrode is lower than the

calculated value. As a result, actual electron density should be higher than the calculated value.

4.4.5. Functions of air flow

The airflow inside the DBD has a special function to reduce the degree of big arcing. It is well known that a DBD consists of many micro arcs. Some of these extremely small arcs are distinguished automatically, and some new small arcs are generated at the same time. These two aspects are balanced in a stable DBD. Without airflow, we can see the small arcs inside the DBD. With certain airflow, no apparent arcs can be seen with bare eyes. The reason has not been investigated. One possible reason is that the air flow changes the shape of the arcs from straight (no air flow) to curvature (with air flow). The shape change may increase the length of the small arcs and decrease the intensity of the arcs (or make the plasma more uniform). Hence, the airflow is beneficial for the DBD. Without airflow, our DBD may begin to arc at relatively lower power. With certain airflow, the DBD can work at relatively higher power without arcing.

4.4.6. The optimal AC frequency for our experiment

The AC high voltage frequency influences the DBD power. We used a low frequency (1k to 7 kHz) high voltage transformer to get to higher power. While changing the AC frequency, we monitored the emission from the DBD. We found that the height of the peak at 317 nm increased with AC frequency (Figure 4.11). We also calculated the total power on DBD. We also found that the total power also increased with AC frequency (Figure 4.12). Our DBD is pulsed plasma. With a higher AC frequency, more pulses are generated and more power can be consumed. On the other hand, a high AC

frequency may reduce the width of the plasma pulse. As a result of the two effects, the total power increasing rate decreases with AC frequency.

From 1 kHz to 7 kHz, the highest power we reached was below 20 W. In order to increase the power, we used another transformer to go to higher frequency, from 25 kHz to 50 kHz. Since the highest frequency for the power amplifier is 40 kHz, we tried 40 kHz first. We got only 20 W. We measured the waveforms of the high voltage and the total current (Figure 4.13). The frequency of the voltage was 40 kHz, but the frequency of the total current was not. The current had a high frequency component at about several hundred kHz. This high frequency component corresponds to the pulsed plasma. This frequency is beyond the frequency range of the power amplifier. Therefore, we cannot get more power at 40 kHz. Then we tried lower frequencies. We got 52 W, 69 W and 88 W at 35 kHz, 30 kHz and 25 kHz respectively. Considering that the lowest frequency for the high voltage transformer is 25 kHz, we believe that the optimal AC frequency should be 25 kHz for our experiment.
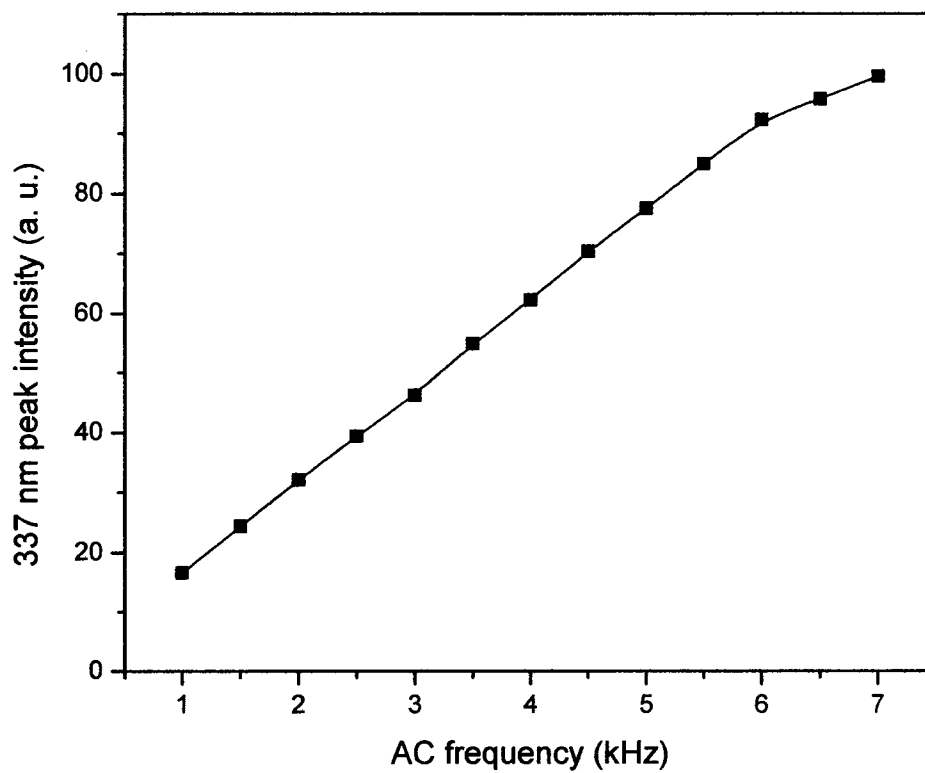
Figure 4.11. 337 nm peak intensity versus AC frequency.
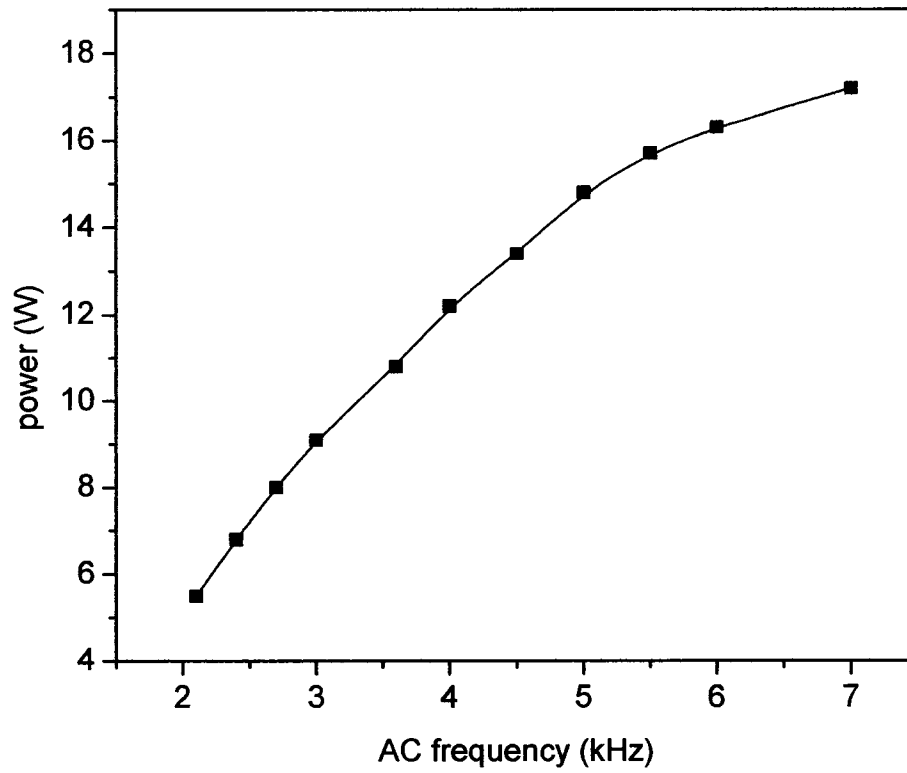
Figure 4.12. DBD power versus AC frequency.
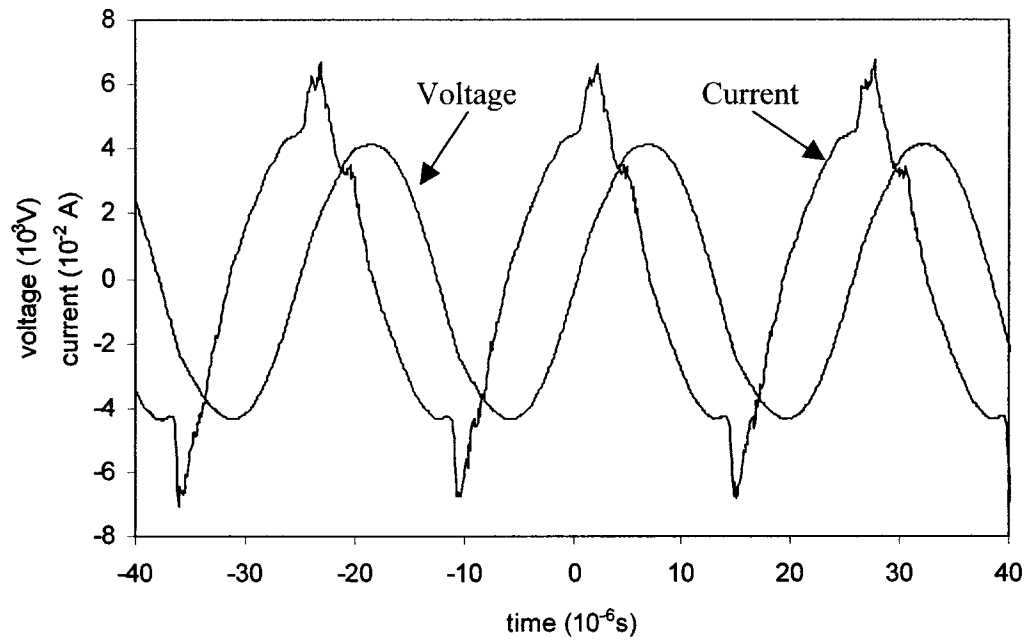
Figure 4.13. Voltage and current waveforms at 40 kHz.

4.4.7. Why only one dielectric sheet

In our experiment, we used only one dielectric sheet to cover the electrode connected to high AC voltage. We also used two dielectric aluminum sheets cover both electrodes, but the result was not good. The main problem was generation of visible arcs in the plasma. With one dielectric sheet, no apparent arcs shown up. Due to the high relative dielectric constant (between 9 and 10), the dielectric does not take a large percentage of the AC voltage. When both electrodes are covered with dielectric sheets, charges accumulate on the dielectric surface, and then are expelled into the plasma. If only one electrode is covered with dielectric sheet, the grounded electrode can absorb all the arriving charges. If both electrodes are covered, more charges may accumulate on the two dielectric surfaces, because they cannot conduct the charges away. As a result, it is easy to arc.

Chapter V

PET surface modification by two plasmas

5.1. Modification setup

The polymer sample was 0.04 mm thick Mylar film from Nova Plastics Inc., Norfolk, Virginia. The sample was cut into two-centimeter-wide slides. The slide was placed at the middle of the plasma exits. The distance between the sample and the tops of the two electrodes was zero. The sample slide was pulled by a roller on a rotary stage at 10 different speeds, which correspond to ten different exposure durations. Table 5.1 shows the roller speed numbers, the corresponding pulling speeds and the exposure duration for the helium plasma. For the air plasma, a smaller roller was used, and the exposure durations were twice compared with the helium plasma case. The modification setup with the helium RF plasma is shown in Figure 5.1. After modification, the sample was taken off, and water drop contact angle measurements were performed with a gonionmeter (Tantec's CAM-Micro).

The goniometer is shown in Figure 5.2. A water drop from the syringe is placed on the sample on the platform. A light beam from the lamp shines at the water drop. An inverted image of the water drop is formed on the vertical screen. The contact angle can be read directly from the screen [90]. In Figure 5.2, the contact angle was 69 degrees.

The resultant contact angles are different at different experimental parameters. The main parameters are the RF power, the sample speed or exposure duration, and the gas flow rates. Higher RF power leads to high plasma intensity, and hence smaller contact angle. Lower sample speed means longer modification duration, and hence smaller contact angle. Helium flow rate, oxygen flow rate should also influence the

modification significantly. The main modification parameters for the air plasma are total power and exposure durations. How these parameter influences the resultant contact angles will be shown later.
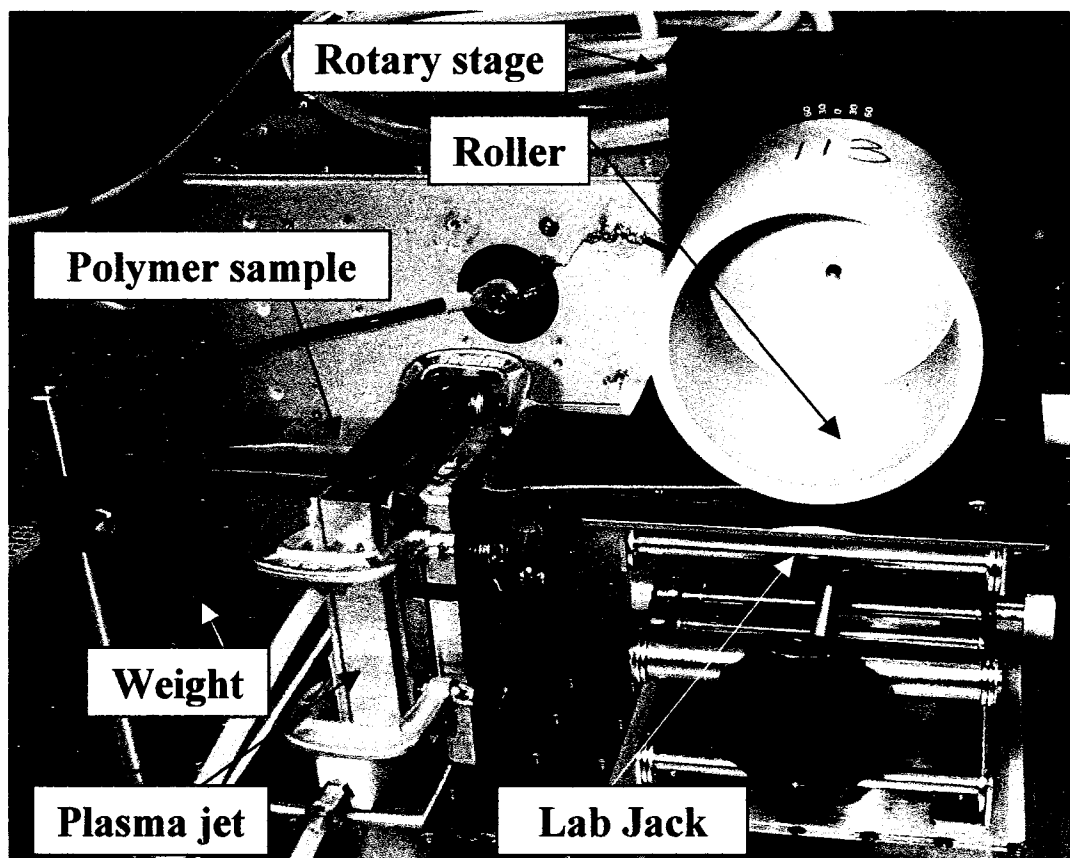
Figure 5.1. The setup for polymer surface modification.

Speed #	Angular speed (degree/min)	Linear speed (mm/min)	Exposure duration (second)
1	49	43	2.2
2	60	53	1.7
3	125	110	0.81
4	193	171	0.53
5	258	228	0.40
6	318	281	0.32
7	378	334	0.27
8	450	398	0.23
9	500	443	0.20
10	490	434	0.21

Table 5.1. Speed # of the rotary stage and conresponding exposure duration.
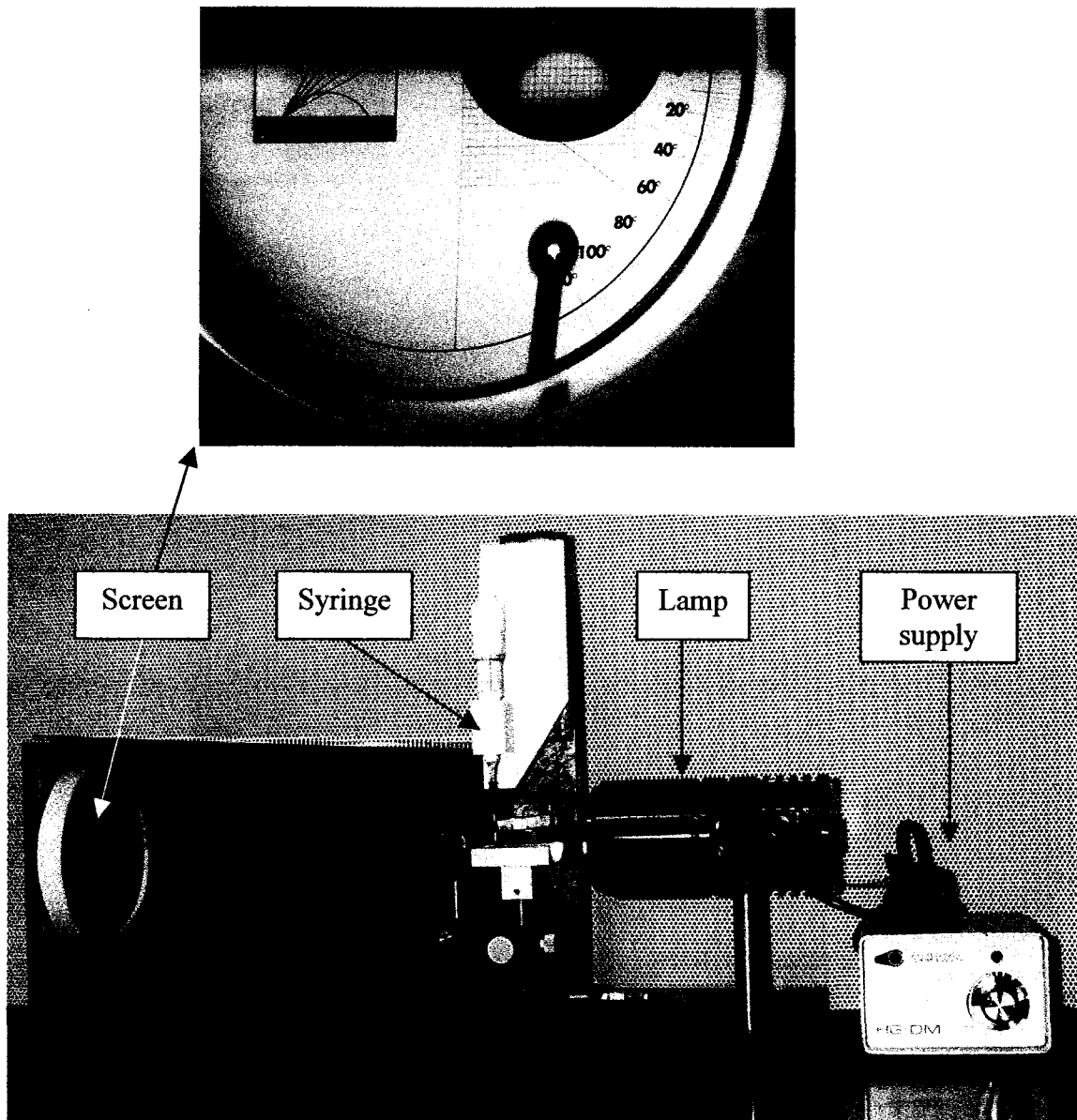
Figure 5.2. Goniometer (lower picture) and contact angle (upper picture).

5.2. Modification results

5.2.1. Modification results by the helium plasma

5.2.1.1. Decreased contact angles

The RF plasma operated with helium or a mixture of helium and oxygen resulted in reduced contact angles and hydrophilic surfaces. During the modification process, PET surfaces were oxidized and polarized groups were generated at the surfaces. PET samples were modified with different operational parameters. Helium flow rate was kept at 12 slm. RF power, exposure duration and oxygen concentration were variable parameters. For each set of operation parameters, contact angles were measured for three times at different positions on the sample surface, and the average value was taken as the final result. The measurement error for contact angles was within one degree.

The unmodified sample showed a contact angle of 70 degrees. Results are shown in the Figure 5.3 and Figure 5.4. The modification effect saturated after certain amount of processing, and the smallest contact angle that could be reached was around 28 degrees. Oxygen concentration in the mixture of helium and oxygen influenced the modification process significantly. Even without oxygen added into the feeding helium gas, the surfaces were still modified and reduced contact angles were observed. This is because of the oxygen impurity in the helium gas. At lower oxygen concentrations (less than about 0.1%) the contact angle decreased with higher oxygen concentration, and above certain oxygen concentrations, the contact angle leveled off.

In certain ranges, the resultant contact angle decreased with higher RF power and longer modification durations. The saturation effect was evident. When the RF power was 80 W, the three curves were separated (Figure 5.3.a). When the RF power was

increased to 100 W, the right part of the middle curve approached the lower curve (Figure 5.3.b). When the RF power was increased to 120 W, the right part of the two lower curves overlapped (Figure 5.3.c). For 0.2 s duration, the three curves were separated (Figure 5.4.a). For 0.4 s duration, the lower two curves were very close (Figure 5.4.b). For 2.2 s duration, the modification was saturated and the three curves were overlapped at about 28 degrees.
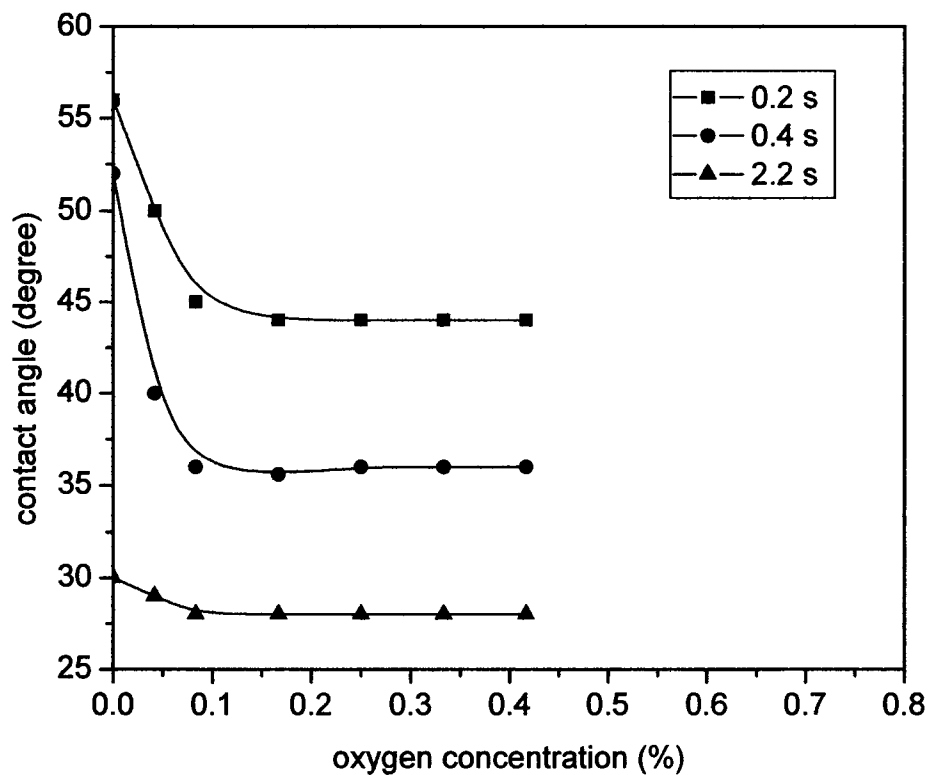
Figure 5.3.a. Contact angle versus oxygen concentration for selected exposure durations at 80 W.
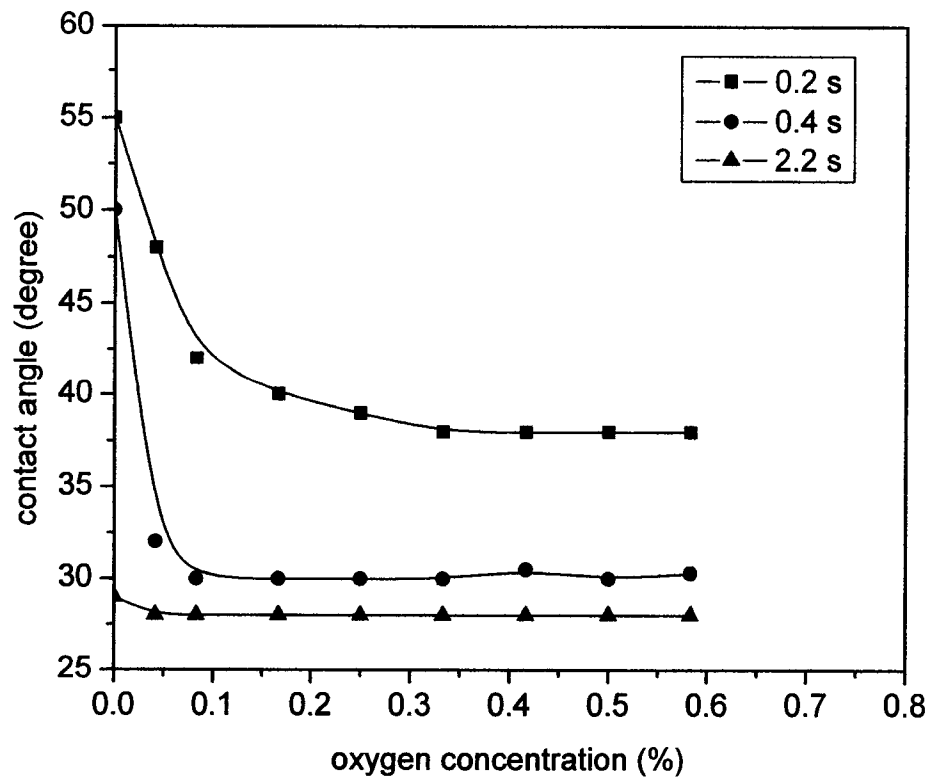
Figure 5.3.b. Contact angle versus oxygen concentration for selected exposure durations at 100 W.
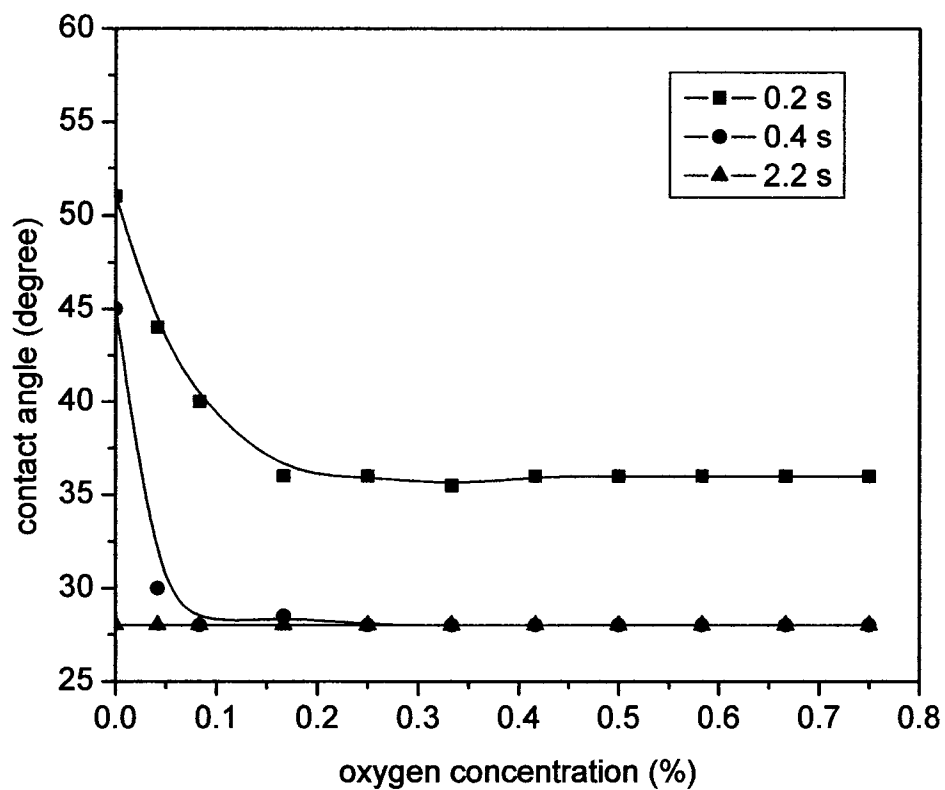
Figure 5.3.c. Contact angle versus oxygen concentration for selected exposure durations at 120W.
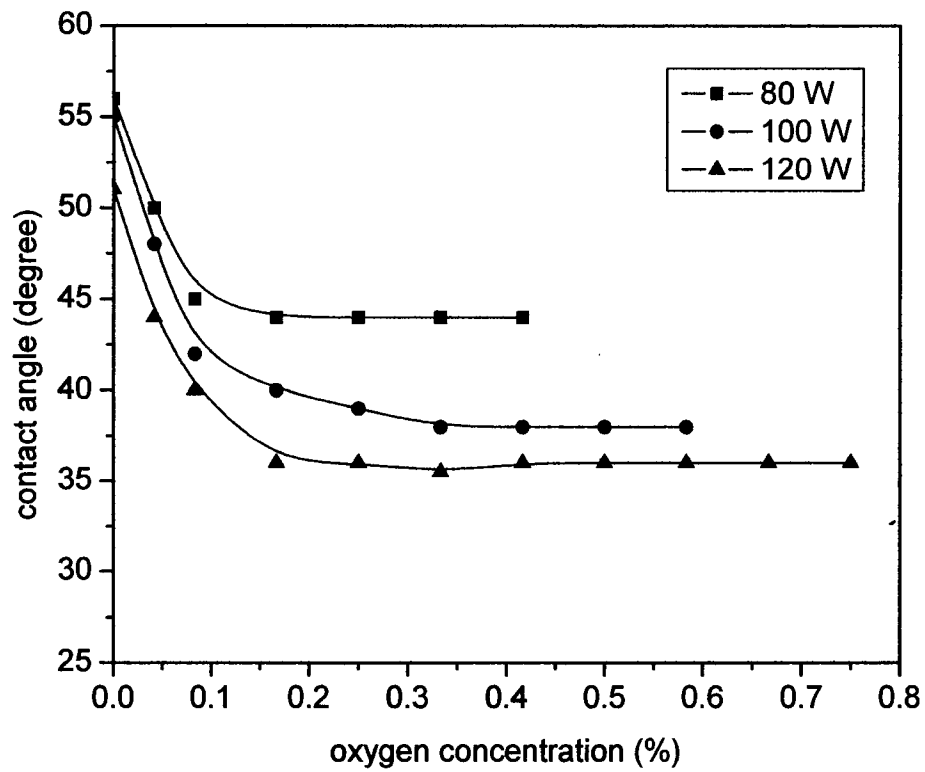
Figure 5.4.a. Contact angle versus oxygen concentration at selected powers for 0.2 s exposure duration.
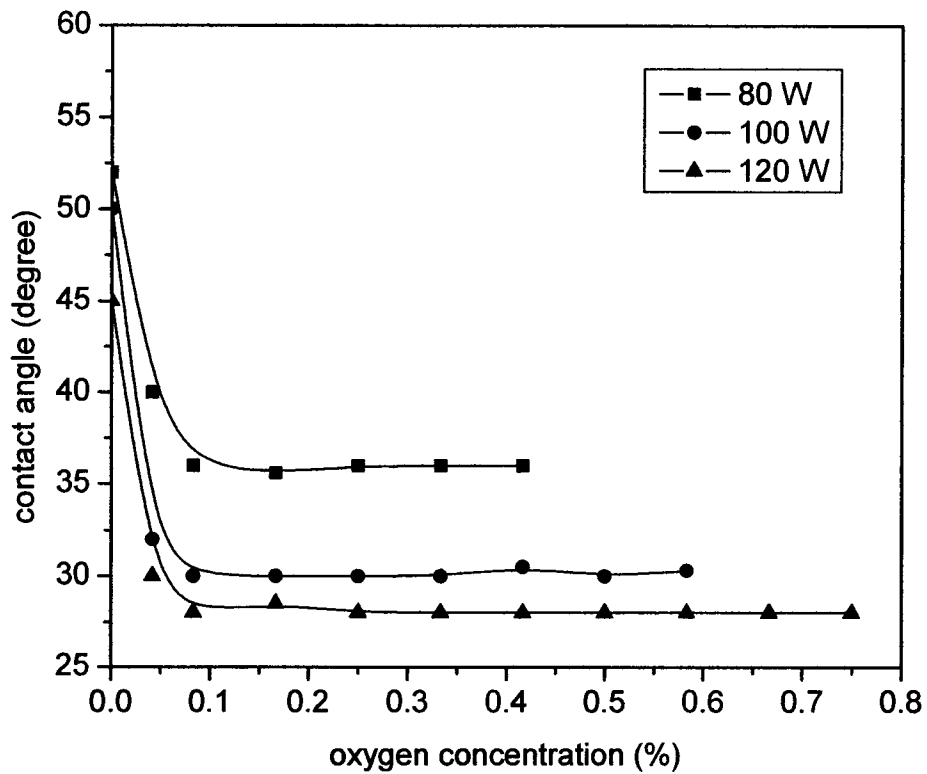
Figure 5.4.b. Contact angle versus oxygen concentration at selected powers for 0.4 s exposure duration.

5.2.1.2. Increased contact angles

The modification by the He-PFH plasma resulted in increased contact angles and hydrophobic PET surfaces. Through the processing, fluorine element was incorporated into the PET surface. The main helium flow rate was kept at 12 slm (standard liter per minute). The small helium-PFH flow rate was 10 sccm and 40 sccm (standard cubic centimeter per minute). The RF power was set at 120 W and 150 W. The modification duration was 2.2 s, 0.4 s and 0.2 s respectively. The sample was PET film. After processing, water contact angles were measured on the sample surface immediately. The results are listed in table 5.2.

He-PFH flow rate (sccm)	RF power (W)	Exposure duration (second)	Contact angle (degree)
1	20	0.2	104
	100	2.2	106
	100	0.2	104
	140	0.2	104
4	20	0.2	104
	100	2.2	106
	100	0.2	104
	140	0.2	104
10	20	0.2	104
	100	0.2	104
	120	0.2	103
	120	0.4	104
	120	2.2	108
	150	0.2	102
	150	0.4	104
	150	2.2	109
40	120	0.2	104
	120	2.2	108
	150	0.2	105
	150	2.2	112

Table 5.2. Contact angle versus He-PFH flow rate, RF power, and exposure duration.

5.2.2. Modification results by the air plasma

5.2.2.1. Reduced contact angles

Air plasma surface modification of PET surfaces resulted in reduced contact angles. During the modification process, PET surfaces were oxidized and polarized groups were generated at the surfaces. Figure 5.5 shows the modification results using the air plasma. The resultant contact angle decreased with longer modification duration and higher power. At different power levels, above certain modification durations, there was no significant change in contact angle.
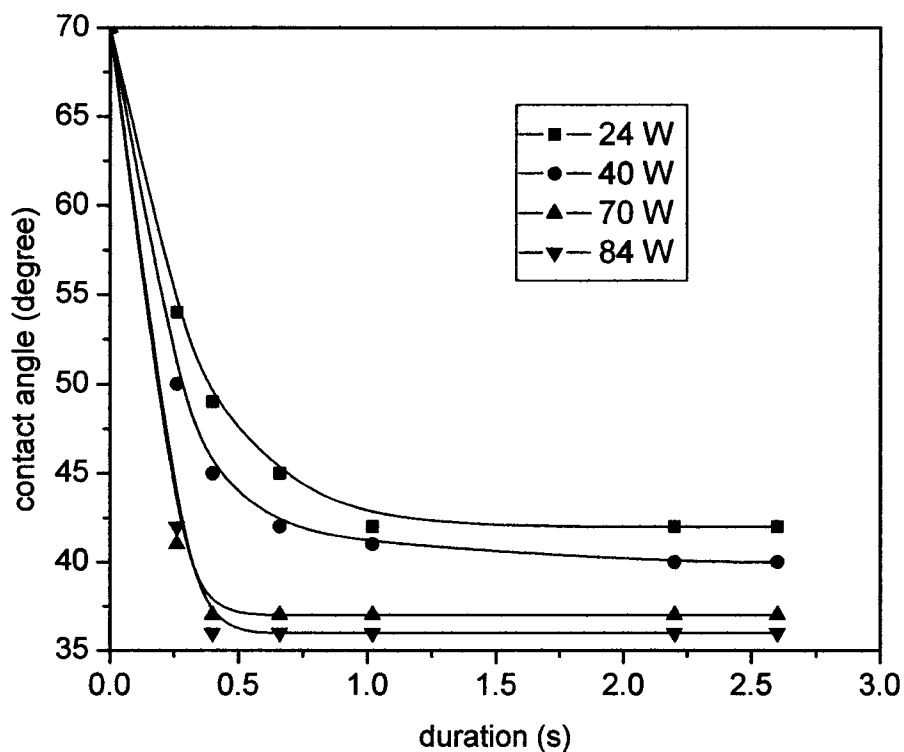
Figure 5.5. Contact angle versus modification duration at selected power levels.

5.2.2.2. Atomic Force Microscope (AFM) measurements

The surface profiles of the unmodified and modified PET surfaces were measured with an AFM (Digital Instruments Nanoscope). The modified PET sample was treated for 2.6 s at 84 W power level. The AFM was running in tapping mode to eliminate any damage to the relatively soft PET sample. The results are shown in Figure 5.6 and Figure 5.7 respectively. The scan area was 1 μm by 1 μm on both samples. The vertical unit was only 15 nm, which is much smaller than the horizontal units. The untreated PET surface was not absolutely flat, but only had smaller and lower mountains. The treated PET surface became rougher, and had a different profile. Many higher and larger peaks were generated. The generation mechanisms of these peaks are unknown. They might come from the plasma etching effect. We believe that these new peaks are low molecular weight oxidized material (LMOM) [1, 19]. It is apparent that the modification increased PET surface area.

Digital Instruments NanoScope
Scan size   1.000 μm
Scan rate   0.3733 Hz
Number of samples   256
Image Data   Height
Data scale   15.00 nm
Engage X Pos
Engage Y Pos

view angle
light angle

0.2
0.4
0.6
0.8
μm

X   0.200 μm/div
Z 15.000 nm/div

0 °
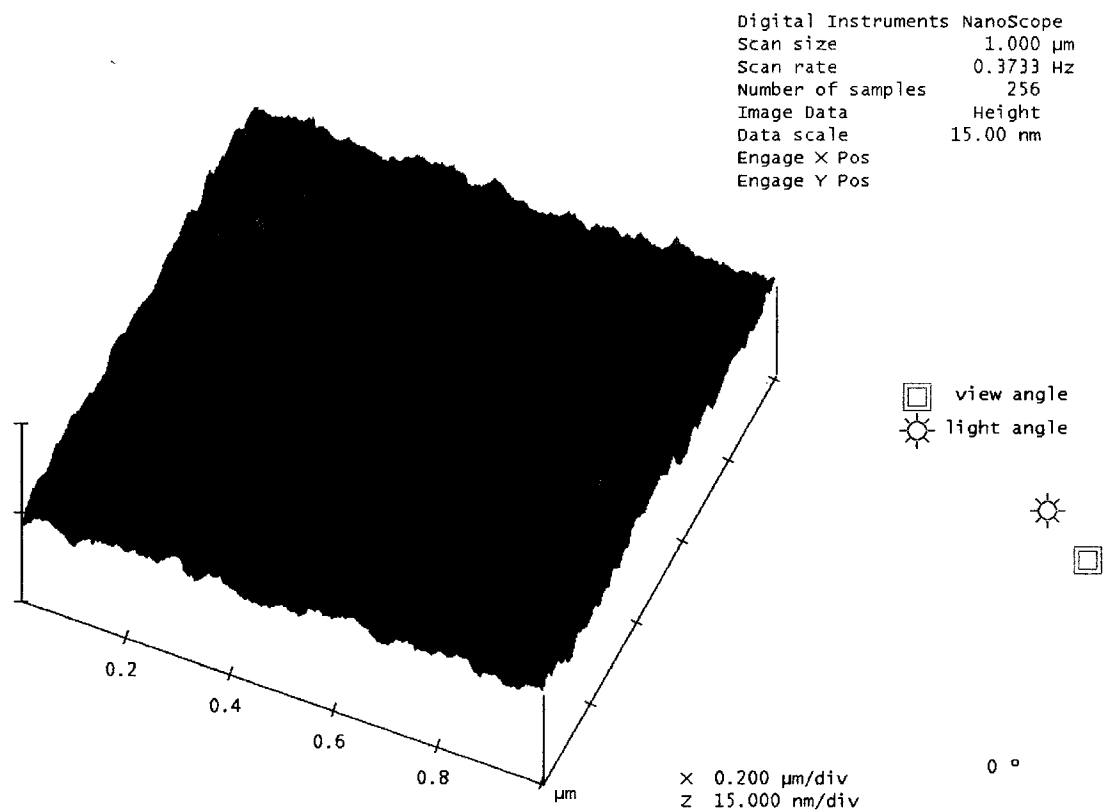
Figure 5.6. An AFM image of an untreated PET surface.

```
Digital Instruments NanoScope
Scan size          1.000 µm
Scan rate        0.2701 Hz
Number of samples      256
Image Data          Height
Data scale       15.00 nm
Engage X Pos
Engage Y Pos
```

view angle
light angle

µm

0.8

0.6

0.4

0.2

X 0.200 µm/div
Z 15.000 nm/div

0 °
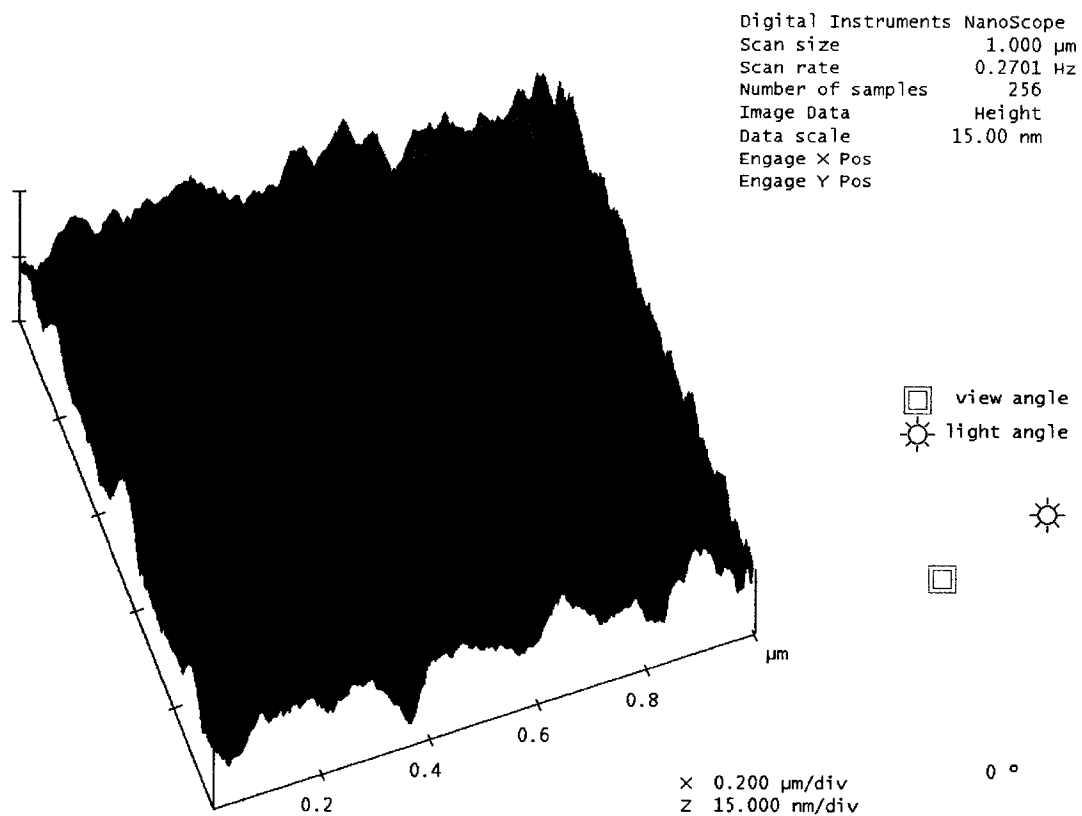
Figure 5.7. An AFM image of a PET surface treated by air plasma.

5.2.3. Decay of the modification effect

We examined the stability of the modified surfaces. We observed an aging effect by monitoring the change of the contact angle with time. For the RF plasma, samples were treated at a 100 W RF power level for 2.2 s (Figure 5.8.a). For the air plasma, the power was held at 84 W with modification durations of 0.66 s and 2.6 s (Figure 5.8.b). During the first three days, the contact angle increased steadily. Beyond three days, the contact angle increased very slowly. For the three samples treated at 100 W RF power level for 2.2 s, the contact angle increased from 28 degrees to 36 degrees after one day of aging. After three days of aging, the contact angle increased to 42 degrees. From then on, the contact angle increased slowly, and reached 48 degrees after three weeks. The modified PET surface was not stable. The possible reasons can be summarized as the reorientation of polar groups at the surface layer, the diffusion of unpolar groups from the sub-surface to the surface, and the reactions of free radicals at the surface [1]. No effect of oxygen concentration in the helium-oxygen plasma on the aging process was observed.

We also examined stability of the PET surfaces modified with the helium-PFH plasma. Four modified samples were monitored. The results are shown in Figure 5.8.c. In the first three weeks, the contact angles decreased several degrees. From the fourth week to the eighth week, the contact angles remained almost unchanged.
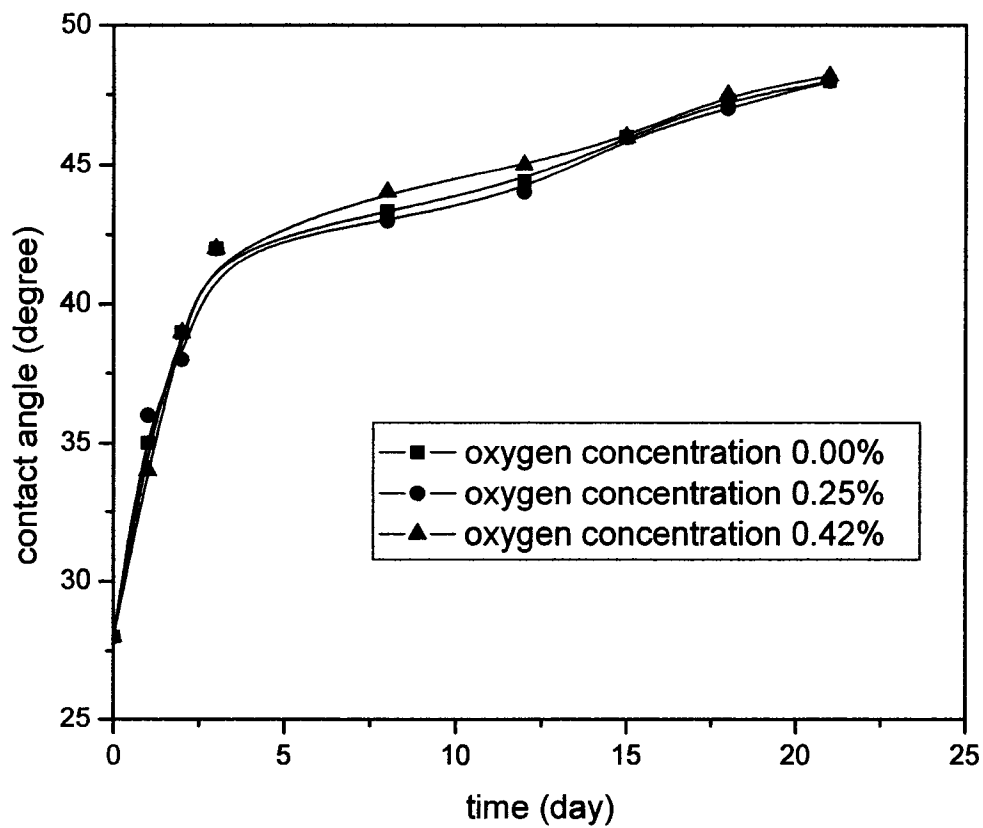
Figure 5.8.a. Contact angle versus time for PET samples treated by the RF He-O_2 plasma.
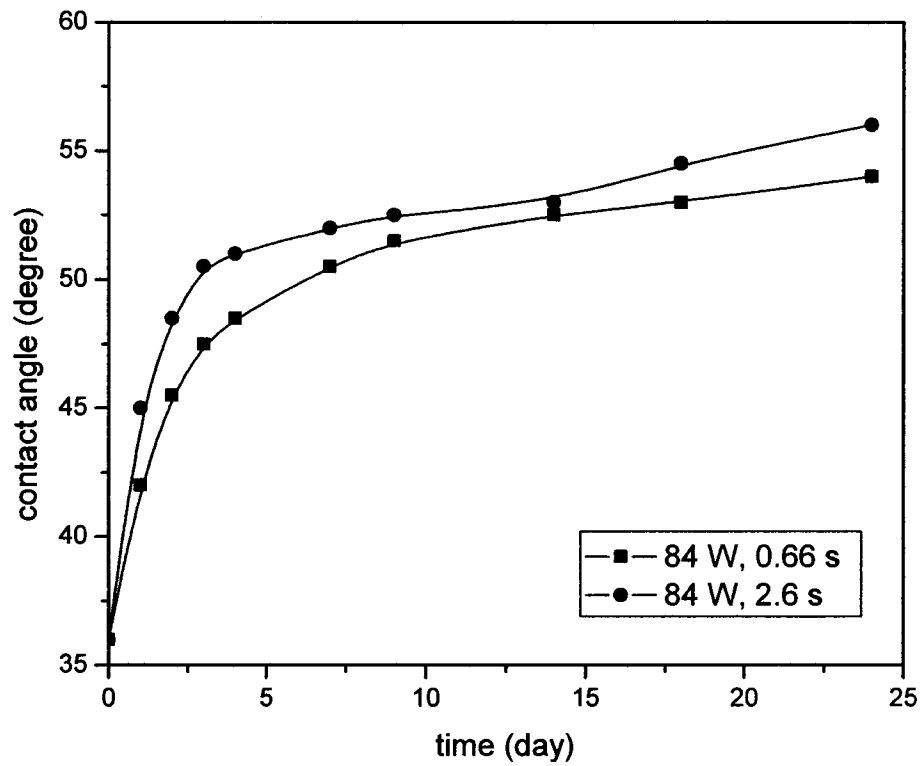
Figure 5.8.b. Contact angle versus time for PET samples treated by air plasma.
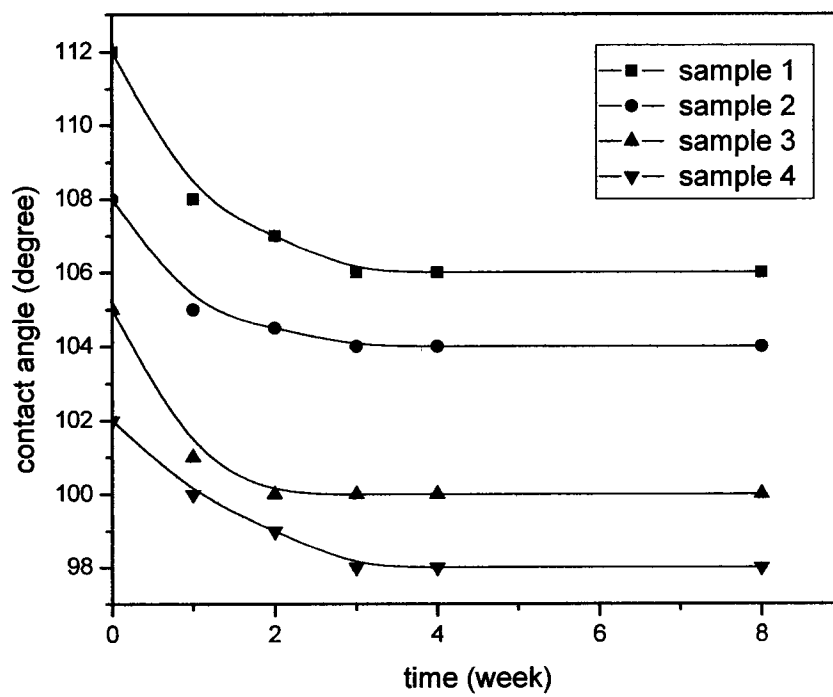
Figure 5.8.c. Contact angle versus time for PET samples treated by RF He-PFH plasma.

5.3. Open-chamber operation of the RF helium plasma

5.3.1. Setup of open-chamber operation

In the preview setup for polymer surface modification, the sample strip passes the exit of the plasma jet. The interaction length of the plasma and the polymer surface equals to the quartz thickness, namely only 1.5 mm. The polymer film never enters the plasma chamber. In order to increase the interaction length and to improve the modification efficiency, we need to put the polymer sample inside the plasma chamber. Hence, open-chamber operation of our plasma is needed.

The idea is shown in Figure 5.9. The quartz slides are cut half in height, and the polymer strip can be placed inside the plasma. The interaction length is the width of the plasma body, namely 10 cm, instead of 1.5 mm. Top of the plasma jet is open. The plasma jet is also open at two sides from of the top of the quartz slide to the top of the plasma jet.

The polymer strip was placed against the RF electrode, the ground electrode, or in the middle of the two electrodes. When the polymer strip was against one electrode, only one side open to plasma was modified uniformly while the other side was poorly modified. Water contact angle was also measured on this well modified side. When the polymer strip was placed in the middle of the two electrodes, both two sides were modified.
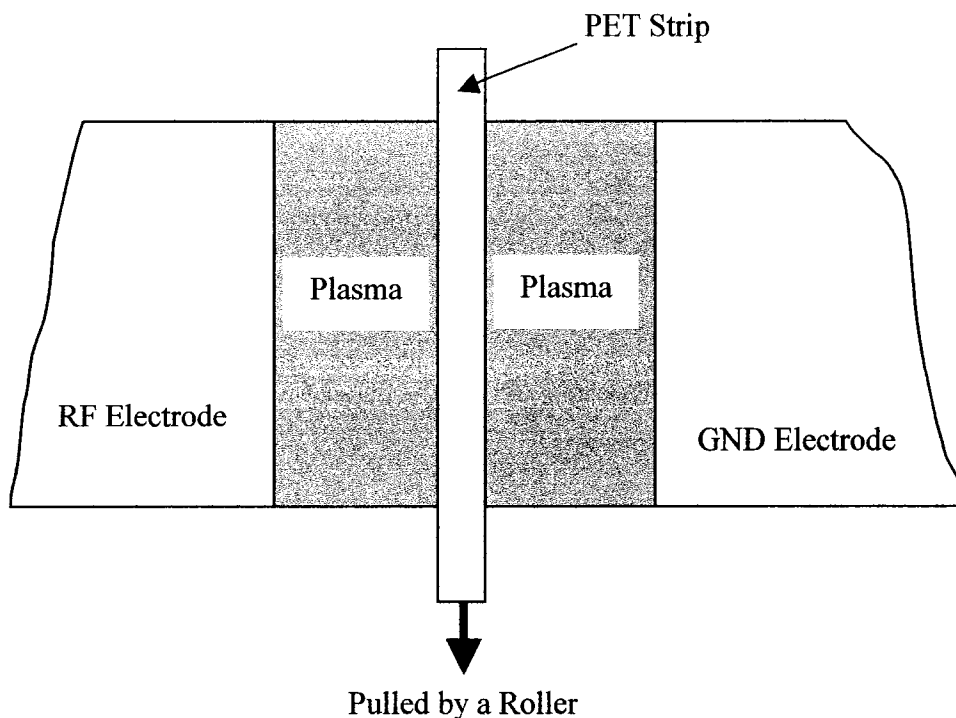
Figure 5.9. Schematic setup of open-chamber operation.

5.3.2. Results of open chamber operation

Top of the plasma jet is open. The plasma jet is also open at two sides, from the top of the quartz slide to the top of the plasma jet (Figure 5.10). The left picture is the plasma jet without the polymer sample, while the right picture is the plasma with a polymer strip inside. As we can see, the polymer sample decreases the plasma density around the polymer sample. When the sample is placed against the RF and the ground electrodes, we got similar results. For speed #5 and #10, the resultant contact angles were all around 36 degrees. We got smaller contact angles (around 30 degrees) when the sample speed was #0. When the sample was placed in the middle of the two electrodes,

we got similar results as when the sample was against the RF or the ground electrode.

The only difference is the two sides of the sample were modified at the same time.
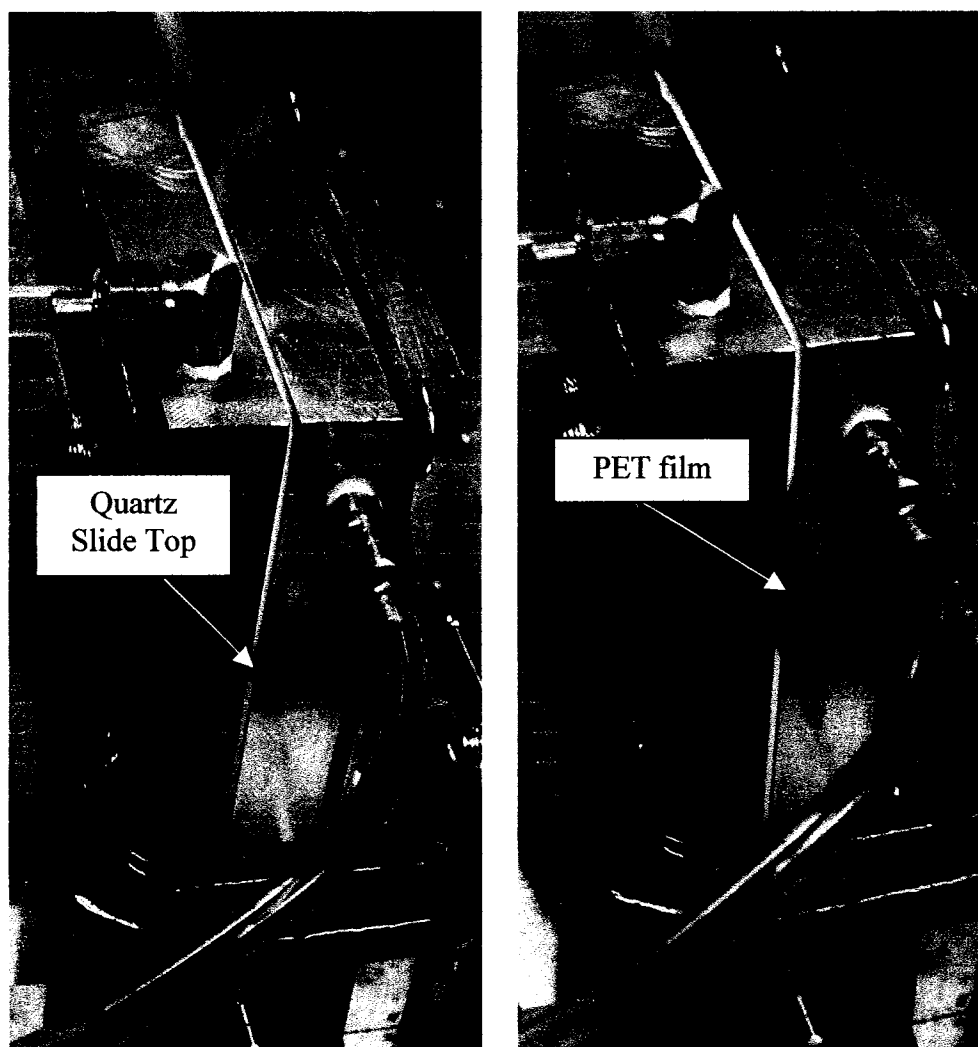
Figure 5.10. Picture of the open-chamber plasma with (right) and without PET.

5.4. Modification mechanisms

5.4.1. A brief review on modification mechanisms

There are three basic theories on the mechanisms of plasma surface modification of polymer [1,2]. They are ultraviolet photochemistry, ion bombardment, and direct reactions. These three theories are being widely accepted, although people still have disputes over some special cases. These three theories are introduced next.

According to ultraviolet photochemistry theory, UV photons from a plasma source have short wavelengths and high energy, and they can break chemical bonds at a polymer surface and in its surrounding gases. These broken bonds lead to a series of chemical reactions at the surface layers. Through these chemical reactions, elements from the surrounding gases can be incorporated into the surface layers. There are three cases in this kind of modification. The first case is that UV light only breaks chemical bonds at polymer surfaces, and no broken bonds are formed in the surrounding gas. In this case, the surrounding gas reacts with the broken bonds at the surface. The second case is that broken bonds are only formed from the surrounding gas, and these broken bonds react with the surface. The third case is that broken bonds are formed in both surrounding gas and polymer surface.

According to the ion bombardment theory, some ions inside the plasma have enough energy to break chemical bonds on polymer surfaces, and then initiate a series of chemical reactions. These reactions change the polymer surface composition and structure. In some cases, ion dose can be the main factor of polymer surface modification.

The third theory is called direct reaction. According to this theory, chemically active species generated by the plasma may react directly with polymer surfaces, and the

reactions modify the polymer surfaces. This kind of modification is mainly a pure chemical effect.

Our atmospheric-pressure plasma source produces a large mount of ions, UV photons, and chemically active species. Above three theories can be applied to our experiment. Next, we check these theories through some experiments and analysis on UV light, ions, oxygen atoms and ozone molecules.

5.4.2. The function of ions

From Langmuir probe measurement and theoretical calculations, we estimate that the ion density is on the order of 10^{11}cm^{-3} for the RF helium plasma. For the air plasma, peak ion density was on the order of 10^9cm^{-3}. The density of neutrals is on the order of 10^{19}cm^{-3}. Ions mainly collide with neutrals and their energy should be balanced with neutrals. For both plasmas, gas temperature was under 60°C. Hence, ion energy should be on the order of 10^{-2} eV. This estimation agrees well with others [69]. The activation energy of chemical bonds at the polymer surface is on the order of a few eV [91]. The ion energy is too low to break any chemical bonds at the polymer surface. Therefore, these low energy ions should have no direct contributions to the surface modification. This conclusion agrees well with one of our Langmuir Probe measurement results and the results on contact angle versus oxygen concentration. From Langmuir Probe measurements, we found that ion density decreased with higher oxygen concentration (higher flow rate). Contact angle measurements showed that in certain ranges, higher oxygen concentration led to higher modification efficiency. In this situation, lower ion density corresponded to higher modification efficiency.

5.4.3. The function of UV light

In order to test the function of the pure UV light, we need to separate the UV light from the plasma. We placed a plate between the RF He plasma and the polymer sample. Only some UV photons could reach the polymer surface, and other compositions from the plasma were blocked. The setup is shown in Figure 5.11. The plate was a piece of 6 mm thick LiF crystal, 1.5 mm thick quartz slide, and 1mm thick glass slides. The transmittance of the LiF crystal is shown in Figure 5.12. Its transmittance is above 90% from 200 to 400 nm. We do not have the transmittance data of the quartz slide and the glass slide, but we know the cutoff wavelength of quartz is about 160 nm, and cutoff wavelength of glass slides is larger.

An unmodified sample showed a contact angle of 70 degrees. After 30 minutes modification, the samples showed contact angle of 50, 64, and 70 degrees modified in the setup with LiF crystal, quartz, and glass slide respectively. LiF crystal led to the most modification, and quartz is less, and glass gave no modification. Shorter wavelength UV light has more contributions in the modification.

The modification efficiency of pure UV light is limited, and it took 30 minutes for the contact angle to decrease 20 degrees. While in the setup without the UV window, it took less than one second for the contact angle to decrease more than 20 degrees. Hence, UV light is not the main contributor in the plasma surface modification process. On the other hand, we found the intensities of UV photons with wavelengths longer than 200 nm decrease with higher oxygen concentration. Oxygen molecules should absorb UV photons whose wavelengths are shorter than 200 nm. In certain ranges, higher oxygen

concentration gives higher modification efficiency. Therefore, UV radiation is not the main factor during the modification process.
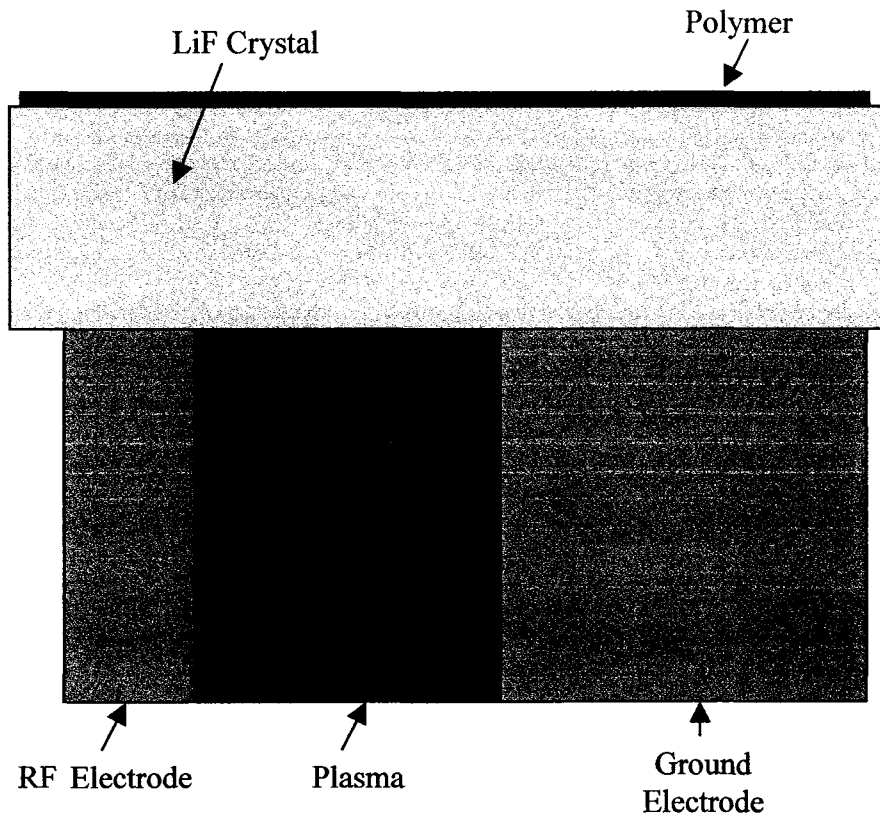
Figure 5.11. Experimental setup on UV light.
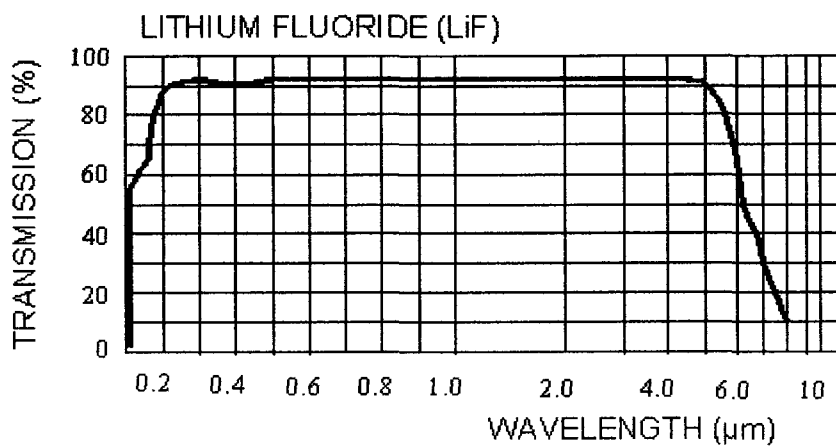
Figure 5.12. LiF crystal transmittance.

We also did similar experiment with LiF plate for our air plasma. We found that the contact angle only decreased a few degrees after 30 minutes processing. This lower efficiency showed that the UV light only had a minor role in the modification process.

5.4.4. Direct reactions

From the absorption spectroscopy measurement, we found that ozone density could reach $10^{15} cm^{-3}$ and $10^{15} cm^{-3}$ in the down plasma region for the two plasmas. Inside the plasma, oxygen molecules are dissociated into oxygen atoms. An oxygen atom reacts with an oxygen molecule to form an ozone molecule. Ozone molecules can also be dissociated to generate oxygen atoms. In the down plasma region, oxygen atoms also react with oxygen molecules to form ozone molecules, but ozone molecule cannot be dissociated through the electric power applied to the plasma. Hence, inside the plasma, the density of ozone is lower than the density of oxygen atoms while in the down plasma region, the ozone density is higher than oxygen atom density. It is reasonable to estimate that the oxygen atom density inside the plasma and the ozone density in the down plasma region are on the same order.

Oxygen atoms and ozone molecules can react directly with polymer surface, and extra polarized groups can be generated in the surface layer. As a result, the polymer surface is modified. The direct reactions of oxygen atom and ozone with polymer surface are likely to be the main modification mechanisms. On the other hand, UV photons break chemical bonds at the polymer surface. With these broken bonds, the surface may react with active species from the plasma at higher efficiencies. We believe UV photochemistry may be another modification mechanism.

In brief, based on the analysis and experiments on ions, ultraviolet photons, oxygen atoms and ozone molecules, we believe that the surface modification was mainly a chemical and photochemical process.

5.5. Discussions

5.5.1. No optimal oxygen flow rate for surface modification

The flow rate of oxygen gas influenced the modification effect for the RF helium-oxygen plasma. For relatively low RF powers or short exposure durations, the contact angle first decreased with the oxygen flow rate, and then leveled off. For high RF powers or long exposure durations, the contact angle was constant at 28 degrees. In other words, no optimal oxygen flow rate was found for the surface modification. This effect can be explained by three theories.

In the first theory, the concentrations of active species are the key factor. A higher oxygen flow rate does not mean high concentrations of active species. When higher oxygen concentration, the plasma density decreases, and the efficiency to generate oxygen atoms and zone molecules decreases. As a result, the number of oxygen atoms and ozone molecules may level off with oxygen flow rate, and the resultant contact angles are the same.

According to the second theory, oxygen atoms at different excited states have different effects for the surface modification [92]. Oxygen atoms at one excited state are positive for the modification, while oxygen atoms at another excited state are negative for the modification. The ratio of the numbers of the oxygen atoms at these two states determines the surface reaction rate. With different oxygen flow rates, this ratio may be the same, and the resultant contact angle is also the same.

The third theory emphasizes the critical step in the surface reactions. This theory is widely accepted in surface chemistry. The surface modification is a complicated reaction process with many steps, and the control step limits the reaction rate [93]. The

explanation is a bottleneck effect. In the region where contact angle decreases with the oxygen concentration, the control step is the formation of active species from oxygen. More oxygen may generate higher density of active species and higher reaction rates. In the region where the contact angle levels off with the oxygen concentration, the control step changes to other steps, and oxygen concentration has no effect on the reaction rate and resultant contact angles. Other control steps may be the adsorption of active species on the surface, the diffusion of some active species on the surface, the formation of active sites on the surface, the reactions of surface radicals with the adsorbed active species, and etc.

5.5.2. On surface analysis

We analyzed PET surfaces modified by the He-O_2 plasma with XPS at College of William and Mary. XPS is a very reliable instrument to do surface analysis. No apparent difference was found on the modified and unmodified sample surfaces. The reason may be due to the etching effect. The etching rate of PI by the He-O_2 plasma was found to be on the order of a few microns per minute [68]. We also found that the etching of PET by our air plasma was on the order of several hundreds nm per minutes. The surface modification is the competition or the combination of the formation of new surface layer and etching. New materials are formed at the surface, and they are also removed continuously. It is a dynamic process. As a result, a very thin new layer is left. Because of its sensitivity limitation and detection depth, this XPS could not detect the modified layer. Evans East also analyzed our PET samples with XPS modified by the He-PFH

plasma. They did not find any big difference between modified and unmodified PET surfaces. More research is needed in this area.

5.5.3. Decay of the modified surface

We examined the stability of the PET surfaces modified by the He-O_2 plasma and the air plasma. We observed an aging effect by monitoring the change of the contact angle with time. The modified PET surface is not stable. The decay process was much slower than the case in the modification by corona discharge, but it is faster than the case in the low-pressure plasma surface modification. The general reasons for the decay can be summarized as the reorientation of polar groups at the surface layer, the diffusion of unpolar groups from the sub-surface to the surface, and the reactions of free radicals at the surface. The etching effect may be another reason for the decay. Our plasma has a strong etching effect on PET sample. As a result of etching, the modified layer may be very thin, and the modified surface is relatively easy to be influenced by the diffusion of unpolar groups from the sub-surface to the surface and the reactions of free radicals at the surface. Hence, the modification effect decays at a relatively high rate.

The surface modified by the He-PFH plasma was relatively stable. The reason may be the different modification effect. The He-PFH plasma has a deposition effect while the He-O_2 plasma and the air plasma have an etching effect. We found new materials were deposited on the electrodes for a long-term operation, such as 30 minutes. We also found new films were formed on PET surface for 3 minutes treatment. By the He-PFH, the modified layer is thicker, and hence the modified PET surfaces are more stable than those modified with the He-O_2 plasma and the air plasma.

5.5.4. Open-chamber operation

Open-chamber operation of our plasma is feasible, and the plasma was also very stable. Polymer surface modification by open-chamber operation was also investigated. The efficiency of open-chamber operation was lower compared with close-chamber operation. The main reason is that the plasma is weaker during the open-chamber operation process.

When the PET sample was placed inside the plasma, the plasma density was decreased around the polymer sample. There are at least three reasons why the polymer sample decreases the plasma density around it. First, the polymer sample influenced the electric field distribution in the plasma. Second, the interaction of the plasma and the polymer sample generates byproducts. These byproducts act as impurities in the plasma, and hence decreases the plasma intensity. Thirdly, the polymer sample decreases the average electron energy. Without the polymer sample, electrons oscillate between the two electrodes inside the plasma. With the polymer sample inside the plasma, electrons collide with the polymer sample, and electron mean free path length is decreased, and hence, so is the mean electron energy. The plasma relies on the high-energy electrons to excite and ionize neutrons, or to sustain the plasma. The low electron energy will decrease the plasma density.

5.5.5. Comparison of the two plasmas

These two plasmas have some common characteristics. First, both of them do not need any vacuum, since they are operated in atmospheric-pressure. Second, they are both cold plasmas. They do not damage the material processed by any thermal effect. Thirdly, both have UV radiations, although UV light is not the main contributor for surface modification. Fourth, polymer surface modification mechanisms are similar for both plasmas. The surface modification is mainly a chemical process.

The two plasmas have a lot of differences. First, the cost of the RF helium plasma is higher, since it uses a lot of helium gas and the RF power supply is more complicated than the AC power supply used for the air DBD. Second, electron density of the helium RF plasma is about two orders higher. Third, the ozone density in the air DBD is about one order higher since the air plasma has more oxygen inside. Fourth, the air DBD can only get hydrophilic polymer surface while the RF helium plasma can get both hydrophilic and hydrophobic surfaces. Fifth, the RF helium plasma may have more potential applications in material processing. Helium is noble gas, and any chemical agent or gas can be added to the feeding helium gas to generate different active species needed.

Chapter VI

Summary

6.1. Summary of this research

Low-pressure plasmas are being widely used to modify polymer surfaces. To eliminate vacuum limitations of low-pressure plasmas, two atmospheric-pressure plasmas were generated to modify polymer surfaces. These two plasmas were cold and stable. Both plasmas were characterized on electron density, emission spectrum, and ozone density. It was demonstrated that both plasmas could be used to modify PET surfaces with very high throughput. The surface modification was a combination of chemical and photochemical process.

An atmospheric-pressure helium plasma was generated through RF capacitive discharge. The capacitive discharge chamber consists of two aluminum electrodes, two quarts slides, and a ceramic manifold. The distance between the two electrodes was kept at 1.50 mm by the two quartz slides. The two electrodes were installed on the top of the ceramic manifold, and helium gas was fed into the chamber through small holes on the top of the manifold. The structure was airtight except that its top was completely open to air. Helium was kept flowing out of the open top during the operation of the plasma. RF power was applied to the plasma chamber through a RF tuner to minimize power reflection. The plasma was very stable without apparent arcing. The gas temperature was below 60 °C. The plasma also works with a mixture of majority helium and another minority gas. Liquid PFH could be added to the feeding helium gas through a bubbler.

The RF helium plasma was characterized. A Langmuir Probe was developed to measure the total ion flux only. The collector of the probe was placed at exit of the

plasma source. The flux increased with negative bias and decreased with positive bias. The flux also decreased with a higher minority gas flow rate. The total ion flux was found to be on the order of 10^{13} cm^{-2}s^{-1} with zero bias. Based on this flux and the gas flow rate, electron density was determined to be on the order of 10^{11} cm^{-3}. Electron density was also calculated without the measurement by this probe. The calculated electron density agrees with the measurement value. The emission spectra from 200 nm to 800 nm were measured. The peaks in the spectrum of pure helium plasma were mainly from the impurities of the feeding helium gas. The UV peaks were mainly from the impurities of N_2. New peaks in the UV spectrum of He-PFH plasma were from CF_2 radicals. Ozone density at the exit of the helium-oxygen plasma was measured by absorption spectroscopy. A 253.6 nm wavelength absorption line was selected from a mercury lamp. The ozone density was estimated to be on the order of 10^{15} cm^{-3}.

The atmospheric-pressure helium plasma was used to modify PET surface. The PET samples were treated for various durations by scanning the samples at various speeds. Immediately after the surface modification process, water contact angle measurements were performed on the PET samples. It was found that contact angle could be reduced from 70 to 28 degrees in less than one-second of exposure duration. In certain operation ranges, resultant contact angle decreased with RF power, exposure duration and oxygen flow rate. Oxygen concentration in helium gas mixture influenced the modification efficiency, but no optimal value was found. The aging effect of the modified PET surfaces was observed by monitoring the change of the contact angle with time.

An atmospheric-pressure air plasma was generated through DBD to eliminate the usage of a large mount of expensive helium. The structure of this plasma chamber was

similar to that of the RF helium plasma except that one electrode was covered by a 1.00 mm thick Al_2O_3 dielectric sheet. The gas gap was kept at 1.00 mm. A high AC voltage was applied between the two electrodes. The AC frequency was set at 25 kHz to reach a maximum total power of about 88 W. The plasma was also cold and very stable.

The air plasma was also characterized. An equivalent circuit was used to calculate the discharge current from measurements of total voltage and total current. Based on the discharge current, the peak electron density was found to be on the order of $10^9 \, cm^{-3}$. The emission spectrum of the plasma was measured. The peaks in the emission spectrum were all from N_2, and no O_2 peaks were observed. The ozone density at the exit of the plasma was determined to be on the order of $10^{16} \, cm^{-3}$ by absorption spectroscopy.

The air plasma was also used to modify PET surfaces in a similar way as the helium plasma. It was found that contact angle could be reduced from 70 to 36 degrees in less than one second of exposure duration. In certain operation ranges, resultant angle decreased with AC power and exposure duration. An aging effect was also found for the modified PET surfaces.

Surface modification mechanisms were investigated on both plasmas. Ions mainly collide with neutrals, and their temperature should be balanced with neutrals. These low-energy ions cannot break chemical bonds at PET surface. Therefore, they should have no direct contributions for the modification. To test the role of UV light, UV light was separated from both plasmas. Experiments with UV light alone suggested that UV light itself could not give such high modification efficiencies. On the other hand, both plasmas produced a large mount of ozone and oxygen atoms. They could react directly with PET

surface and played main roles in the modification. Hence, the surface modification with both plasmas was a combination of chemical and photochemical process.

6.2. Future developments

The RF helium plasma has been operated below 150 W with only RF electrode cooled by circulating water. At high power, the plasma chamber might become unstable due to the heating effect. In fact, the plasma works well with both electrodes cooled with circulating water. In this way, the plasma will work well at higher power levels as long as it does not transfer to arc. With higher RF power, surface modification efficiency may be further improved.

Another way to improve the modification efficiency is to combine the two plasmas. The setup can be based on the RF helium plasma. An extra electrode will be placed at the exit of the helium plasma. The polymer sample will be placed under the new electrode. A high AC voltage will be applied to the new electrode, or a series of high voltage pulses will be applied. In this setup, the plasma will be started by the RF power, but its intensity will be increased by the DBD structure at exit of the helium plasma. More research is needed in this direction.

Modification duration was very short for both plasmas, but the sample speed was not very fast. The limitation comes from the fact that both plasmas are very narrow, and the interaction lengths are only 1.5 and 1.0 mm respectively. To over come this limitation, a series of parallel plasma arrays can be established. In this setup, the interaction length will be longer, and the sample speed will be increased. To save power, the height of the plasma chambers needs to be reduced a lot.

PFH was fed to the RF helium plasma to get hydrophobic PET surface. The plasma should work well other chemicals. Different chemical will have different modification effect. In this research, only PET samples were used. The materials that can

be surface modified are not limited to PET, or to polymer. This plasma was also used to modify aluminum foil surface. The surface modification of carbon fibers by this plasma was also proposed.

Both plasmas were only used to modify material surfaces. Other applications by both plasmas are possible, such as material deposition. The RF helium plasma should be able to deposit different kinds of films if proper chemicals are added to the feeding helium. Even the air plasma should be able to deposit SiO_2 film if tetraethoxysilane is added to the feed air.

Open-chamber operation of the RF helium plasma was demonstrated. In this setup, solid powder materials can be input into the plasma chamber from the open side. The untreated powder material can be collected at the exit of the plasma. Detailed structure of this setup needs more investigation.

Both plasmas were very narrow, and the efficiency of processing large material piece by both plasmas will be very low. To increase the processing efficiency, a large volume of atmospheric-pressure plasma is needed. To generate such plasmas, microwave power will be used, instead of RF or low-frequency AC power. The plasma can be started with a RF coil or high voltage pulses, and microwave energy can be applied afterwards. As long as the initial plasma frequency is higher than the microwave frequency, the applied microwave energy can be absorbed to increase the plasma density.

References

1. E. M. Liston, L. Martinu, and M. R. Wertheimer, in *Plasma Surface Modification Of Polymers: Relevance To Adhesion*, edited by M. Strobel, C. S. Lyons and K. L. Mittal, chapter 1, VSP: Utrecht, The Netherlands (1994).

2. M. R. Wertheimer, A. C. Fozza, and A. Hollander, Nucl. Instrum. Methods Phys. Res. B **151**, 65 (1999).

3. P. Matousek, G. Kruger and O. D. Hennemann, International Polymer Science and Technology **23**, 630 (1996).

4. Seok-Keun Koh, Seok-Kyun Song, Won-Kook Choi, Hyung-Jin Jung, Sung-Nam Han, J. Mater. Res. **10**, 2390 (1995).

5. P. Bertrand, P. Lambert, Y. Travaly, Nuclear Instruments and Methods in Physics Research B **131**, 71 (1997).

6. B. J. Bachman, and M. J. Vasile, J. Vac. Sci. Technol. A 7, 2709 (1989).

7. J. S. Cho, Young-Whoan Beag, Sung Han, Ki-Hwan Kim, J. Cho, and Seak-Keun Koh, Surface and Coatings Technology **128-129**, 66 (2000).

8. David L. Pappas and Jerome J. Cuomo, J. Vac. Sci. Technol. A **9**, 2704 (1991).

9. A. Hollander, J. E. Klemberg-Sapieha, and M. R. Wertheimer, Macromolecules 27, 2893 (1994).

10. B. W. Callen, M. L. Ridge, S. Lahooti, A. W. Neumann, and R. N. S. Sodhi, J. Vac. Sci. Technol. A **13**, 2023 (1995).

11. J. Heitz, H. Niino, and A. Yabe, Appl. Phys. Lett. **68**, 2648 (1996).

12. H. Niino, and A. Yabe, Appl. Phys. Lett. **63**, 3527 (1993).

13. J. E. Klemberg-Sapieha, L. Martinu, S. Sapieha, and M. R. Wertheimer, "Control and modification of surfaces and interfaces by corona and low pressure plasma", in G. Akovali(ed.), The Interfacial Interactions in Polymeric Composites, 201-222, Kluwer Academic Publishers, Netherlands (1993).

14. Christine (Qin) Sun, Dong Zhang, and Larry C. Wadsworth, Advances in Polymer Technology 18, 171 (1999).

15. Dong Zhang, Qin Sun, and Larry C. Wadsworth, Polymer Engineering and Science 38, 965 (1998).

16. M. Matsunaga, and P. J. Whitney, Polymer Degradation and Stability 70, 325 (2000).

17. J. Friedrich, L. Wigant, W. Unger, A. Lippitz, H. Wittrich, Surface and Coatings Technology 98, 879 (1998).

18. P. Matousek, G. Kruger and O. D. Hennemann, International Polymer Science and Technology 23, 632 (1996).

19. Mark Strobel, Christopher Dunatov, Joan M. Strobel, Christopher S. Lyons, Stephen J. Perron and Mark C. Margen, J. Adhesion Sci. Technol. 3, 321 (2000).

20. M. A. Lieberman, A. J. Lichtenberg, Principles of Plasma Discharges and Materials Processing, John Wiley & Sons, Inc. (1994).

21. H. Elesayed-Ali, ECE 875 Plasma Surface Interactions, Department of Electrical and Computer Engineering, Old Dominion University, Norfolk, Virginia (1999).

22. P. Fauchais and A. Vardelle, IEEE Trans. Plasma Sci. 25, 1258 (1997).

23. R. W. Smith, D. Wei, and D. Apelian, Plasma Chem. Plasma Process. 9, 135S (1989).

24. S. Ramakrishnan and M. W. Rogozinski, J. of Appl. Phys. D **30**, 636 (1997).

25. V. A. Nemchinsky, J. of Appl. Phys. D **30**, 2566 (1997).

26. D. R. Mac Rae, Plasma chem. Plasma Process. **9**, 85S (1989).

27. J. Heberlein and E. Pfender, "Thermal plasma chemical vapor deposition" in Materials Science Forum, J. J. Pouch and S. A. Alterovitz, Ed. Aedermannsdorf, Switzerland: Tran. Tech. Publications Ltd., **140-142**, 477-496 (1993).

28. P. Fauchais, M. Vardelle, A. Vardelle, and L. Bianchi, Ceram. Int. **22**, 295 (1996).

29. T. Yoshida, Materials Trans., JIM **31**, 1 (1990).

30. H. Koinuma, H. Ohkubo, and others, Appl. Physics Lett. **60**, 816 (1992).

31. K. Inomata, H. Koinuma, and others, Appl. Physics Lett. **66**, 2188 (1995).

32. K. Inomata, H. Ha, and others, Appl. Physics Lett. **64**, 46 (1994).

33. H. Ha, K. Inomata, and others, J. Electrochem. Soc. **142**, 2726 (1995).

34. H. Ha, M. Yoshimoto, and others, Appl. Physics Lett. **68**, 2965 (1996).

35. H. Ha, B. K. Moon, and others, Mater. Sci. Eng. B **41**, 143 (1996).

36. B. Lee, Y. Kusano, and others, Jpn. J. Appl. Phys. **36**, 2888 (1997).

37. K. Inomata, N. Aoki, and H. Koinuma, Jpn. J. Appl. Phys. **33**, L197 (1994).

38. M. Goldman and R. S. Sigmond, IEEE Trans. Elect. Insulation **17**, 90 (1982).

39. Y. P. Raizer, Gas Discharge Physics, New York: Spring-Verlag (1991).

40. J. R. Roth and Y. Ku, in Abstracts IEEE int. conf. Plasma Sci., Madison, WI, 251 (1995).

41. J. Salge, Surf. Coat. Technol. **80**, 1 (1996).

42. K. Schoenback, R. Verhappen, T. Tessnow, F. E. Peterkin, and W. W. Byszewski, Appl. Phys. Lett. **68**, 13 (1996).

43. E. E. Kunhardt, IEEE Transactions on Plasma Science **28**, 189 (2000).

44. A. J. Beaulieu, Appl. Phys. Lett. **16**, 504 (1970).

45. M. Sugawara, K. Murata, T. Ohshima, and K. Kobayashi, J. Phys. D: Appl. Phys. **14**, L137 (1981).

46. H. Aiyama, T. Takamatsu, C. Yamabe, and K. Horii, J. Phys. E: Sci. Instrum. **17**, 1014 (1984).

47. K. Nakamura, N. Yukawa, T. Mochizuki, S. Horiguchi, and T. Nakaya, Appl. Phys. Lett. **49**, 1493 (1986).

48. M. D. Wheeler, S. M. Newman, A. J. Orr-Ewing, and M. N. R. Ashfold, J. chem. Soc. Faraday Trans. **94**, 337 (1998).

49. F. M. Levinton and others, Physical Review Letters **63**, 2060 (1989).

50. Louis H. Sharpe, "Interfaces, Interphases and 'Adhesion': A perspective", in "The interfacial Interactions in Polymeric Composites", Edited by G. Akovali, Kluwer Academic Publishers, 1-20 (1993).

51. K. L. Mittal, Journal of Vacuum Science and Technology **13**, 19 (1976).

52. Adamson, Arthur W., Physical chemistry of Surfaces, Wiley-Interscience, New York, 424 (1982).

53. Louis H. Sharpe, and Harold Schonhorn, Advances in Chemistry **43**, 189 (1964).

54. B. V. Deryagin, V. P. Smilga, Proc. 3rd Intern. Congress Surface Activity, Cologne, Universitatsdruckerei, Mainz **2**, 349 (1960).

55. S. S. Voyutskii, Polymer Review **4**, Interscience, New York (1963).

56. J. J. Bikerman, The Science of Adhesion Adhesive Joints, second edition, Academic Press, New York (1968).

57. Hiroyuki Niino and Akira Yabe, Applied Physics Letters **63**, 3527 (1993).

58. J. Heitz, H. Niino, and A. Yabe, Applied Physics Letters **68**, 2648 (1996).

59. S. Beil, H. Horn, A. Windisch, C. Hilgers, and K. Pochner, Surface and Coatings Technology **116**, 1195 (1999).

60. B. W. Callen, M. L. Ridge, S. Lahooti, A. W. Neumann, R. N. S. Sodhi, Journal of Vacuum Science and Technology A **13**, 2023 (1995).

61. A. Hollander, J. E. Klemberg-Sapieha, and M. R. Wertheimer, Macromolecules **27**, 2894 (1994).

62. P. Groning, M. Collaud, G. Dietler, and L. Schlapbach, Journal of Applied Physics **76** (1994).

63. S. Nowak, P. Groning, O. M. Kuttel, M. Collaud, and G. Dietler, Journal of Vacuum Science and Technology A **10**, 3419 (1992).

64. RFII 1250 and 3000 Generators user manual, Advanced Energy Industries, Inc. (1998).

65. AZX series tuner user manual, Advanced Energy Industries, Inc. (1994).

66. J. Park, I. Henins, H. W. Herrmann, and G. S. Selwyn, Applied Physics Letters **76**, 288 (2000).

67. J. Park, I. Henins, H. W. Herrmann, and G. S. Selwyn, Journal of Applied Physics **89**, 15 (2001).

68. J. Y. Jeong, J. Park, I. Henins, S. E. Babayan, V. J. Tu, G. S. Selwyn, G. Ding, and R. F. Hicks, Journal of Physical Chemistry A **104**, 8027 (2000).

69. J. Park, I. Henins, H. W. Herrmann, and G. S. Selwyn, Journal of Applied Physics **89**, 29 (2001).

70. Yuzhi Wang, Vacuum Technology, Sichuan Scientific and Technological Press (1985).

71. "E. C. Y. Inn and Y. Tanaka, J. Opt. Soc. Am. **43**, 870 (1953).

72. R. W. B. Pearse and A. G. Gaydon, *The Identification of Molecular Spectra*, 4th ed. John Wiley & Sons, Inc., New York (1976).

73. P. Vidaud, S. M. A. Durrani, and D. R. Hall, Journal of Physics D **21**, 57 (1988).

74. H. E. Wagner, R. Brandenburg, K. V. Kozlov, A. Sonnenfeld, P. Michel, and J. F. Behnke, Vacuum **71**, 417 (2003).

75. S. Stucki, Process Technologies for Water Treatment, Asea Brown Boveri Ltd., Baden, Switzerland (1987).

76. A. V. Phelps, in Gaseous Dielectrics V, Proceedings of the Fith International Symposium on Gaseous Dielectrics Knoxville, TN, USA, edited by L. G. Christophorou, and D. W. Bouldin, 1 (1987).

77. J. Tepper and M. Lindmayer, HAKONE VII International Symposium on High-Pressure, Low Temperature Plasma Chemistry, Breifswald, Germany (2000).

78. X. Lu, F. Leipold, and M. Laroussi, Journal of Physics D: applied Physics **36**, 2662 (2003).

79. S. Ishikawa, K. Yukimura, K. Mtsunaga, and T. Maruyama, Surface and Coating Technology **130**, 52 (2000).

80. S. Kodama, H. Habaki, H. Sekiguchi, and J. Kawasaki, Thin Solid Films **407**, 151 (2002).

81. E. S. Lee, H. II. Park, H. K. Baik, S-J. Lee, K. M. Song, M. K. Hwang, and C. S. Huh, Surface and Coatings Technology **171**, 328 (2003).

82. J. Salge, Surface and Coatings Technology **80**, 1 (1996).

83. R. Seebock, H. Esrom, M. Charbonnier, M. Romand, and U. Kogelschatz, Surface and Coatings Technology **142-144**, 455 (2001).

84. R. Foest, F. Adler, F. Sigeneger, and M. Schmidt, Surface and Coatings Technology **163-164**, 323 (2003).

85. J. G. Kang, H. S. Kim, S. W. Ahn, and H. S. Uhm, Surface and Coatings Technology **171**, 144 (2003).

86. H. Barankova, and L. Bardos, Surface and Coatings Technology **174**, 63 (2003).

87. L. Bardos and Barankova, Surface and Coatings Technology **133-134**, 522 (2000).

88. J-K. Park, W-T. Ju, K-H. Paek, Y-H. Kim, Y-H. Choi, J-H Kim, and Y-S. Hwang, Surface and Coatings Technology **174-175**, 547 (2003).

89. HV Transformer and Power Amplifier Manual, Industrial Test Equipment Inc. (2004).

90. Contact Angle Meter Manual, Tantec Inc.

91. J. Xu, Fundamentals of Organic Chemistry (in Chinese), Chapter one, High Education Press, Beijing (1986).

92. L. F. Macmanus, M. J. Walzak, N. S. Mcintyre, J. Polym. Sci. A **37**, 2489 (1999).

93. R. I. Masel, Principles of Adsorption and Reaction on Solid Surfaces, chapter 6, John Wiley & Sons (1996).